Development of a New Fully Flexible Hydraulic Variable Valve Actuation System

by

Mohammad Pournazeri

A thesis
presented to the University of Waterloo
in fulfillment of the
thesis requirement for the degree of
Doctor of Philosophy
in
Mechanical Engineering

Waterloo, Ontario, Canada, 2012

AUTHOR'S DECLARATION

I hereby declare that I am the sole author of this thesis. This is a true copy of the thesis, including any required final revisions, as accepted by my examiners.

I understand that my thesis may be made electronically available to the public.

Mohammad Pournazeri

Abstract

The automotive industry has been in a marathon of advancement over the past decades. This is partly due to global environmental concerns about increasing amount of air pollutants such as NOx (oxides of nitrogen), CO (carbon monoxide) and particulate matters (PM) and decreasing fossil fuel resources. Recently due to stringent emission regulations such as US EPA (Environmental Protection Agency) and CARB (California Air Resource Board), improvement in fuel economy and reduction in the exhaust gas emissions have become the two major challenges for engine manufacturers. To fulfill the requirements of these regulations, the IC engines including gasoline and diesel engines have experienced significant modifications during the past decades. Incorporating the fully flexible valvetrains in production IC engines is one of the several ways to improve the performance of these engines. The ultimate goal of this PhD thesis is to conduct feasibility study on development of a reliable fully flexible hydraulic valvetrain for automotive engines.

Camless valvetrains such as electro-hydraulic, electro-mechanical and electro-pneumatic valve actuators have been developed and extensively studied by several engine component manufacturers and researchers. Unlike conventional camshaft driven systems and cam-based variable valve timing (VVT) techniques, these systems offer valve timings and lift control that are fully independent of crankshaft position and engine speed. These systems are key technical enablers for HCCI, 2/4 stroke-switching gasoline and air hybrid technologies, each of which is a high fuel efficiency technology. Although the flexibility of the camless valvetrains is limitless, they are generally more complex and expensive than cam-based systems and require more study on areas of reliability, fail safety, durability, repeatability and robustness. On the contrary, the cam-based variable valve timing systems are more reliable, durable, repeatable and robust but much less flexible and much more complex in design. In this research work, a new hydraulic variable valve actuation system (VVA) is proposed, designed, prototyped and tested. The proposed system consists of a two rotary spool valves each of which actuated either by a combination of engine crankshaft and a phase shifter or by a variable speed servo-motor. The proposed actuation system offers the same level of

flexibility as camless valvetrains while its reliability, repeatability and robustness are comparable with cam driven systems. In this system, the engine valve opening and closing events can be advanced or retarded without any constraint as well as the final valve lift. Transition from regenerative braking or air motor mode to conventional mode in air hybrid engines can be easily realized using the proposed valvetrain.

The proposed VVA system, as a stand-alone unit, is modeled, designed, prototyped and successfully tested. The mathematical model of the system is verified by the experimental data and used as a numerical test bench for evaluating the performance of the designed control systems. The system test setup is equipped with valve timing and lift controllers and it is tested to measure repeatability, flexibility and control precision of the valve actuation system. For fast and accurate engine valve lift control, a simplified dynamic model of the system (average model) is derived based on the energy and mass conservation principles. A discrete time sliding mode controller is designed based on the system average model and it is implemented and tested on the experimental setup. To improve the energy efficiency and robustness of the proposed valve actuator, the system design parameters are subjected to an optimization using the genetic algorithm method. Finally, an energy recovery system is proposed, designed and tested to reduce the hydraulic valvetrain power consumption.

The presented study is only a small portion of the growing research in this area, and it is hoped that the results obtained here will lead to the realization of a more reliable, repeatable, and flexible engine valve system.

Acknowledgements

I would like to thank my supervisors, Professor Amir Khajepour for all his guidance, support, and constant encouragement during my research.

I would also like to express my gratitude to the examining committee members Professor Ehsan Toyserkani, Professor Naser Lashgarian, and Professor Soo Jeon, whose comments and suggestions were extremely helpful in improving my manuscript. Special thanks to Professor Ridha Ben Mrad, from the University of Toronto, for serving as my external examiner.

Over the last three years, I have been privileged to work with and learn from my colleagues, Babak Ebrahimi, Amir Fazeli, Masoud Ansari, Saman Mohammadi, Alireza Kasaizadeh, Ehsan Parvizi, Saleh Tanabdeh, Mohsen Azimi, Saman Hoseini, and Roozbeh Borjian. Especially, I would like to thank my lovely wife Neda Darivandi, for her endless support, patience, and dedication during past years.

I wish to express thanks to all my family members, Shahrzad Esparham, Bahram Pournazeri, Shaghayegh Pournazeri, and Sam Pournazeri for their constant support and love.

Dedication

For Neda Darivandi, Shahrzad Esparham and Bahram Pournazeri, my lovely wife and parents, whose steadfast support and unconditional love fuelled my drive to the end.

Table of Contents

List of Figures

List of Tables

Nomenclature

A_{HPSV}	HPSV port opening area [m^2]
A_{LPSV}	LPSV port opening area [m^2]
A_{Piston}	Engine piston area [m^2]
C	Hydraulic cylinder viscose coefficient [Ns/m]
C_d	Rotary valves port discharge coefficient
C_p	Exhaust gas specific heat at constant pressure [kJ/kg.K]
C_v	Exhaust gas specific heat at constant volume [kJ/kg.K]
$C_{v,bleed}$	Bleed valve flow coefficient
d	Distance between spool edge and port center in rotary spool valve [mm]
D_{tube}	Hydraulic tube diameter [m]
e	Engine valve lift tracking error [m]
$EHVVA$	Elecro-hydraulic variable valve actuation
$F_{friction}$	Coulomb friction force [N]
$F_{preload}$	Engine valve return-spring preload [N]
F_{gas}	Engine cylinder gas force [N]
h_{cyl}	Enthalpy of the exhaust gas inside the engine cylinder [kJ/kgK]
$HPSV$	High pressure rotary spool valve
K	Engine valve return-spring stiffness [N/m]
k	engine cycle
k	Isentropic gas coefficient (C_p/C_v)
K_{spring}	Valve return-spring stiffness [N/m]
K_{fb}	Feedback control law gain
l	Rotary spool valve port length [m]
l_{Rod}	Engine piston rod length [m]
L_f	Engine valve lift [m]
$L_{f,ref}$	Reference engine valve lift [m]
$LPSV$	Low pressure rotary pool valve
L_{tube}	Hydraulic tube length [m]

m	Engine valve moving mass [kg]
m_{cyl}	Exhaust gas mass trapped in the cylinder [kg]
$\dot{m}_{ex}$	Exhaust gas mass mass flowrate through the valve [kg/s]
n	Gas polytropic coefficient
N_{engine}	Engine speed [rpm]
N_{pump}	Hydraulic pump speed [rpm]
$P_{cyl,0}$	Cylinder pressure at the beginning of the exhaust stage [pa]
P_{in}	Upstream pressure [pa]
P_{HP}	High pressure hydraulic source [pa]
P_{LP}	Low pressure hydraulic source [pa]
P_{out}	Downstream pressure [pa]
P_O	Exhaust manifold pressure [pa]
$P_{reservoir}$	Oil reservoir pressure [pa]
P_1	Air accumulator pressure [pa]
$P_{1,0}$	Precharge air accumulator pressure [pa]
P_2	Hydraulic cylinder pressure [pa]
Q_{bleed}	Flow through the bleed valve [m^3/s]
Q_{HPSV}	Flow through HPSV [m^3/s]
Q_{LPSV}	Flow through LPSV [m^3/s]
$Q_{leakage}$	leakage flow [m^3/s]
Q_{pump}	Pump flowrate [m^3/s]
r_c	Rotary spool valve casing radius [m]
r_{cs}	Crankshaft radius [m]
r_{pe}	Pump to engine speed ratio
r_s	Rotary spool valve spool radius [m]
r_{valve}	Engine Valve Radius [m]
R	Gas constant [kJ/kg.K]
R_b	Cam base diameter [m]
Re	Reynolds number
S	sliding mode
t	time [s]
T	Engine cycle period [s]

$T_{cyl,0}$	Engine cylinder gas temperature at the beginning of the exhaust stage [K]
u_{eq}	Equivalent control law
u_{fb}	Feedback control law
$V_{cyl,0}$	Engine cylinder dead volume [m^3]
V_{disp}	Pump displacement volume [m^3/rev]
VVA	Variable valve actuation
VVT	Variable valve Timing
V_1	Air accumulator gas volume [m^3]
$V_{1,0}$	Precharge air accumulator gas volume [m^3]
V_2	Hydraulic cylinder volume [m^3]
x	Egine valve displacement [m]
β	Hydraulic fluid bulk modulus [pa]
ε	Hydraulic tube surface roughness
$\eta_{volumetric}$	Pump volumetric efficiency
θ	Spool angular position [rad]
θ_{CA}	Crankshaft angle [deg]
$\theta_{opening}$	Engine valve opening angle [CA°]
$\theta_{closing}$	Engine valve closing angle [CA°]
μ	Oil dynamic viscosity [pa.s]
ρ	Oil density [kg/m^3]
φ	Rotary spool valve port angle [rad]
ω	spool angular velocity [rad/s]

Chapter 1

Introduction

In this chapter, the scope and motivation behind this research are discussed. Complexity and control issues involved in current cam-based and camless valvetrains are addressed followed by an outline of the contributions of this thesis.

1.1 Motivation for Flexible Engine Valvetrain

Valvetrain systems, in automotive engine applications, have been mainly designed to accurately control the admission and rejection of intake and exhaust gases to the cylinder within each cycle. Throughout the decades of engine development, the conventional cam-follower mechanisms have been the primary means of engine valve actuation. In this system, the engine valves open and close with a fixed lift and timings. Although this design provides reliable and accurate valve operation during various speed ranges, the engine cannot be operated at its most efficient performance over wide range of speed and load [1]. Because the dynamic behavior of gas flow in a cylinder varies over different operating conditions, fixed valve timing is always a compromised setting for a given design goal. Hence, some desirable performance characteristics such as minimum emission or fuel consumption are sacrificed for other requirements such as maximum power and torque [2].

Varying the engine valve event duration, timing and lift is a well-known method of improving the engine performance, lowering the exhaust emission and therefore has been the object of considerable amount of researches since 1880 [3]. Many studies have shown that optimizing the engine valve timing at all engine loads and speeds significantly improves engine efficiency, power, torque, smoothness and cleanness. A minimum engine efficiency improvement of about 15% over typical driving cycles has been observed using variable valve timing systems and a potential of up to 20% improvement has been estimated [4].

Some of the advantages of applying flexible engine valve actuation technology in different types of engines are as follows:

- Gasoline Engines
    - Reduction in pumping losses by wide open throttle (WOT) through controlling the intake valve opening duration [5],
    - Improvement in brake mean effective pressure (BMEP) throughout the speed range by controlling intake valve closing (IVC).
- Diesel Engines
    - Cylinder deactivation,
    - Engine torque improvement,
    - Turbocharger efficiency improvement by optimizing intake valve closing and exhaust valve opening timings [6],
    - NOx emission reduction by internal exhaust gas recirculation (iEGR) [7],
    - Improvement in catalyst efficiency by influencing the temperature,
    - Reduction of particulate matters (PMs) by optimizing intake charging.
- Air Hybrid Engine
    - Realizing three modes of operation including regenerative braking, air motor and conventional combustion modes [8].

To date, several variable engine valve actuation system (VVA) have been proposed. These system are either cam-based or cam-less. Limited degrees of control freedom are allowed by cam-based VVAs while significantly complex as well as heavy and expensive mechanical systems have to be adopted [10]. On the other hand, camless valvetrains offer unlimited and programmable flexibility of engine valve motion owing to the use of engine independent actuators; however, sophisticated control systems are required in order for the camless valvetrain to operate properly. Low reliability, poor repeatability, high engine valve seating

velocity and high power consumption are other significant factors affecting the applicability of these systems in production engines.

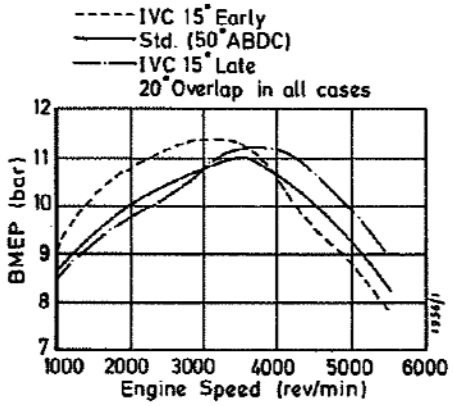

Figure 1-1: Effect of IVC on BMEP in 2 liter gasoline engine [9]

1.2 OBJECTIVES

In this research, following goals are pursued:

- Proposing a new variable valve actuation system with the following capabilities:
    - Valve opening and closing timings can be varied independently from 0 to 720CA° at any engine speed,
    - 100CA° change in valve timing can be completed within one engine cycle [11],
    - Maximum engine valve timing variability maintains below 5CA°,
    - Final engine valve lift can be varied continuously from 0mm (valve deactivation) to minimum 10mm at any engine speed from 600 to 6000rpm,
    - Maximum valve lift variability of 1mm is maintained at all transient operating conditions and engine cycle to cycle variations,
    - The valve actuation system should be able to continue operating during any failure in electric power or electric components (fail safe),
    - The valve seating velocity is maintained close to 100mm.s^{-1} [12], [13].

- Prototype design, fabrication, instrumentation and testing for a single engine valve actuation,
- Controller design, implementation and testing,
- System optimization to lower the power consumption to be comparable with conventional cam-follower mechanism (~2.2kW for 16 valve engine at 5000rpm engine speed).

1.3 Overview and Contribution of the Dissertation

This dissertation addresses a novel hydraulic variable valve actuation system developed, modeled and tested in Chapter 3 and Chapter 4. The proposed system can change the engine valve opening /closing timings from 0 to 720CA^{o} independently and it can change the valve lift from 0 to 10mm even at 6000rpm engine speed. One of the advantages of this system is that it is fail-safe mechanism in the event of failure in the electrical components. A control system is proposed in Chapter 5 for valve timing control. Although the proposed control system is much simpler than those used in camless valvetrain, it can change the valve timing by 100CA^{o} within only one engine cycle.

A new engine valve lift control strategy is developed in Chapter 6 based on the average model of the system. A non-linear discrete sliding-mode controller is designed based on the system average model and its stability is proved. As it will be shown, the proposed lift control strategy can be applied in any electro-hydraulic camless valvetrain. In most of the current electro-hydraulic camless valvetrain, the desired valve lift is achieved by accurate control of the closing instant of the high pressure solenoid valve; however, due to slow solenoid actuator response, precise control of these devices becomes difficult and sometimes impracticable during high engine speeds. In contrast to current lift control methods, in the proposed lift control technique, the desired valve lift is obtained by controlling the supply pressure. This reduces the problems caused by limited solenoid actuator response and results in more accurate and robust control.

In Chapter 7, the power consumption and robustness of the proposed engine valve system is studied numerically. An optimization problem is set up to maximize the system power efficiency while maintaining its robustness. A new formulation is proposed for objective function and constraints calculations. The optimization problem is solved using the genetic algorithm. The proposed optimization structure can be generalized to any hydraulic variable valve actuation system. An energy recovery system is designed and implemented to eliminate the tradeoff between the system power consumption and its robustness. Using this system it is possible to restore a portion of the energy consumed to compress the engine valve return spring during engine valve rise interval. The proposed energy recovery system is also applicable in electro-hydraulic valvetrains with single acting hydraulic cylinder whose valve closure is performed with the aid of the return spring.

Chapter 2

Literature Review

2.1 Conventional Valvetrains

Poppet valves are used in combustion engines to open and close intake and exhaust ports located in the engine cylinder head. These valves usually consist of a flat disk with a tapered edge rigidly connected to a long rod at one end, called a valve stem (shank). The valve stem is used to push down or pull up the valve against the tapered seat during opening and closing stages. The retaining spring is usually used to close the valve when the stem is not being pushed on. In valvetrain system, the valve is raised from its seat by pushing the stem using a cam-follower mechanism. The cam profile and its location with respect to the cam follower determine the valve translational motion as well as its opening and closing timings (Appendix A). In the conventional designs, the camshaft is placed relatively close to the crankshaft and the translational motion from the cam follower is transferred to the valve stem through pushrods or rocker arms. This mechanism is very common in the V-type engines and allows for the actuation of the valves of both cylinder banks using a common camshaft.

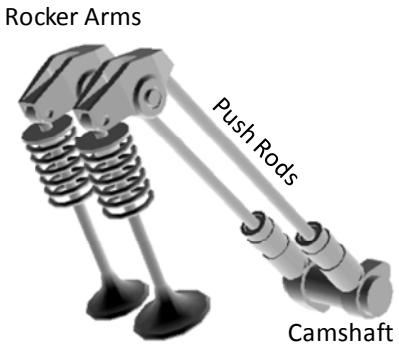

Figure 2-1: Push-rod mechanism [14]

However, this design leads to considerable energy losses in the engine. In modern engines, the camshaft is located on the top of the cylinder head and the valve stem is pushed directly

by the cam follower. This design is called overhead camshaft. In this design, if there is only one camshaft on the top of the cylinder head, the system is called single overhead camshaft (SOHC), and if there are two camshafts, one for intake and one for exhaust, the system is called double overhead camshaft (DOHC).

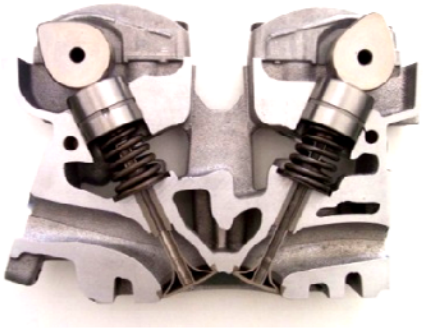

Figure 2-2: Double Overhead Cam System [15]

The cams are usually fixed on the camshaft and rotate with the same speed as the camshaft. The camshaft obtains its rotary motion from the engine crankshaft using an intermediate mechanism such as chain, gear or belt. The camshaft speed is half the crankshaft speed in 4-stroke engines and equal to that in 2-stroke engines.

In addition to zero flexibility of the cam-follower valvetrains, another drawback of the cam-driven valvetrains is that the minimum possible engine valve opening angle (β) is limited due to the cam profile limitations. In a cam with flat faced follower (Figure 2-3), a negative radius of curvature on the cam cannot be accommodated [16] and this limits the minimum cam rise or fall angle ($\beta/2$) for a specific cam size. The following correlation is used to determine the minimum engine valve opening angle (β) using cam-follower mechanism:

$$\beta = 2Cos^{-1}\left(\frac{R_b}{R_b + L_f}\right) \tag{2.1}$$

where, L_f is engine valve lift and R_b is cam base radius.

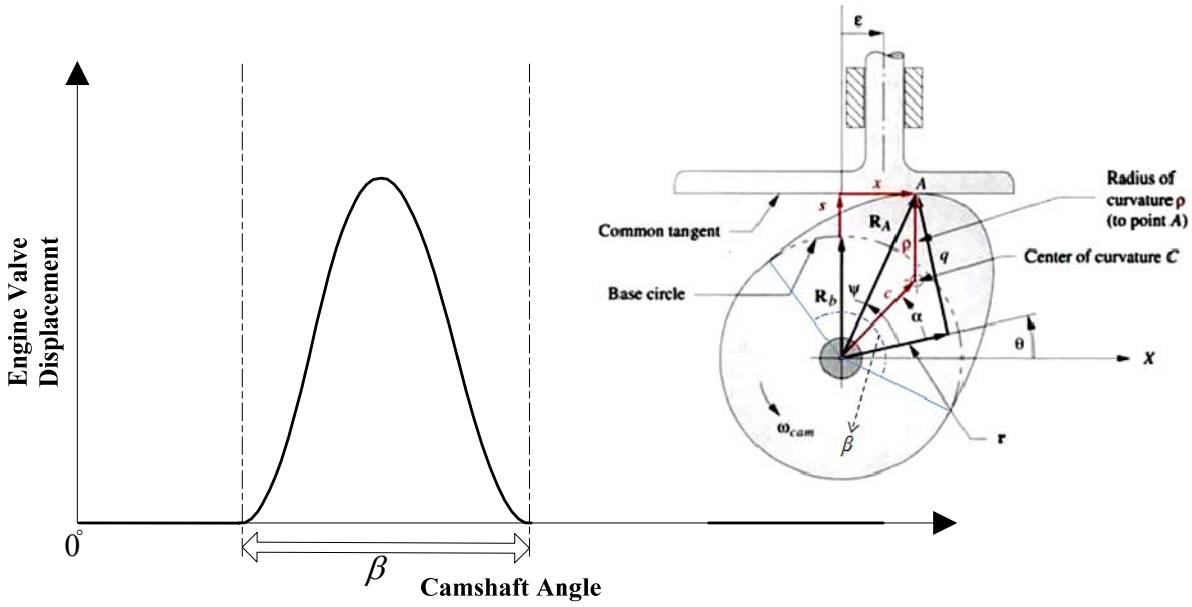

Figure 2-3: Cam with Flat Faced Follower [16]

As shown in Figure 2-4, in order to reduce the valve rise/fall interval, the ratio of the engine valve lift to base circle radius must decrease. On the other hand, decreasing this ratio with a constant valve lift, will lead to an increase in radius of the cam base-circle which is not always feasible due to space limitation.

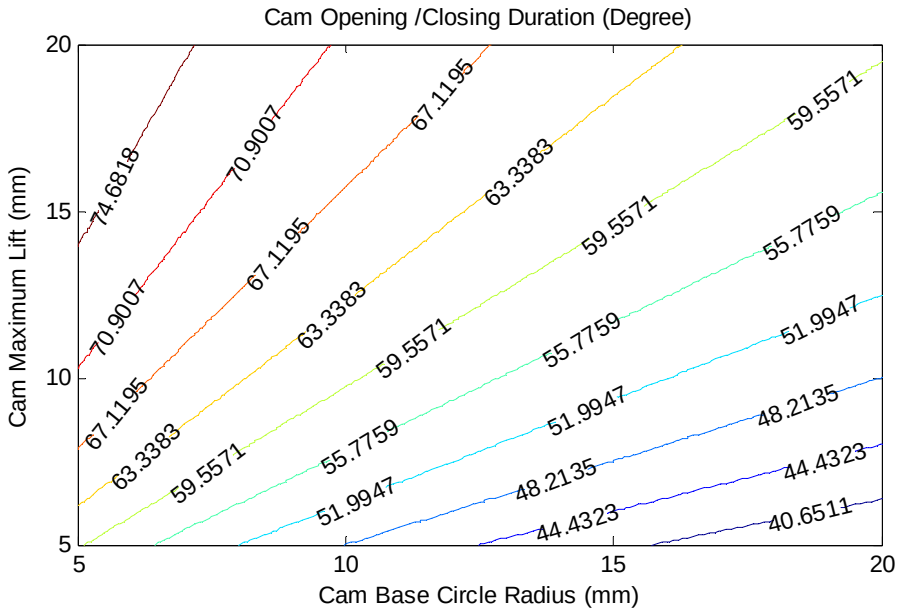

Figure 2-4: Minimum required rise/fall angle (β/2) for flat-faced cam-follower mechanism

2.2 VARIABLE VALVE ACTUATION (VVA) TECHNOLOGY

Recently due to the stringent environmental regulations, improvement in fuel economy and reduction in the exhaust gas emissions have become the two major challenges in the automotive section. To fulfill the requirements of these regulations, the internal combustion engines have experienced significant improvements during the past decades. Incorporating the flexible valvetrains in production engines is one of the several ways to improve the performance of the internal combustion engines. For several years, the engine camshaft has been the primary solution for valve actuation and timing. In the cam-follower valvetrain, engine valves open and close with the fixed lift and timing. Although these systems offer a reliable and accurate valve operation, the engine cannot be operated efficiently over a wide range of engine operation [1].

One of the major disadvantages of the conventional spark ignition (SI) engines is energy loss through the inhaling of sub-atmospheric gases at the intake process and the expelling of exhaust gases at the exhaust stage. These losses are referred to as pumping losses. In conventional SI engines, the engine load and speed are controlled by positioning the throttle valve from fully open to fully closed. In these engines, the pumping losses are very dependent on the position of the throttle valve and are inversely proportional to the engine load. Thus, the pumping losses increase significantly during low engine load operation, which increases fuel consumption and exhaust emissions. However, a throttle-less control of airflow in direct injection engines and air-fuel mixture in indirect injection engines can be realized through variation of the valve-opening period [17] and also valve lift. In addition, exhaust gas recirculation (EGR) can be controlled by adjusting the intake and exhaust valve overlap to improve the engine performance and reduce oxides of nitrogen (NOx) emission. Thus, variable valve timing systems have the capability to reduce pumping losses and exhaust emissions and consequently improve the overall efficiency of SI engines by about 7~10% [6] [18].

Many studies have shown that significant improvement in power density, volumetric efficiency, emission and fuel consumption could be achieved by variable valve actuation

systems (VVA). The ever-increasing number of production engines using different types of VVAs is an evidence for this fact [12]. Hundreds of patents and implementation of prototype systems have been already proposed for VVA systems; however only few types with less flexibility have entered into production stage and the rest have been remained at the research level.

2.3 EXISTING VVA SYSTEMS

In general, VVA systems are divided into two main categories: camless and cam-based valvetrains. In the camless systems, there is no mechanical connection between the engine crankshaft and the valvetrain. High level of flexibility in valve timing and valve lift is the main advantage of these systems over cam-based valvetrains. Electro-mechanical, electro-hydraulic and electro-pneumatic valvetrains are all in this category. Although these systems are the most flexible valve actuation systems, some concerns including high cost, low reliability (i.e. not being fail-safe), high power consumption (>2.2kW for 16 valve engine at 5000 rpm engine speed), high seating velocity (>100mm.s^{-1}) and control complexity (requires ultra fast actuator with response time of less than 3 ms) prevent these systems from being incorporated into the production engines.

In contrast to camless valvetrains, the cam-based VVA systems are mechanically linked to the engine crankshaft. Due to their high reliability, durability, repeatability and robustness, many of these systems have been already designed and implemented in production engines. Limited flexibility and high mechanism complexity are the major disadvantage of the cam-based valvetrains compared with the existing camless systems.

2.3.1 Cam-based VVA Systems

Nowadays, Cam-based VVA systems are widely used by engine manufacturers due to their higher reliability, durability and control simplicity. One of the main advantages of cam-based systems is that their operating speed is synchronized by the crankshaft and thus there is no limitation in their working speed. Because valve motion is controlled by the cam and the follower mechanism, the valve seating velocity is laid within an acceptable range.

2.3.1.1 Cam Phaser

Cam phaser is a standard mechanism for valve timing. By using this mechanism, it is possible to change the cam angular position relative to the crankshaft and consequently shift the valve opening and closing events simultaneously. However, using this mechanism, the total engine valve opening duration and lift remain constant. Cam phasers are categorized into oil actuated, helical gear drives, differential drives, chain drives, worm gear drives and planetary gear drives [19].

2.3.1.2 Cam Profile Switching

Cam Profile Switching (CPS) is another technique introduced by Honda to vary valve timing, duration and lift simultaneously. In this technique, the valve motion is switched between two different sets of cam lobs. During low engine speed operation, the cam with low lift profile is engaged with the valve stem, while at high engine speed operation, the cam with high lift profile is engaged. The shift from one cam to another is realized by either an electric or hydraulic system. In this system, the cams profiles are compromised settings for the desired objectives during two engine speed ranges.

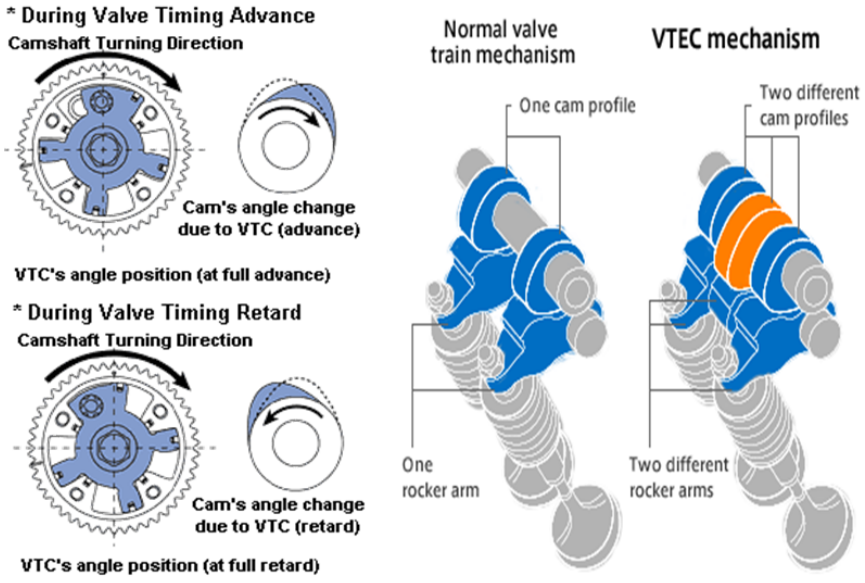

Figure 2-5: Hydraulic cam phaser (left figure) and cam profile switching (right figure) mechanisms [20], [21]

2.3.1.3 Three-dimensional Cam Mechanism

One of the problems of cam profile switching is that the valve motion is switched only between two specific cam profiles. However, the use of a three-dimensional cam design allows the engine to continuously change the valve timing, lift and duration over a wide range of engine operating conditions. In this mechanism, the cam profile continuously varies along the cam axis, and the axial movement of the camshaft with respect to follower brings a different profile of the cam into engagement with the follower, prompting a change in valve opening profile. A combination of three-dimensional cam mechanism and cam phaser has been also implemented by Nagaya et al. to control both valve timing and valve lift independently [22].

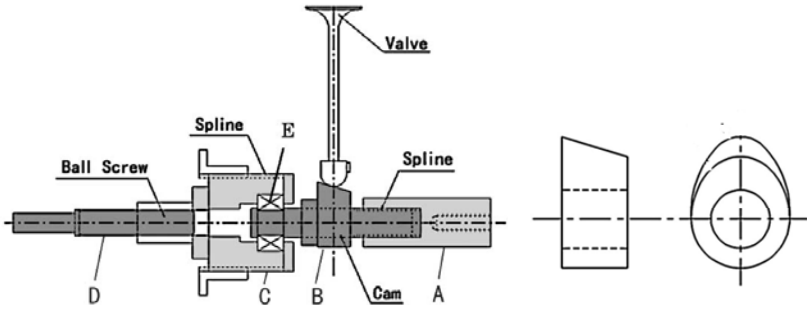

Figure 2-6: Three-dimensional cam mechanism with ball follower [22]

2.3.1.4 Electro-Hydraulic Lost Motion VVTs

In this mechanism, the cam motion is transmitted via a cam-follower to the reciprocating hydraulic pump. Oil is then pumped into a high pressure hydraulic line, connected to the valve actuator, and a normally open two-way solenoid valve.

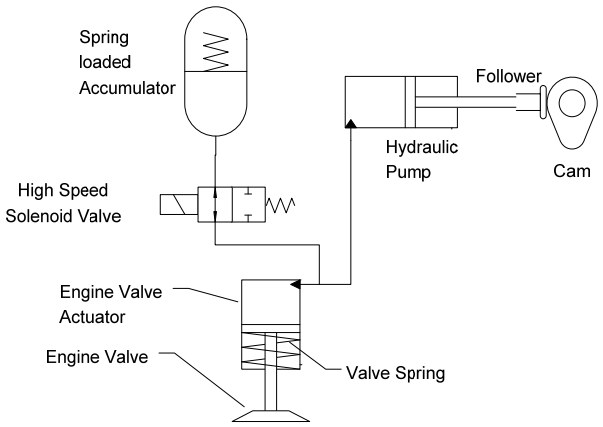

Figure 2-7: Electro-hydraulic VVT system based on the "lost motion" principle [23]

When the solenoid valve is closed, the engine valve follows exactly the cam motion. However, when the solenoid valve is opened, the oil is directed into the lower pressure accumulator instead of the hydraulic cylinder and consequently, the engine valve is closed earlier. Fiat has recently implemented this principle to control the valve opening and closing timings as well as valve opening duration [23], while Hyundai, Jacobs Vehicle System and IVECO have already implemented this technology in their engines [24], [25], [26]. Engine valve lift dependency to valve opening duration and also limitation in solenoid response time are the two major drawbacks of this system.

2.3.1.5 Other Cam-based VVTs

In addition to the above mechanisms, many other complex designs have been proposed and implemented by several automotive manufacturers. "Valvetronic" by BMW, "Valvematic" by Toyota and two cam mechanism by Meta Motorten [27] are some examples of these systems.

2.3.2 Camless Systems

Although cam-based designs have been successfully implemented by several car manufacturers, due to their limitations and high dependency on engine speed, there is still a tremendous interest in developing a more flexible valve system. Thus, many researches are now focusing on improving camless systems. Aside from the laboratory use, history shows that the idea of the camless engine originated as early as 1899 [28].

2.3.2.1 Electro-Mechanical Actuation System

Electromagnetic valve actuators generally consist of two magnets and two balanced springs. The moving parts of the electromagnetic valve are connected to the engine valve. When both magnets are off, the armature is held in the intermediate position between the coils by balanced springs [29].

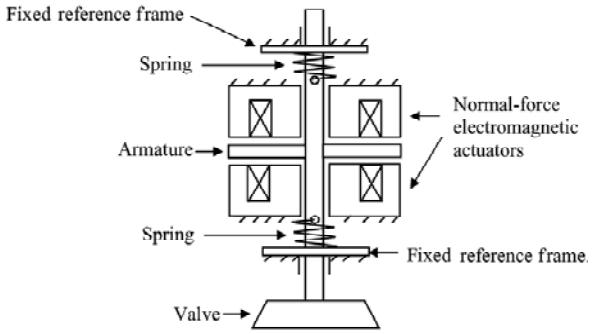

Figure 2-8: Camless electro-mechanical valve system [29]

At engine start-up, the upper electromagnet is activated and it pulls up and holds the armature, and the potential energy is stored in the retaining springs [29]. To open the valve, the upper electromagnet is deactivated and the stored energy is released and converted into kinetic energy which carries the armature toward the lower magnet. At a distance of less than one millimeter from the lower magnet, the moving part is captured and held. During the valve closing stage, similar events are repeated. Due to high non-linearity in magnetic force characteristics, there are several difficulties preventing this technology from being commercially implemented [30]. These difficulties include:

- High landing velocity (>0.5 m/sec at 1500 rpm)
- High transition time (>3.5 msec)
- Higher power losses than conventional cam drive system
- Requirements for robust feedback control
- High sensitivity to in-cylinder gas pressure

2.3.2.2 Electro-hydraulic Variable Valve Actuation (EHVVA) System

As shown in Figure 2-9, the basic electro-hydraulic camless valvetrain consists of a hydraulic cylinder, two solenoid valves and two check valves. In this design, the solenoids and the check valves control the submission and rejection of the high pressure oil into and out of the hydraulic cylinder during valve operation. Using an additional oil path, a constant force is always applied to the bottom of the piston, and when the high pressure oil is removed from the piston top, the valve returns to its seated position. By controlling the solenoid valves timing and opening duration, it is possible to precisely control the valve timing, duration, and lift. By activating the high pressure solenoid valve (HPSV), the high pressure oil is admitted into the hydraulic cylinder. The opening period of this HPSV determines the amount of oil submitted into the cylinder chamber and consequently determines the valve lift. By activating the low pressure solenoid valve (LPSV), the oil is discharged from the upper cylinder chamber thanks to the presence of high pressure oil at the lower chamber. The LPSV opening duration determines how far the valve moves in its closing descent.

Similar to electro-mechanical valve systems, a closed loop electronic control is required to reduce valve seating velocity, transition time, and cyclic variability [31]. One of the problems of this VVT system is servo valve response time. Due to solenoid coil inductance and non-linear force to displacement relation, the solenoid maximum operating frequency is reduced and, as a result, the system shows poor performance during high engine speeds.

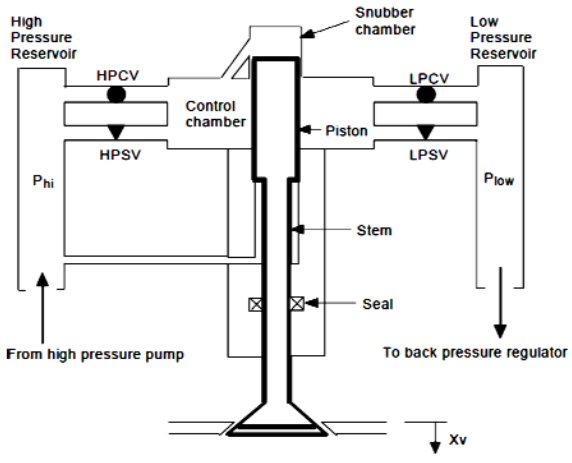

Figure 2-9: Basic electro-hydraulic valvetrain [31]

As shown in Figure 2-10, the required valve actuation time reduces significantly as engine speed increases, and consequently the minimum valve opening angle becomes limited. For example, at an engine speed of 6000 rpm and a total opening angle of 100 degrees, the total time available for the actuation process is about 3ms, which almost exceeds the speed of the high bandwidth solenoid valves which are currently on the market. This causes the electro-hydraulic valve manufacturers to use either a double-stage mechanism (i.e., two pilot valves) or employ ultra high frequency actuators such as piezoelectric.

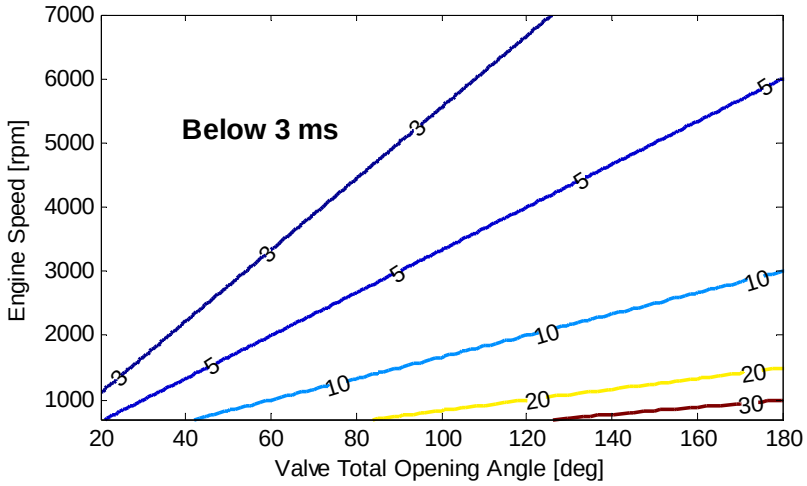

Figure 2-10: Total valve actuation duration (ms) at different engine speeds and opening angles

Lotus and Sturman have already introduced their camless electro-hydraulic valvetrains to the industry [32], [12], [33]. In the electro-hydraulic VVA system, the major part of the system cost is for high speed servo-valves which control the oil flow to and from the hydraulic cylinder. To solve this problem, Lotus Engineering has developed a design that not only achieves a similar level of flexibility but also costs much less. In this design, a high speed servo valve is split into a digital three-way valve and two proportional valves. The digital three-way valve directs hydraulic fluid either from a high pressure source toward the hydraulic cylinder or from the hydraulic cylinder to the reservoir. However, the two-way proportional valves control the valve timing, valve lift/fall duration, valve lift and valve velocity [12].

To increase the system bandwidth, Rocheleau et al. [32] have proposed an electro-hydraulic valvetrain in which the solenoid actuators are replaced with piezoelectric stacks (Figure 2-11). The proposed system is capable of having maximum valve lift of 12.4 mm and bandwidth frequency of up to 500 Hz. In this mechanism, an electric signal sent from a control system causes a piezoelectric stack to expand. This linear expansion is transferred to the spool valve via a solid hinge mechanism. The reason for using this mechanism is to overcome the displacement limitations in the piezoelectric stacks while maintaining its efficiency and operating frequency. Using this mechanism, the movements of the stacks can be amplified from 30μm to 150μm, which is sufficient for spool valve actuation.

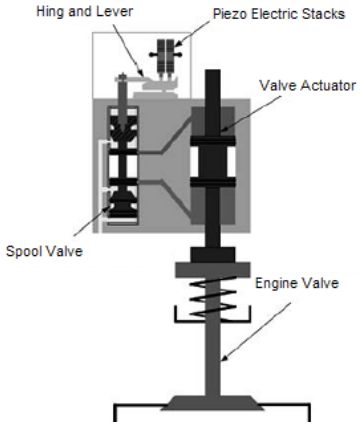

Figure 2-11: Piezoelectrically controlled actuator for a camless engine [32]

2.3.2.3 Electro-pneumatic Variable Valve Actuation System

In addition to electro-hydraulic and electro-mechanical valvetrains, Cargine has proposed an electro-pneumatic variable valve actuation system (EPVVA) [34], [35], [36].The combination of hydraulic and pneumatic mechanisms allows the system to extract maximum work from the air flow and thus it can function under low air pressure. To reduce the energy consumption and also control valve seating velocity, a hydraulic latch was also employed in this system. This mechanism is capable of controlling valve lift, valve timing, and opening duration as desired by the engine.

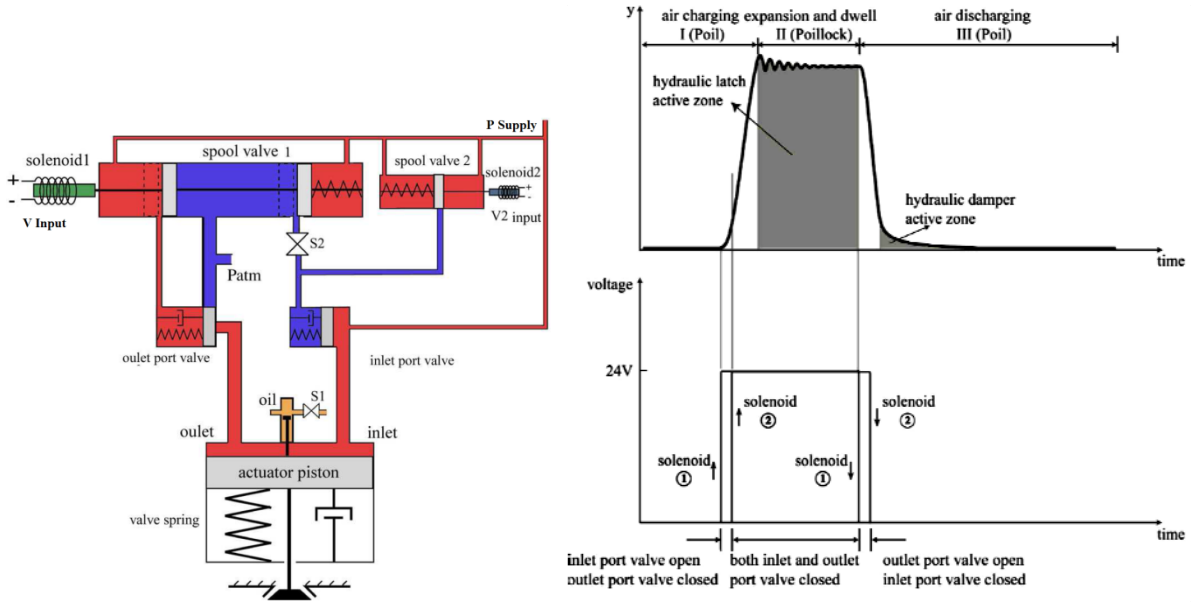

Figure 2-12: Electronically controlled pneumatic hydraulic valve [34]

One of the main problems of this system is its high dependency on the in-cylinder gas pressure. Due to low working pressure of this system compared to hydraulic systems and gas compressibility, the valve opening and closing are highly affected by the engine in-cylinder pressure. Thus, having pre-knowledge of the cylinder pressure and also solenoid response time is necessary to predict the exact timing of solenoid activation or deactivation. For this reason, a model-based predictive control was implemented by Ma et al. to estimate the solenoid activation timing for the desired engine valve trajectory [37]. Aside from the above difficulty, the solenoids response time also limits the system's bandwidth.

Chapter 3

A New Variable Valve Actuation System

In this chapter, a new hydraulic variable valve actuation (VVA) system is proposed and designed. In this system, each engine valve is actuated with a hydraulic cylinder which is charged and discharged using two rotary spool valves. The rotary spool valves are rotated by the engine crankshaft while their phases are controlled by hydraulic or electric phase shifters. Similar to camless valvetrains, the new engine valve system is capable of flexible engine valve timings (0 -720CAº) and lift (0-10mm) at any engine speed (600-6000rpm) without drawbacks of existing camless valvetrains including high control complexity, low reliability and slow actuator response (5.5 ms for 8mm lift [38]). The mathematical model of the system is derived based on Newton's second law and fluid mechanics equations.

3.1 Proposed VVA System Configuration

Figure 3-1 illustrates the diagram of the proposed VVA system for a single engine valve. As shown in this figure, the system consists of two rotary spool valves, two differential phase shifters and a single-acting spring-return hydraulic cylinder for each engine valve. The engine valve is connected to the piston of the hydraulic cylinder. The two rotary spool valves including high pressure rotary spool valve (HPSV) and low pressure rotary spool valve (LPSV) are responsible for charging and discharging the hydraulic cylinder. These spool valves obtain their rotary motion from the engine crankshaft and their speeds are half of the engine speed in four-stroke engines. Although the velocities of the spool valves are proportional to the engine speed, their phases could be independently altered by two differential phase shifters. These phase shifters are either electric or hydraulic types and they could flexibly change the angular position of the output shaft (spool shaft) with respect to its original position without changing the input/output speed ratio. As shown in Figure 3-2, each rotary spool valve consists of a rotary spool and a stationary casing each of which has an

opening area. The spool valve casing interior cavity is connected to a high or low pressure hydraulic source. The casing port connects the hydraulic cylinder to the spool valve inner chamber when it is lined up with the spool port (slot).

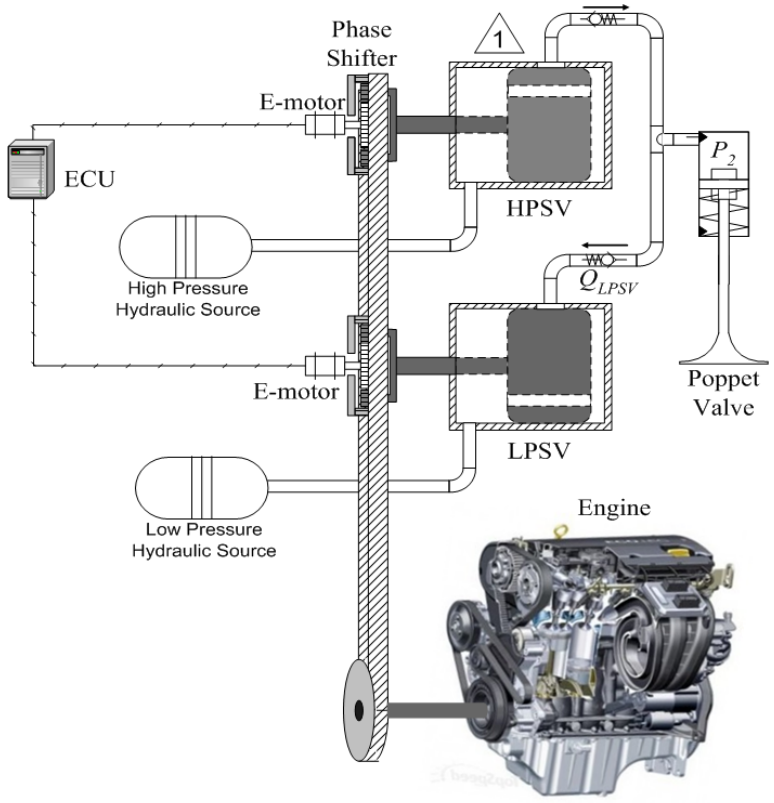

Figure 3-1: Schematic drawing of the proposed VVA system for single-valve actuation

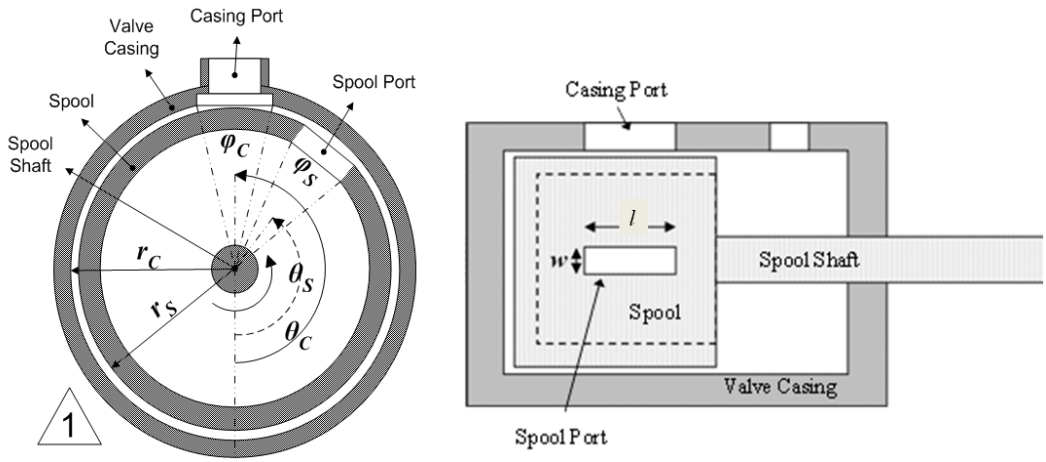

Figure 3-2: The proposed rotary spool valve construction

Using the proposed VVA system, the engine valve operation in every engine cycle is divided into four stages (Figure 3-3): opening, stay open, closing and stay closed.

(a) Opening: when the spool slot of the high pressure spool valve (HPSV) is lined up with the casing port, the high pressure hydraulic fluid from the high pressure hydraulic source flows into the hydraulic cylinder pushing the piston down resulting the valve starts to open. The valve opening interval continues until the overlap area between the spool slot and the casing port of HPSV becomes zero. At this stage, the final engine valve lift depends on the HPSV opening interval and the hydraulic fluid supply pressure.

(b) Stay Open: After the high pressure rotary spool valve is closed, the oil is trapped in the hydraulic cylinder chamber and the engine valve stays open until the low pressure rotary spool valve (LPSV) is opened.

(c) Closing: when the spool port of the LPSV is lined up with the casing port, the trapped oil in the hydraulic cylinder flows into the low pressure hydraulic source and the engine valve starts to close thanks to the return-spring force. The engine valve closing interval ends upon the low pressure rotary spool valve is closed. Hence, the spring force should be high enough for full engine valve closure. The hydraulic cylinder is also equipped with a hydraulic cushion to avoid high contact velocity.

(d) Stay Closed: After the low pressure spool valve is closed, the engine valve remains closed until the HPSV is opened again.

Since the rotating velocities of rotary spool valves are half of the engine speed, they open and close only once in every engine cycle. Hence, the engine valve operating frequency is passively controlled by the engine speed; however, the opening and closing timings along with opening duration could be actively controlled by phase shifting the rotary spool valves. A similar method is used for the LPSV to flexibly control the engine valve closing event and consequently control the total opening duration. The engine valve opening and closing times remain constant when the phase shifters are idle.

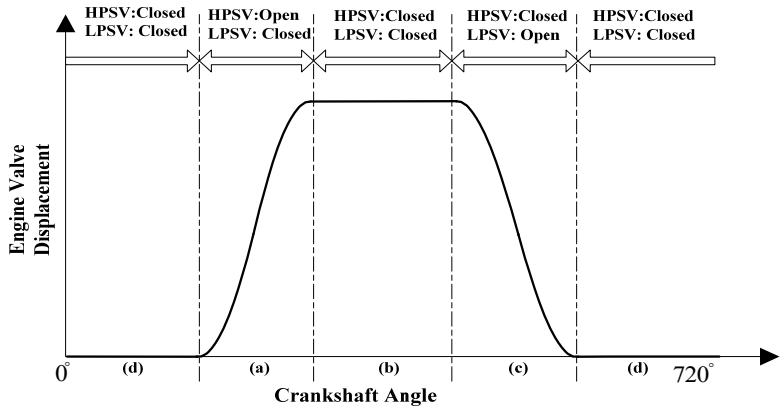

Figure 3-3: The status of the high and low pressure rotary spool valves at different engine valve operating intervals

3.2 SYSTEM PROS AND CONS

The proposed system advantages with respect to existing cam-based and camless systems are as follows:

- 0-720CAº flexibility in valve opening/closing timings at any operating condition
- Continuous valve lift variation (zero to maximum allowable valve lift) independent of the valve timing
- No need to any solenoid actuator or servo valve
- Less expensive and simple components
- Complete fail-safe system (system continues operating with fixed timings and lift during electric power or any electric component failure)

The main system disadvantage with respect to camless valvetrains is that multiple engine valve opening within an engine cycle is not possible; however, multiple valve opening is not usually required in the conventional IC engines and may be only needed in air hybrid engines.

3.3 MATHEMATICAL MODEL

In the following, the governing equations of each component shown in Figure 3-1 are derived and assembled into a system of algebraic differential equations. Most of the equations given in this section are discussed in detail in Appendix B .

Hydraulic Cylinder:

The governing equations for the hydraulic cylinder include piston's equation of motion and hydraulic fluid pressure gradient. Using the Newton's 2nd law, the piston equation of motion is:

$$m\ddot{x} = -Kx - F_{preload} - sign(\dot{x})F_{friction} - F_{gas} + A_p P_2 \tag{3.1}$$

where, x, m, K, A_p, P_2, $F_{friction}$, $F_{preload}$ and F_{gas} are piston displacement (engine valve displacement), total moving mass (piston, shaft, valve, transducer and etc.), spring stiffness, piston area, hydraulic cylinder pressure, friction, spring preload and the engine cylinder gas force respectively.

During the exhaust stage, the amount of engine cylinder gas force on the exhaust valve is considerably high. As the exhaust valve opens, the combustion gas is discharged from the engine cylinder and consequently the cylinder pressure reduces. Hence, the intensity of gas force imposed on the poppet valve varies during valve opening interval. To estimate the amount of in-cylinder gas force on the exhaust valve, the engine cylinder pressure is modeled mathematically.

Figure 3-4 illustrates the schematic drawing of the engine cylinder with a single exhaust valve. In this figure m_{Cyl}, P_{Cyl} and T_{Cyl} are the mass, pressure and temperature of the exhaust gas, respectively. A_{Piston} is the piston area and x and y are the exhaust valve and engine piston displacements respectively. In this figure, P_O and T_O are exhaust manifold pressure and temperature.

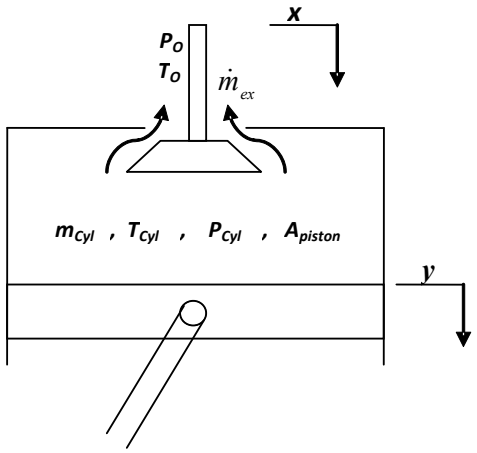

Figure 3-4: In-cylinder pressure model

The mass flow rate of the exhaust gas through the engine cylinder valves is determined by [39]:

$$\dot{m}_{ex} = \frac{-dm_{Cyl}}{dt} = C_m P_{Cyl} A_{ex} \sqrt{\frac{1}{T_{Cyl}}} \tag{3.2}$$

where A_{ex} is the gas flow area and is determined by:

$$A_{ex} = 2\pi r_{valve} x \tag{3.3}$$

In (3.2), the gas flow coefficient C_m is calculated as follows:

$$C_m = \begin{cases} \sqrt{\dfrac{2k}{R(k-1)}} \left(\dfrac{2}{k+1}\right)^{\frac{1}{k-1}} & \dfrac{P_{cyl}}{P_O} \geq \left(\dfrac{k+1}{2}\right)^{\frac{k}{k-1}} \\ \sqrt{\dfrac{2k}{R(k-1)} \left[\left(\dfrac{P_O}{P_{Cyl}}\right)^{\frac{2}{k}} - \left(\dfrac{P_O}{P_{Cyl}}\right)^{\frac{k+1}{k}} \right]} & else \end{cases} \tag{3.4}$$

where, $k = \dfrac{C_p}{C_v}$ and $R = C_p - C_v$. Using ideal gas law, the engine cylinder pressure is determined by:

$$P_{Cyl} = \frac{m_{Cyl} R T_{Cyl}}{V_{Cyl}} \tag{3.5}$$

where,

$$V_{Cyl} = A_{Piston} y + V_{Cyl,0} \tag{3.6}$$

In the above equation, y is the piston displacement which is calculated by:

$$y = r_{CS} + l_{Rod} - r_{CS}\cos\left(\theta_{CS}\right) - \sqrt{{l_{Rod}}^2 - r_{CS}^2 \sin^2\left(\theta_{CS}\right)} \tag{3.7}$$

where, r_{CS}, l_{Rod} and θ_{CS} are crank radius (half stroke), piston rod length and crank angle respectively. During exhaust stage, the engine cylinder gas temperature varies as the pressure reduces. First law of thermodynamics is used to determine the cylinder gas temperature:

$$\frac{dU_{Cyl}}{dt} = -\dot{m}_{ex} h_{Cyl} + \frac{dQ}{dt} - \frac{dW}{dt} \tag{3.8}$$

where, W is the piston work and is determined by:

$$\frac{dW}{dt} = P_{cyl}\frac{dV_{Cyl}}{dt} = P_{Cyl} A_{piston} \dot{y} \tag{3.9}$$

The piston velocity $\dot{y}$ is calculated by:

$$\dot{y} = \frac{dy}{dt} = r_{CS}\dot{\theta}_{CS}\sin\left(\theta_{CS}\right) + r_{CS}^2 \dot{\theta}_{CS}\sin\left(\theta_{CS}\right)\cos\left(\theta_{CS}\right)\left({l_{Rod}}^2 - r_{CS}^2\sin^2\left(\theta_{CS}\right)\right)^{-\frac{1}{2}} \tag{3.10}$$

The rate of change of the internal energy of the cylinder gas is determined by:

$$\frac{dU_{Cyl}}{dt} = \frac{d}{dt}\left(m_{Cyl} u_{Cyl}\right) = u_{Cyl}\frac{dm_{Cyl}}{dt} + m_{Cyl}\frac{du_{Cyl}}{dt} = m_{Cyl}\frac{du_{Cyl}}{dt} - u_{Cyl}\dot{m}_{ex} \tag{3.11}$$

Using cold-air standard assumption, the rate of change of the internal energy and enthalpy is approximated by:

$$\frac{du_{Cyl}}{dt} = C_v \frac{dT_{Cyl}}{dt} \tag{3.12}$$

$$\frac{dh_{Cyl}}{dt} = C_p \frac{dT_{Cyl}}{dt} \tag{3.13}$$

Therefore, the rate of change of the combustion gas temperature during exhaust stage is calculated by:

$$\frac{dT_{Cyl}}{dt} = \frac{1}{m_{Cyl}C_v}\left(u_{Cyl}\dot{m}_{ex} - \dot{m}_{ex}h_{Cyl} + \frac{dQ}{dt} - P_{Cyl}A_{piston}\dot{y}\right) \tag{3.14}$$

In the above equation, the heat transfer through the cylinder and piston bodies can be neglected during the exhaust stage.

In (3.1), the friction force *($F_{friction}$)* of the hydraulic piston and cylinder is modeled as a transition from stiction friction to coulomb friction force. At the sealing, the coulomb friction can be 2 or 3 times lower than the stiction friction. To avoid any discontinuity in the friction model, the stiction friction is modeled as a force which varies linearly with the change in relative displacement ($F_{Stiction} = \alpha x$) until the specified maximum stiction friction is reached.

When the piston displacement exceeds the specified threshold, the friction force becomes coulomb friction. To prevent instantaneous transition from stiction force to dynamic force, it is possible to consider the dynamic friction as a function of relative velocity, maximum stiction force and dynamic friction. This effect is known as Stribeck effect and can be shown as follows:

$$F_{Dynamic} = F_{Coulomb} + \left(F_{Stiction} - F_{Coulomb}\right)e^{-3|\dot{z}|/\sigma} \tag{3.15}$$

The coulomb friction forces for the piston with o-ring can be determined using the analytical friction model proposed by Al-Ghathian et. al. [40]:

$$F_{Coulomb} = 2\pi\,\mu\,D\,r\,E\left(1 - \frac{D-d}{4r}\right)\sqrt{1 - \frac{\left(D-d\right)^2}{16r^2}} \tag{3.16}$$

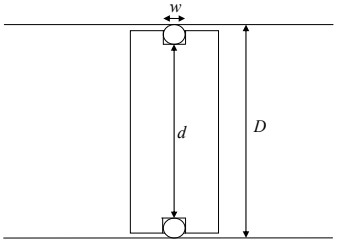

Figure 3-5: Dimension of the o-ring between hydraulic piston and cylinder

where μ is the coulomb friction coefficient, D is the cylinder inner diameter, d is the groove diameter, r is o-ring radius and E is the o-ring material Young modulus.

The pressure gradient in the hydraulic cylinder is calculated based on [41]:

$$\frac{dP_2}{dt} = \frac{\beta}{V_{2,0} + A_p x}\left(Q_{HPSV} - Q_{LPSV} - A_p \dot{x}\right) \tag{3.17}$$

where, β, $V_{2,0}$, Q_{HPSV} and Q_{LPSV} are hydraulic fluid bulk modulus, hydraulic cylinder dead volume and flowrate through the high/low pressure rotary spool valves. The hydraulic fluid bulk modulus β is calculated by:

$$\beta = K_{\beta,1}\left(1 + \frac{\left(K_{\beta,2} - 1\right)P_2}{K_{\beta,1}}\right)\left(1 + \frac{K_{\beta,2}P_2}{K_{\beta,1}}\right) \tag{3.18}$$

where, $K_{\beta,1}$ and $K_{\beta,2}$ are fluid bulk modulus properties (for mineral oil at 40ºC, $K_{\beta,1}$=17000bar , $K_{\beta,2}$=5.6). For the hydraulic fluid, $K_{\beta,2}$ is practically constant at all temperatures while the value of $K_{\beta,1}$ carries a temperature dependency with it [41].

In (3.17), in case of existence of air inside of the hydraulic fluid in the form of bubbles, foam and dissolved air, the oil bulk modulus β must be replaced with the equivalent bulk modulus (β_e) which is determined by [41]:

$$\frac{1}{\beta_e} = \frac{1}{\beta} + \left(\frac{V_a}{V_{2,0} + A_p x}\right)\frac{1}{\beta_a} \tag{3.19}$$

In the above equation, β_a and V_a are air bulk modulus and air volume respectively. Assuming adiabatic air compression and expansion processes, the air bulk modulus is determined by [41]:

$$\frac{1}{\beta_a} = \frac{1}{P_2 k} \tag{3.20}$$

where, k is the ratio of the air constant pressure specific heat to the constant volume specific heat (k~1.4). Assuming air as ideal gas, V_a is determined by the following equation:

$$V_a = \left(\frac{P_{atm}}{P_2}\right)^{\frac{1}{k}} V_{a,atm} \tag{3.21}$$

Where, $V_{a,atm}$ is the volume of the air at atmospheric pressure (P_{atm}). Substituting (3.21) and (3.20) in (3.19), the effective bulk modulus will be estimated by:

$$\frac{1}{\beta_e} = \frac{1}{\beta} + \left(\frac{V_{a,atm}}{V_{2,0} + A_p x} \right) \frac{P_{atm}^{\frac{1}{k}}}{k P_2^{\frac{k+1}{k}}} \tag{3.22}$$

Figure 3-6 shows the amount of engine lubrication oil aeration at different engine speed [42]. As shown in this figure, the maximum air to oil volumetric ratio at atmospheric pressure is about 18%; however, the oil aeration level in the hydraulic systems is much less than this value due to their limited oil-air stirring and splashing intensity.

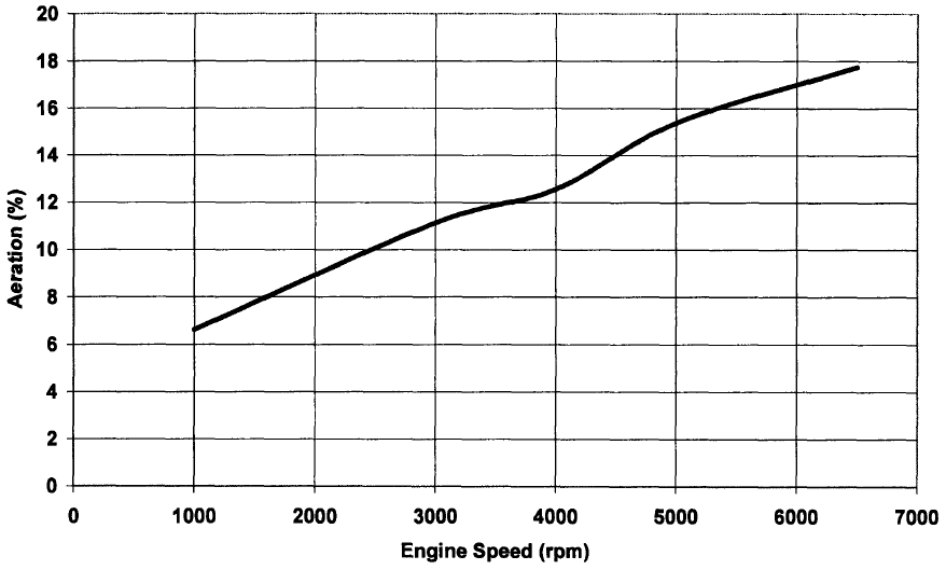

Figure 3-6: The level of oil aeration at different engine speeds [42]

Figure 3-7 illustrates the effect of pressure and air/liquid volume ratio on the effective bulk modulus. As shown in this figure, at higher pressures, the effect of trapped air on the final bulk modulus become low; however, this effect increases quadratically as the pressure reduces.

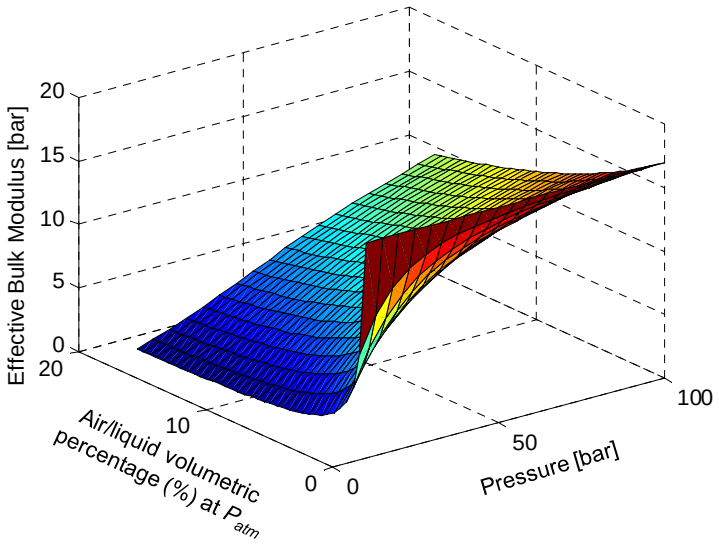

Figure 3-7: Effect of pressure and air/liquid volume percentage on effective bulk modulus

High/low Pressure Rotary Spool Valves (HPSV, LPSV):

As mentioned before, the rotary spool valves are responsible for opening and closing the flow connections between the hydraulic cylinder and high/low pressure hydraulic sources. In these rotary spool valves, at each time instant, the flow opening area (A_{SV}) can be determined based on the spool and casing port sizes (φ , l, r_s), geometries and angular positions (θ_s , θ_c). In this work, it is assumed that the spool and casing ports are both axial slots with length of l and opening angles of φ_s and φ_c respectively (Figure 3-1). Hence, the flow opening area A_{SV} can be written as:

$$A_{SV} = \begin{cases} 0 & \theta_s < \left(\theta_c - \dfrac{\varphi_c + \varphi_s}{2}\right) \\ lr_s \min\left(\varphi_s, \theta_s - \theta_c + \dfrac{\varphi_s + \varphi_c}{2}\right) & \left(\theta_c + \dfrac{\varphi_c - \varphi_s}{2}\right) > \theta_s > \left(\theta_c - \dfrac{\varphi_c + \varphi_s}{2}\right) \\ lr_s \min\left(\varphi_c, \theta_c - \theta_s + \dfrac{\varphi_s + \varphi_c}{2}\right) & \left(\theta_c + \dfrac{\varphi_c + \varphi_s}{2}\right) > \theta_s > \left(\theta_c + \dfrac{\varphi_c - \varphi_s}{2}\right) \\ 0 & \theta_s > \left(\theta_c + \dfrac{\varphi_c + \varphi_s}{2}\right) \end{cases} \quad (3.23)$$

where,

$$\begin{cases} \dot{\theta}_c = 0 \\ \dot{\theta}_s = N_{engine} / 2 \end{cases} \tag{3.24}$$

Based on the calculated opening flow areas, an orifice model is used to determine the flow rates through the rotary spool valves (Q_{HPSV} and Q_{LPSV}):

$$Q_{HPSV} = \begin{cases} A_{HPSV} C_d \sqrt{2\left(P_{HPSV,in} - P_{HPSV,out}\right)/\rho} & P_{HPSV,in1} > P_{HPSV,out} \text{ and } A_{HPSV} \neq 0 \\ Q_{HPSV,leakage} & P_{HPSV,in1} > P_{HPSV,out} \text{ and } A_{HPSV} = 0 \\ 0 & else \end{cases} \tag{3.25}$$

$$Q_{LPSV} = \begin{cases} A_{LPSV} C_d \sqrt{2\left(P_{LPSV,in} - P_{LPSV,out}\right)/\rho} & P_{LPSV,in} > P_{LPSV,out} \text{ and } A_{LPSV} \neq 0 \\ Q_{LPSV,leakage} & P_{LPSV,in} > P_{LPSV,out} \text{ and } A_{LPSV} = 0 \\ 0 & else \end{cases} \tag{3.26}$$

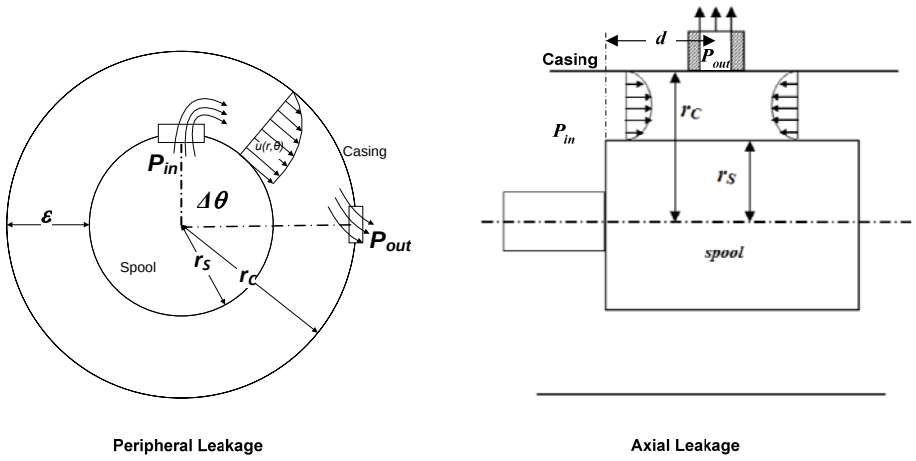

Figure 3-8: Axial and peripheral leakage in rotary spool valves

where, $Q_{HPSV,leakage}$, $Q_{LPSV,leakage}$ and ρ are the leakage flowrates in high pressure and low pressure rotary spool valves and oil density respectively. The effect of pressure on the oil density can be determined by:

$$\frac{\Delta\rho}{\rho} = \exp\left(\frac{\Delta P}{\beta}\right) - 1 \tag{3.27}$$

Based on (3.27), as the oil pressure increases by 100 bar, the oil density will only change by 0.5%.

In fact, due to the clearance exists between the spool outer surface and the casing inner surface, the hydraulic fluid can flow from the high pressure side to the low pressure side either axially or peripherally (Figure 3-8):

$$Q_{leakage} = Q_{leakage,axial} + Q_{leakage,peripheral} \tag{3.28}$$

Using the governing equations of motion for low-Reynolds-number flows [41], following equations have been derived (Appendix B.7 and Appendix B.8) to calculate the amount of axial and peripheral leakage flowrates in the proposed rotary spool valves:

$$\begin{aligned} Q_{leakage,axial} = \left(r_S + r_C\right)\varphi_c \Big(\left(r_C^3 - r_S^3\right)\left(P_{out} - P_{in}\right)\mu^{-1}d^{-1} / 12 + \\ C_{1,axial}\left(r_C\left(\ln r_C - 1\right) - r_S\left(\ln r_S - 1\right)\right) + C_{2,axial}\left(r_C - r_S\right)\Big) \end{aligned} \tag{3.29}$$

$$\begin{aligned} C_{1,axial} &= -\frac{\left(r_C{}^2 - r_S{}^2\right)\left(P_{out} - P_{in}\right)}{4\mu d\left(\ln r_C - \ln r_S\right)} \\ C_{2,axial} &= -\frac{r_C{}^2\left(P_{out} - P_{in}\right)}{4d\mu} - C_1 \ln r_C \end{aligned} \tag{3.30}$$

$$\begin{aligned} Q_{leakage,peripheral} = l\Big(0.5\left(r_c{}^2 - r_s{}^2\right)\left(P_{out} - P_{in}\right)\mu^{-1}\Delta\theta^{-1} \\ + C_{1,peripheral}\left(r_c\ln\left(r_c - 1\right) - r_s\ln\left(r_s - 1\right)\right) + C_{2,peripheral}\left(r_c - r_s\right)\Big) \end{aligned} \tag{3.31}$$

$$\begin{aligned} C_{1,peripheral} &= -\frac{r_s\dot{\theta}_s\mu\Delta\theta + \left(r_c - r_s\right)\left(P_{out} - P_{in}\right)}{\mu\Delta\theta\left(\ln r_c - \ln r_s\right)} \\ C_{2,peripheral} &= \frac{-r_c}{\mu}\frac{\left(P_{out} - P_{in}\right)}{\Delta\theta} - C_1 \ln r_c \end{aligned} \tag{3.32}$$

where, μ and $\dot{\theta}_s$ are hydraulic fluid viscosity and spool angular velocity. Other parameters such as d and $\Delta\theta$ are defined in Figure 3-8. In each rotary spool valve, P_{in} and P_{out} are determined as follows:

$$\left(P_{in}, P_{out}\right) = \begin{cases} \left(P_{HPSV,in}, P_{HPSV,out}\right) & \text{in } HPSV \\ \left(P_{LPSV,in}, P_{LPSV,out}\right) & \text{in } LPSV \end{cases} \tag{3.33}$$

Hydraulic Transmission Lines:

In the developed mathematical model of the proposed VVA system, the effect of pressure waves inside the hydraulic transmission lines are ignored to reduce the model complexity; however, due to the small hydraulic tubes flow area and high fluid velocity, the effect of pressure losses are considerable and could not be neglected. The amount of the pressure drop in the fluid transmission lines is a function of both tube geometry and flow Reynolds number and can be determined by [41]:

$$P_{tube,in} - P_{tube,out} = 8f\left(\mathrm{Re}, \frac{\varepsilon}{D_{tube}}\right)\rho\frac{Q^2 L_{tube}}{\pi^2 D_{tube}^5} \tag{3.34}$$

where, f is obtained from the Moody diagram. Therefore, $P_{HPSV,in}$, $P_{HPSV,out}$, $P_{LPSV,in}$, $P_{LPSV,out}$, P_1, P_2 and P_{atm} can be correlated to each other using Equation(3.34).

3.4 NUMERICAL STUDIES

For preliminary investigation of the proposed VVA system performance and requirements, the system is simulated in Matlab/Simulink software using the developed mathematical model. Due to nature of the hydraulic systems, the governing differential equations of these systems contain both very rapidly changing states such as pressure and flow rate and also very slowly changing states such as engine valve displacement. This causes a wide range of time scales present in the solution of these sets of equations and makes these problems computationally intensive. This type of problems is called stiff problem and requires a stiff solver with dynamic time steps. To this end, the Matlab solver “ode15s” is used to simulate the dynamic system.

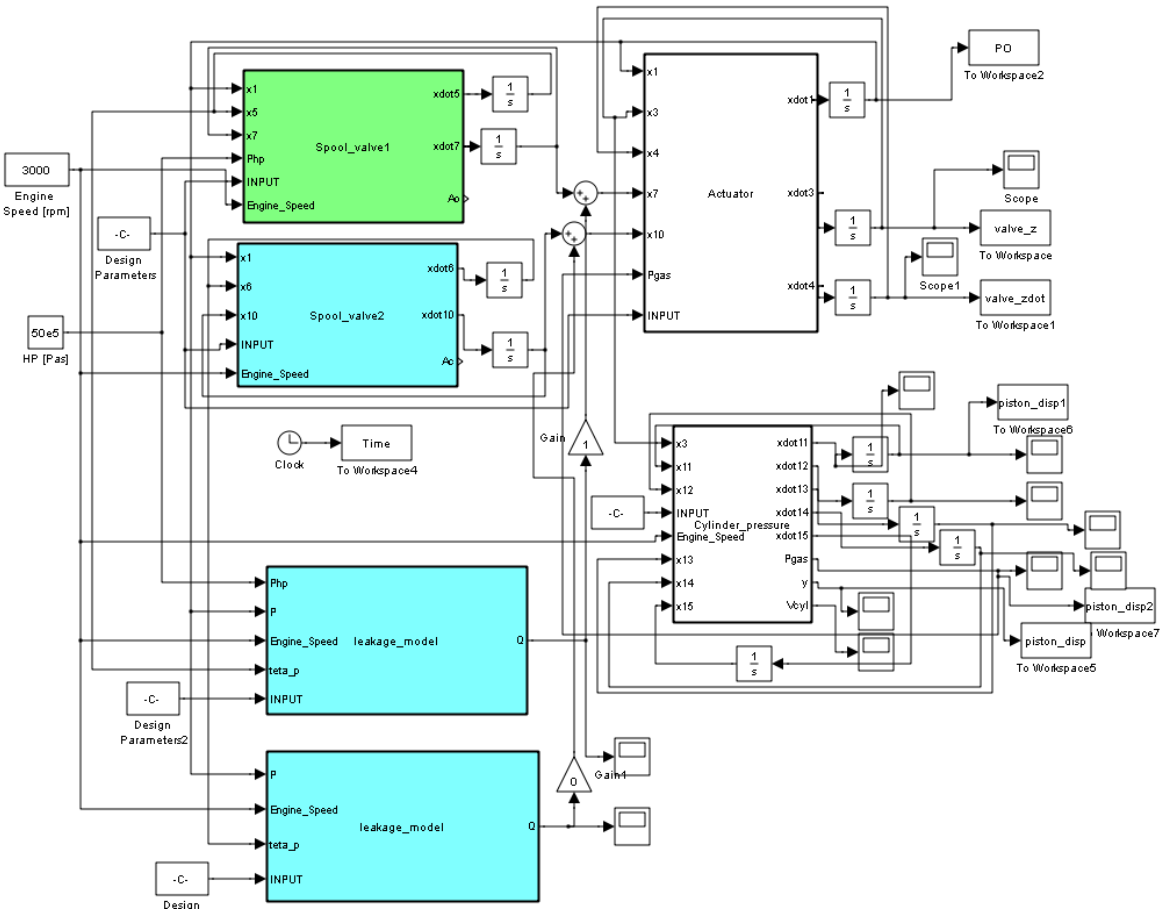

Figure 3-9: The Simulink model of the proposed variable valve actuation system

The simulation is initially run using arbitrary values for the model parameters which are fine tuned after several iterations. Some of the model parameters such as valve actuator moving mass (m), friction ($F_{friction}$) and rotary spool valves flow coefficient (C_d) which are design dependent are presumed as known values in the simulation. Table 3-1 shows the final values selected for the system parameters.

Table 3-1: Tuned Model parameters

K [N/m]	$F_{preload}$ [N]	A_P [mm^2]	l [mm]
60000	400	198.8	8
$V_{2,0}$ [cc]	μ [N.s/m^2]	m [g]	$F_{friction}$ [N]
10	0.051	100	50
φ_c [deg]	φ_s [deg]	r_s [mm]	r_c [mm]
25	25	14.98	15.02
β [bar]	d [mm]	C_d	ρ [kg/m^3]
17000	18	0.5	850

Figure 3-10 illustrates the functionality of the proposed engine valve actuation system at 2000rpm engine speed. The first dotted line on the left shows the high pressure rotary spool valve flow area with respect to engine crankshaft angle while the right one is for the low pressure spool valve. As shown in this figure, there is a time delay in the engine valve opening instant and this is the due to the time required for the hydraulic cylinder pressure to build up. Although the HPSV total open duration is 100CAº, the engine valve opening interval is less than 75CAº. This is due to the equilibrium reached between hydraulic cylinder and supply pressures which depends on the system parameters including hydraulic piston diameter, return spring stiffness and preload. As the engine speed increases, the difference between engine valve opening interval and HPSV open duration decreases due to system dynamics and at some point the HPSV closes before the pressure equilibrium is reached.

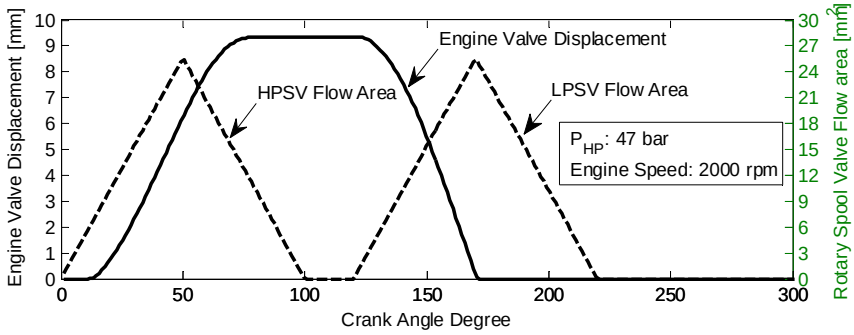

Figure 3-10: Engine valve displacement with respect to rotary spool valves ports opening area

The engine valve starts to close as soon as the LPSV opens. The engine valve closing interval continues until the engine valve returns to its seat. As shown in Figure 3-10, for the current system configuration, at 2000rpm engine speed, the engine valve lands on its seat 50CAº before the LPSV is fully closed. As the engine speed increases, the difference between the engine valve and LPSV closing instants reduces; however, care must be taken to choose system design parameters such that full engine valve closure is guaranteed at maximum engine speed. As the distance between the HPSV and LPSV open intervals (left and right dotted lines in Figure 3-10) changes, the total engine valve opening duration varies (Figure 3-11). However, as show in Figure 3-11, if the difference between LPSV and HPSV opening

times becomes lower than the engine valve rise time, the valve starts to close before it reaches to it final lift.

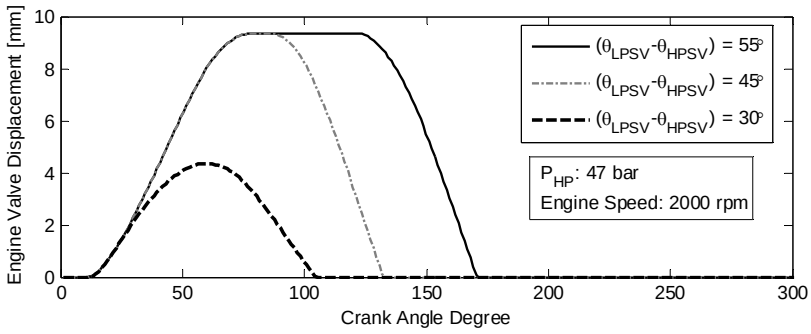

Figure 3-11: Effect of variations in the low and high pressure spool valves phase difference on engine valve total opening duration

Figure 3-12 shows the constant engine valve lift contours for a range of supply pressure and engine speed. As mentioned before, for a constant supply pressure, increase in the engine speed reduces the difference between the engine valve rise time and HPSV opening interval and above a certain engine speed, this difference becomes zero and the engine valve lift starts to decrease. This phenomenon is clearly observed in Figure 3-12. As shown in this figure, in order to have a constant valve lift at wide range of engine speeds, the supply pressure must be changed in a controlled manner.

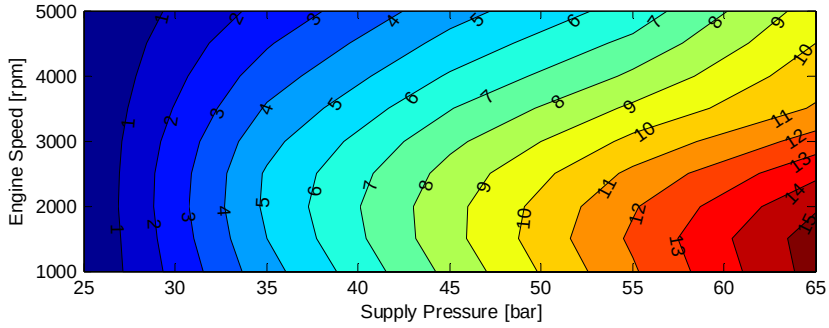

Figure 3-12: Final engine valve lift at various engine speed and hydraulic supply pressure (P_{HP})

The constant valve lift contours varies as the system parameters change. Figure 3-13 shows the effect of change in the high pressure spool valve port angle (φ) on the 10mm valve lift contour. As shown in this figure, reduction in the HPSV port angle results in rise in the

amount of supply pressure required for similar valve lift at higher engine speeds; however, this increase in the supply pressure is much severer at the smaller port angles.

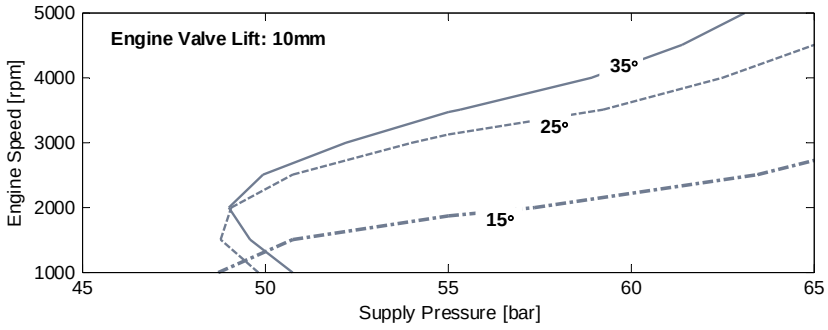

Figure 3-13: Required supply pressure for 10mm valve lift at different HPSV port opening angle (φ_s)

One of the main concerns of the proposed VVA system is the sealing problem in the designed rotary spool valves. In fact, the only sealing technique used in the proposed rotary spool valves is minimizing the clearance between the spool and casing to restrict the oil flow from high pressure to low pressure side when the spool valve is closed. Because the tradeoff exists between the rotary spool valve sealing efficacy and its rotor and casing friction, the maximum allowable radial clearance between the valve rotor and stator guaranteeing the whole VVA system performance must be determined using the numerical model developed for the axial and tangential leakage through the clearance. Figure 3-14 shows the effect of increase in the gap between spool and casing on the leakage flowrate through both HPSV and LPSV and also on the engine valve lift and seating performance. As shown in Figure 3-14c-d, the leakage in both valves increases quadratically as the gap between spool and casing (ε) increases. The leakage through HPSV is low when the engine valve is fully open and it is high during the rest of the cycle. The main disadvantage of leakage through HPSV is unwanted engine valve opening during engine valve close period which is shown in Figure 3-14a for the spool valve with 20mil clearance. In LPSV, the maximum leakage happens during the period when the engine valve is fully open and the hydraulic cylinder pressure is high. The major disadvantage of this leakage is drop in the final engine valve lift as

illustrated in Figure 3-14a. As shown in this figure, the leakage through the rotary spool valves does not affect the engine valve operation for the radial clearances below 4 mils.

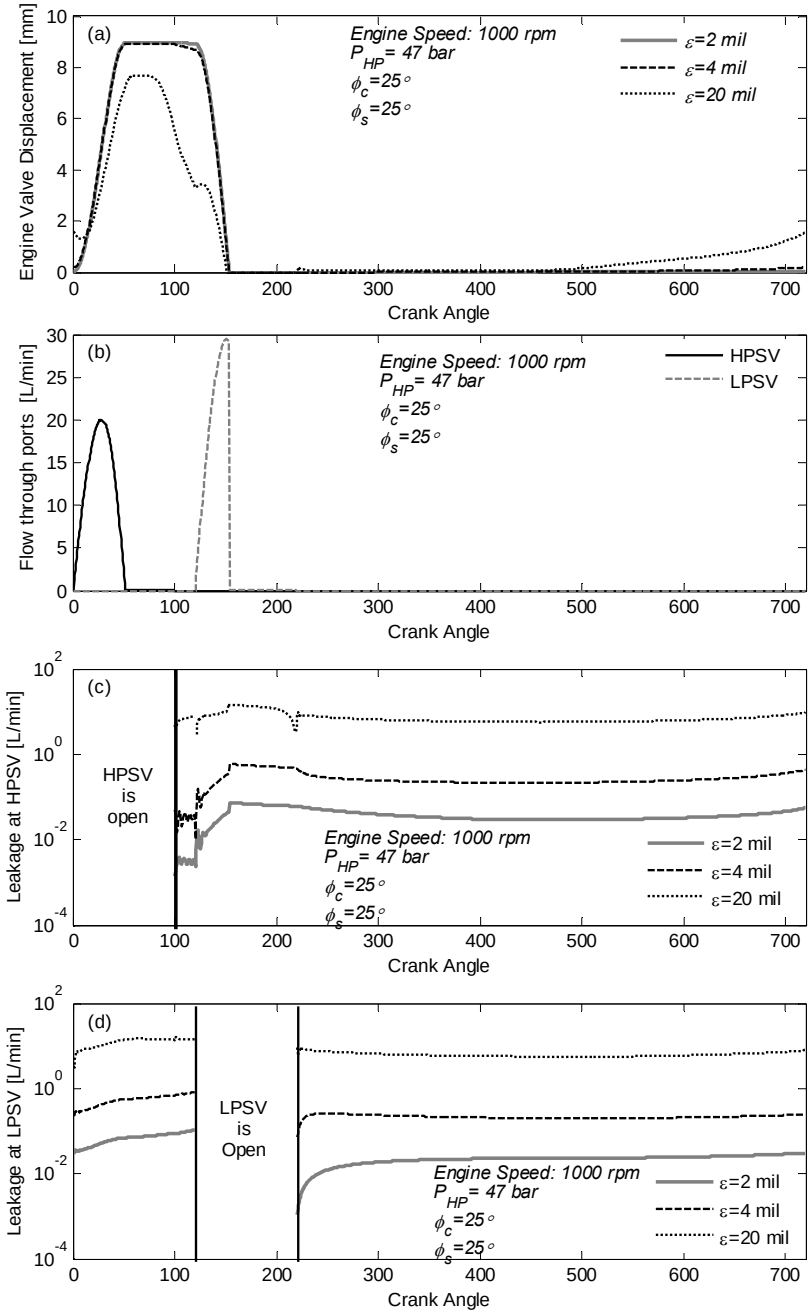

Figure 3-14: Effect of increase in the clearance between rotor and casing of the rotary spool valves (ε) on the leakage flow ($Q_{leakage}$) and consequently on engine valve displacement

Since the engine cycle duration is inversely proportional to the engine speed, the total amount of leakage through one engine cycle decreases as the engine speed increases; however, due to higher supply pressure required for similar engine valve lift at higher engine speed, the instantaneous leakage flowrate may increase. Figure 3-15 shows the total amount of rotary spool valves leakage per engine cycle at different engine speeds and constant engine valve lift. As illustrated in this figure, the effect of leakage is diminished as the engine speed increases.

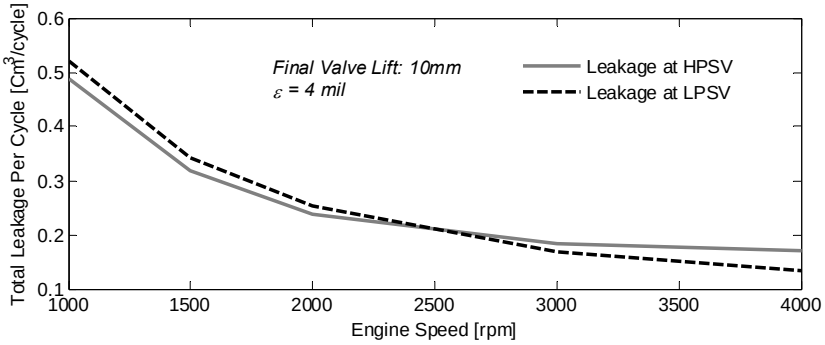

Figure 3-15: Effect of engine speed on the total amount of leakage through the rotary spool valves in one engine cycle

The performances of the hydraulic systems are usually degraded as the amount of trapped air increases. As shown in Figure 3-7, the bulk modulus reduces as the air to liquid volume ratio increases. To study the sensitivity of the proposed VVA system to the amount of the trapped air, the system is run at 4000rpm with 65 bar hydraulic supply pressure and the amount of air to liquid volumetric ratio at atmospheric pressure is changed. As shown in Figure 3-16, increase in the amount of trapped air to oil volumetric ratio from 0 to 18% will affect the valve opening timing by $7CA^{o}$ and lift by 0.53mm.

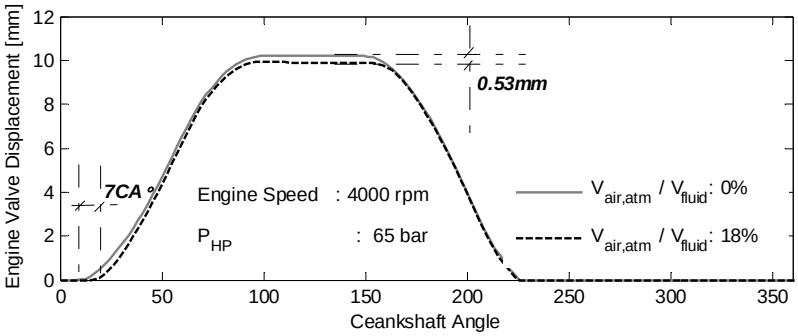

Figure 3-16: Effect of trapped air on engine valve trajectory including timing and lift

One of the important factors in variable valve system is the effects of variability in engine valve timing and lift on cylinder pressure and mass exchange process especially during exhaust stage. This can highly influence the engine fuel penalty and performance due to pumping losses and also incomplete exhaust or intake processes. On the other hand, the engine cylinder gas force on the poppet valve during the exhaust stage can adversely affect the engine valve trajectory. This places a high degree of importance on modeling the engine cylinder pressure and mass exchange process especially during the exhaust stage. For this purpose, the mathematical formulation derived in Section 3.3 is used to study the effects of both exhaust process and exhaust valve on each other. Some of the model parameters including components dimensions, initial conditions and exhaust gas specifications are given in Table 3-2. It is assumed that the cylinder gas has the pressure of 5 bar and temperature of 1000K at the beginning of the exhaust stage and the exhaust manifold has the atmospheric pressure.

Table 3-2: Engine parameters

$T_{Cyl,0}$ [K]	$P_{Cyl,0}$ [bar]	r_{valve} [mm]	r_{cs} [mm]	l_{Rod} [mm]
1000	5	12.5	39.3	169.2
P_O [bar]	A_{piston} [cm^2]	$V_{Cyl,0}$ [cc]	C_p [kJ/kg.K]	C_v [kJ/kg.K]
1.01	64	56	1.0045	0.7175

Figure 3-17 shows the numerical results for the exhaust valve opening trajectory, cylinder pressure and cylinder gas mass during the exhaust stage (540~720CAº). As shown in Figure 3-17c, the cylinder pressure drops to exhaust manifold pressure within a short time (~45CAº) after the exhaust valve opens; however, if the exhaust valve flow area is not sufficient, the

cylinder pressure drops with a slower rate and this increases the piston negative work which consequently reduces the net engine power.

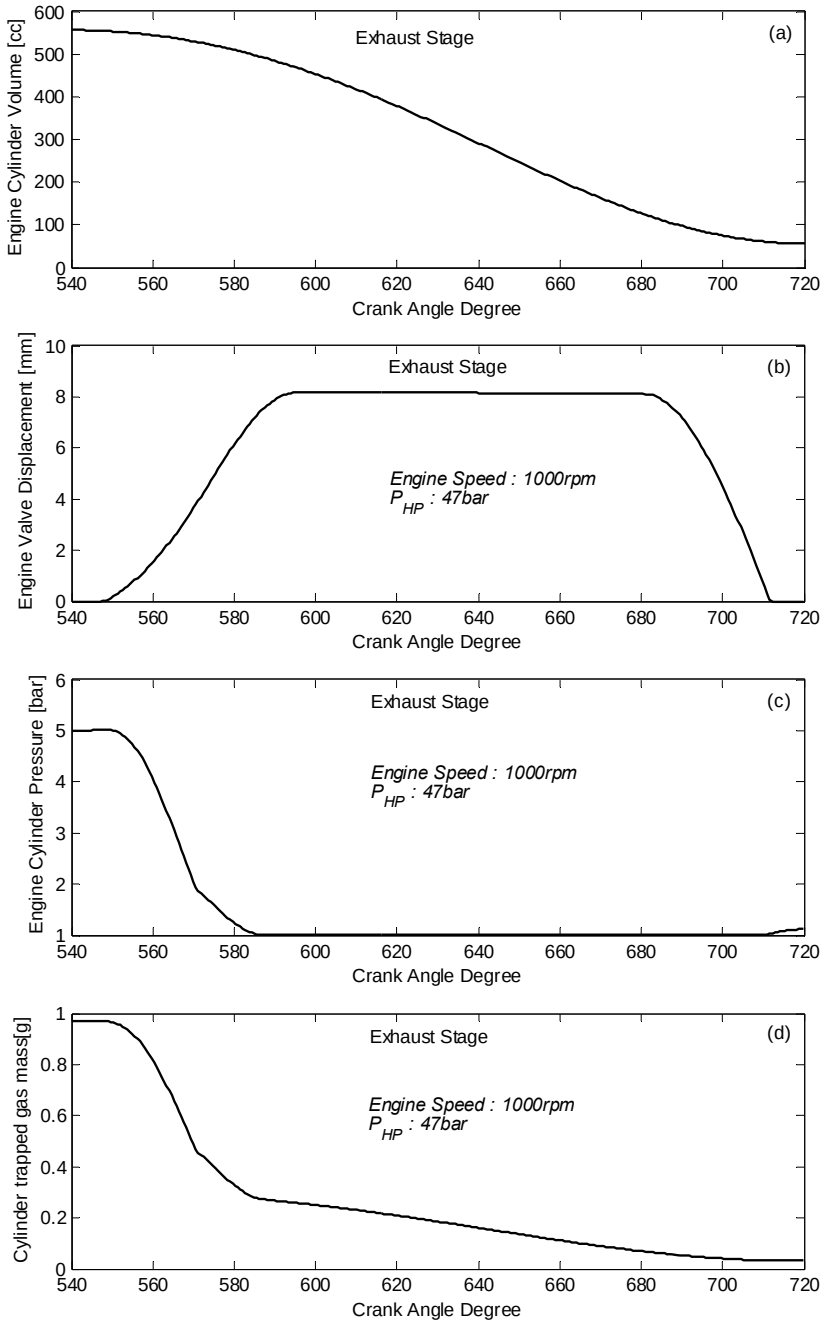

Figure 3-17: In-cylinder pressure and exhaust mass during exhaust stage

As depicted in Figure 3-17d, the gas exchange process continues till the end of exhaust valve opening period. In fact, if the exhaust valve closes before the piston reaches to the cylinder

TDC (top dead center) or opens after the piston leaves the cylinder BDC (bottom dead center), some amount of work produced by the engine is used to compress the trapped exhaust gas and can adversely affect the engine efficiency.

The effect of cylinder gas pressure on the exhaust valve is also shown in Figure 3-18. In this figure, the solid and dotted lines show engine valve trajectories with and without considering the cylinder gas pressure effect respectively. As illustrated, the engine cylinder gas force not only affects the final valve lift (in this case about 10%) but also affects the engine valve timings.

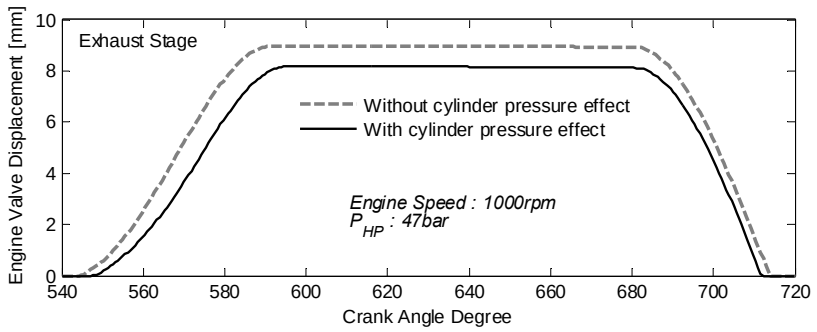

Figure 3-18: Effect of cylinder pressure on the engine valve actuator performance

As discussed before, any change in the exhaust valve timing or lift can affect the engine output power due to the change in the compression work in this stage. Moreover, the engine intake charge quality can also be affected by the trapped exhaust gas from the previous cycle.

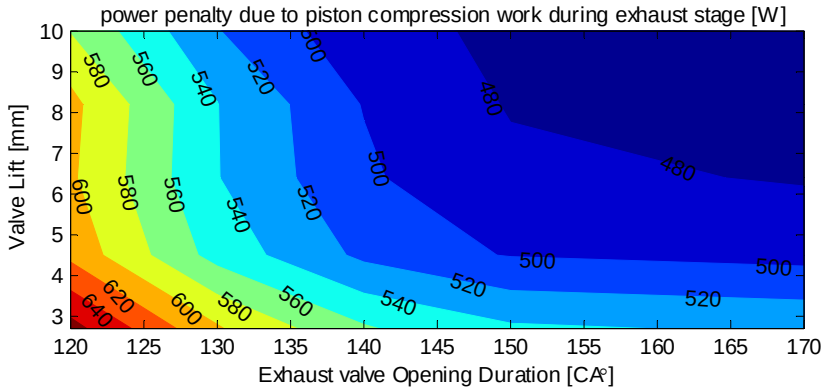

Figure 3-19: Effect of exhaust valve lift and total opening duration on the engine power consumed during exhaust stage for a single cylinder (engine speed: 1000rpm)

Figure 3-19 shows the piston negative power contours for a single engine cylinder during exhaust stage. As shown in this figure, at 1000rpm engine speed, reduction in the exhaust valve opening duration from 170CAº to 120CAº can increase the power losses by 20~27% depending on the final valve lift. In fact, the sensitivity of the power losses to exhaust valve total opening duration decreases as the valve opening duration increases. Also, the effect of final engine valve lift on the piston power consumption during exhaust stage increases as the exhaust valve opening duration reduces; however, the gradient of the engine power losses to the valve lift is more significant at lower engine valve lifts.

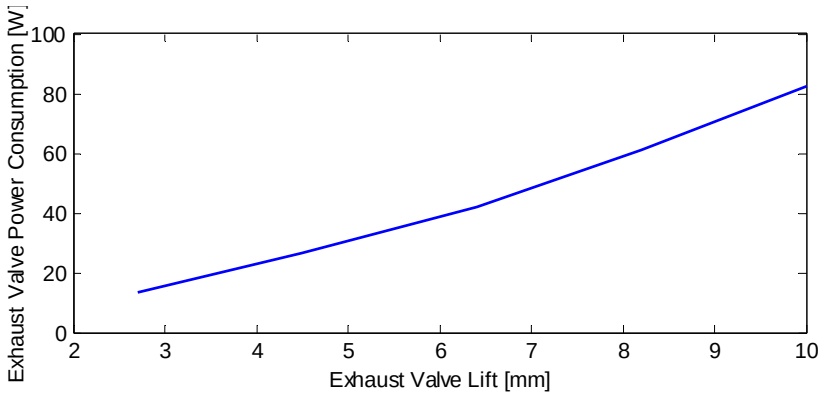

Figure 3-20: The proposed valve system power consumption for different valve lifts for a single engine valve actuation system (engine speed: 1000 rpm)

Although, increase in the engine valve lift reduces the piston power consumption, it increases the power used by the hydraulic VVA system. As shown in Figure 3-20, the power consumption of the single valve actuator increases by about 70W at 1000rpm engine speed as the valve lift increases from 3mm to 10mm. This increase in power consumption is higher than the saving gained by reducing the piston work especially at larger exhaust valve opening duration.

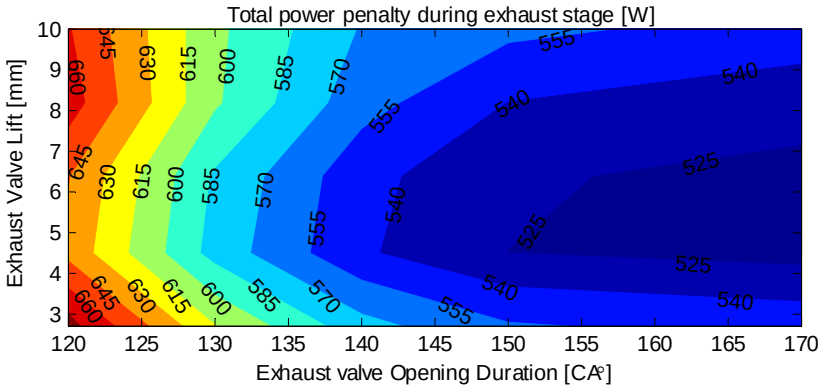

Figure 3-21: Total power consumed by the engine valve actuator and also engine piston during exhaust stage at various engine valve lifts and opening durations (engine speed: 1000rpm)

To find the optimum exhaust valve lift, the contours of total power consumption shown in Figure 3-21 is used. As clearly depicted in this figure, the minimum power penalty at different valve opening durations corresponds to the exhaust valve lift of 6mm at this engine speed. Using the similar methodology, the optimum exhaust valve lift at different engine speeds can also be achieved.

Figure 3-22 shows the effect of exhaust valve opening duration and valve lift on the percentage of exhaust gas left in the cylinder after the exhaust stage. As shown in this figure, reducing the exhaust valve opening duration will increase the amount of unexpelled exhaust gas. However, the change in the engine valve lift from 3mm to 10mm does not have a considerable effect on the amount of exhaust gas left in the cylinder.

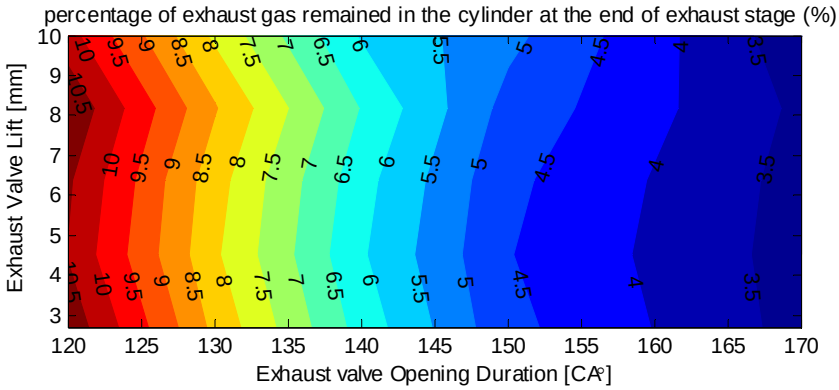

Figure 3-22: The percentage of the exhaust gas remained in the cylinder at the end of exhaust stage at different exhaust valve lifts and opening durations (engine speed: 1000rpm)

3.5 HYDRAULIC SUPPLY PRESSURE CONTROL

As shown in the previous section, in order to have a constant valve lift at different engine speeds, the hydraulic pressure to the VVA system must vary significantly. This requires a variable pressure hydraulic power unit. As shown in Figure 3-23, the hydraulic power unit proposed for the studied VVA system consists of an oil reservoir, a positive displacement pump (i.e. a gear pump) and an air accumulator. The hydraulic pump is rotated by the engine crankshaft through a mechanical transmission whose speed can be slightly varied using a variable speed gearbox. The speed of the gear pump is adjusted such that the flow required by the valve system to achieve a desired lift is provided.

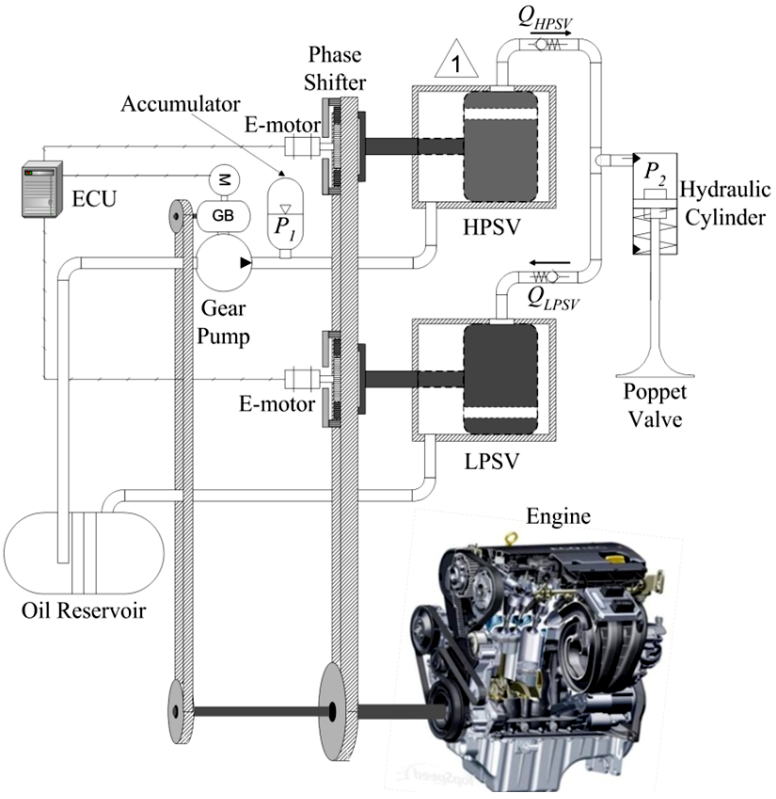

Figure 3-23: The studied VVA system with a variable pressure/flow hydraulic power unit

As the hydraulic pump runs continuously, the system upstream pressure increases when the HPSV is fully closed. During this period, the pumped fluid is stored in the accumulator. As the HPSV opens, the pressurized oil is discharged into the hydraulic cylinder and the

upstream pressure decreases. Considering the trapped air in the accumulator as an ideal gas, the gas expansion and compression processes follow:

$$P_1 V_1^n = P_{1,0} V_{1,0}^n \tag{3.35}$$

where, P_1, V_1, $P_{1,0}$ and $V_{1,0}$ are the current and the initial values for the accumulator pressure and volume. In the above equation, n is the polytropic constant. Assuming zero leakage in the oil supply line, the gas volume is varied according to:

$$\frac{dV_1}{dt} = Q_{HPSV} + Q_{HPSV,leakage} - Q_{pump} \tag{3.36}$$

Differentiating from (3.35) and using (3.36), the accumulator pressure gradient is determined by:

$$\frac{dP_1}{dt} = -nP_1 V_1^{\frac{n-1}{n}} \left(Q_{HPSV} + Q_{HPSV,leakage} - Q_{pump} \right) \tag{3.37}$$

Since the pump is positive displacement, the pump flowrate can be approximated by:

$$Q_{pump} = \eta_{volumetric} N_{pump} V_{disp} \tag{3.38}$$

In the above equation, $\eta_{volumetric}$, V_{disp} and N_{pump} are pump volumetric efficiency, displacement volume and pump speed respectively.

3.6 SUMMARY

In this chapter, a new variable valve actuation system was introduced for the engine valvetrain. Using the proposed system, it is possible to control the engine valve opening and closing angles along with its lift independently. To set up the complete mathematical model of the proposed engine valve actuator, the governing algebraic differential equations of the system were derived based on dynamics, fluid mechanics and heat transfer principles. The system was modeled and simulated in Matlab/Simulink software and the numerical results were discussed.

Chapter 4

Prototyping and Experimental Studies

This chapter addresses the specification of the prototyped variable valve actuation system and the experimental results are also discussed. The parameters of the model developed in the previous chapter are either measured or estimated using experiments and the developed mathematical model is then validated.

4.1 System Prototype and Test Setup

As shown in Figure 4-1, the proposed VVA system is prototyped to study the performance of the proposed VVA system and also to obtain the empirical data required to identify and then validate the numerical model. For this purpose, a test setup for a single valve actuation system is designed and fabricated. The rotary spool valves and hydraulic cylinder are designed based on the results achieved from the numerical simulations and also several design considerations (Figure 4-2).

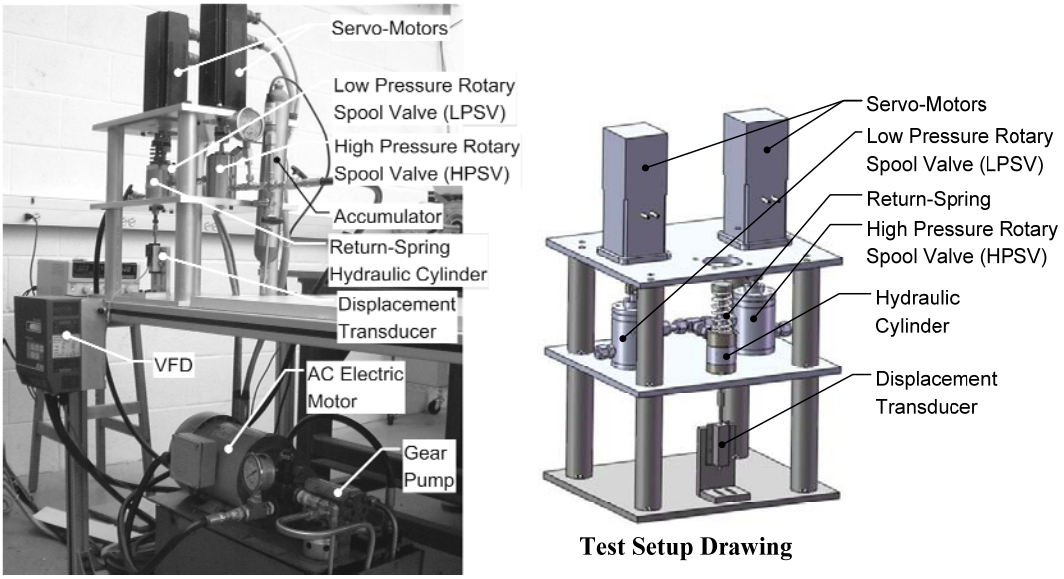

Figure 4-1: The proposed VVA system prototype for a single valve actuation

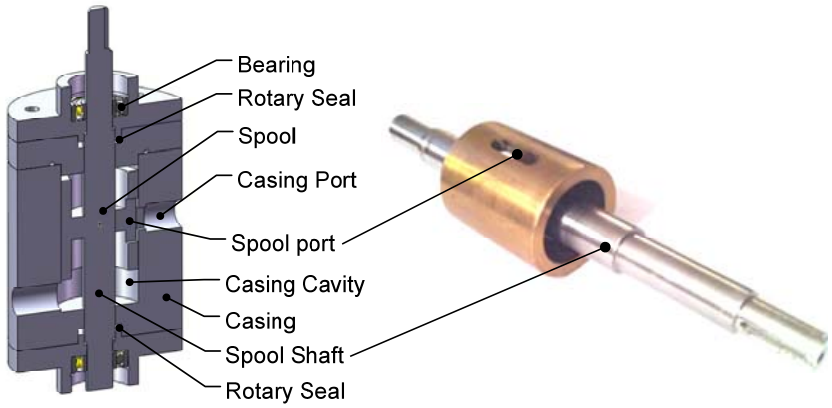

Figure 4-2: Rotary spool valve assembly and design

In the experimental setup, as shown in Figure 4-3, instead of using differential phase shifters, two servo-motors (Emerson brushless motors DXM/E-340W) with two servo drives (Emerson LX-700) are used to rotate the high and low pressure rotary spool valves. In fact, the servo-motors serve as both engine crankshaft and phase-shifters simultaneously. During operation with fixed valve opening and closing timings, both servo motors rotate with half of the engine speed; however, to change the engine valve opening or closing timings, the servomotors should accelerate or decelerate until the desired phase shift is reached. The engine valve actuator is a custom designed miniature single-acting hydraulic cylinder (Mack Corporation) equipped with a return-spring. The hydraulic cylinder shaft is connected to a displacement transducer (Novo Technik) with 0-10 Vdc output signal for lift measurement. The transducer is an analogue potentiometer with accuracy of 50μm and bandwidth of 10 kHz. The shaft acceleration is also measured continuously with a three-axis accelerometer (Kistler Triaxial PiezoBeam accelerometer, Type 8688A5). The hydraulic power unit consists of a gear pump, an oil reservoir and an air-accumulator. In this test setup, instead of using a crankshaft driven variable speed gearbox, the gear pump is rotated by a synchronous electric motor. Since the speed of the synchronous AC-motor is function of supply frequency and number of magnetic poles, its speed can be varied by changing the line frequency. To this end, a variable frequency drive (AC Tech, MC-1000) with a control signal input is employed to precisely control the line frequency and consequently the pump speed. The pressure of air accumulator and hydraulic cylinder are measured with two analogue pressure

transducers (Omegadyne PX309-3KG5V). A Beckhoff control module with an embedded PC is used for communication, control and data acquisition.

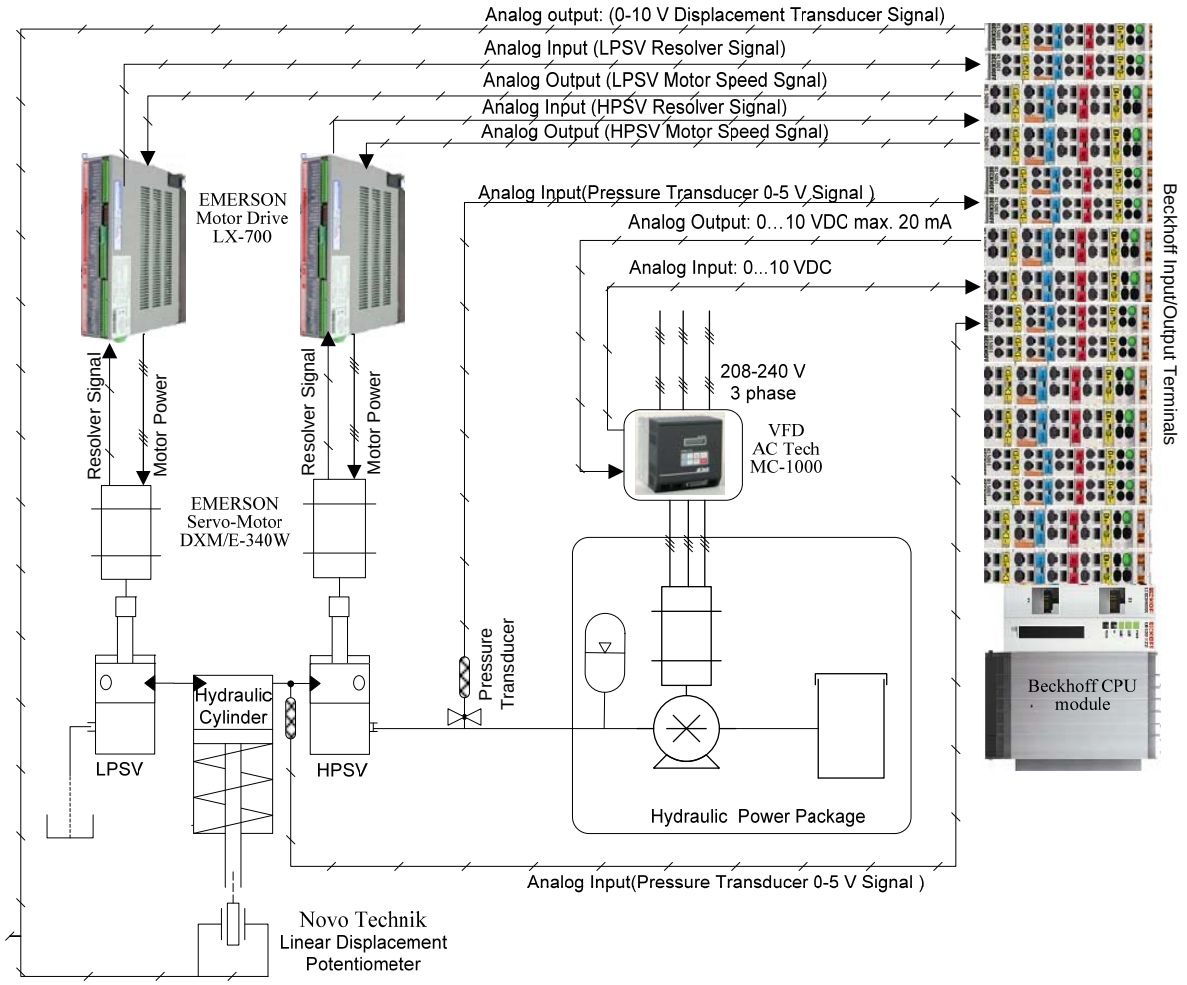

Figure 4-3: The electrical diagram of the experimental setup

4.2 MATHEMATICAL MODEL PARAMETERS ESTIMATION AND VALIDATION

To make the developed mathematical model more accurate numerical platform for future studies, the model parameters should be identified using the experimental results. Some of model parameters such as components dimensions and hydraulic fluid properties are directly measured or known; however, other parameters such as total moving mass (m), equivalent spring rate (K), spring preload ($F_{preload}$) and friction force ($F_{friction}$) need to be identified experimentally. A constant friction force ($F_{friction}$) between hydraulic cylinder and piston is

considered during parameters identification. An experiment is run and the engine valve displacement (x), velocity ($\dot{x}$) and acceleration ($\ddot{x}$) along with hydraulic cylinder pressure are recorded every one millisecond. For k set of measurements, (3.1) can be written in the following matrix form:

$$\underbrace{\begin{bmatrix} \ddot{x}[1] & x[1] & \frac{1-sign\left(\dot{x}[1]\right)}{2} & \frac{1+sign\left(\dot{x}[1]\right)}{2} \\ \ddot{x}[2] & x[2] & \frac{1-sign\left(\dot{x}[2]\right)}{2} & \frac{1+sign\left(\dot{x}[2]\right)}{2} \\ \vdots & \vdots & \vdots & \vdots \\ \ddot{x}[k] & x[k] & \frac{1-sign\left(\dot{x}[k]\right)}{2} & \frac{1+sign\left(\dot{x}[k]\right)}{2} \end{bmatrix}}_{U} \underbrace{\begin{bmatrix} m \\ K \\ F_{preload}-F_{friction} \\ F_{preload}+F_{friction} \end{bmatrix}}_{\Theta} = \underbrace{\begin{bmatrix} P_2(1)A_p \\ P_2(2)A_p \\ \vdots \\ P_2(k)A_p \end{bmatrix}}_{Y} \tag{4.1}$$

Using least square estimation method, the best estimate for Θ can be obtained as follows:

$$\Theta = \left(U^T U\right)^{-1} U^T Y \tag{4.2}$$

Table 4-1 lists the actual system parameters measured or estimated from the experimental data. To verify the developed model accuracy, both simulation and experimental setup are run in an arbitrary operating condition (engine speed: 1000rpm, valve lift: 5mm) different from those used for system identification. Figure 4-4 illustrates the comparison between experimental measurements and simulation results for the accumulator pressure, hydraulic cylinder pressure, engine valve displacement and velocity. As shown in this figure, there is an excellent agreement between the simulation and experimental results.

Table 4-1: The experimental system parameters

K [N/m]	$F_{preload}$ [N]	A_P [mm^2]	l [mm]
59839	438.74	198.8	8
V_{disp} [cc/rev]	n	$P_{1,0}$ [bar]	$V_{1,0}$ [cc]
2.1	1.3	1	50
$V_{2,0}$ [cc]	μ [N.s/m^2]	m [kg]	$F_{friction}$ [N]
10	0.051	0.376	104.32
φ_c [deg]	φ_s [deg]	r_s [mm]	r_c [mm]
25	25	14.98	15.02
β [bar]	d [mm]	C_d	ρ [kg/m^3]
17000	18	0.261	680

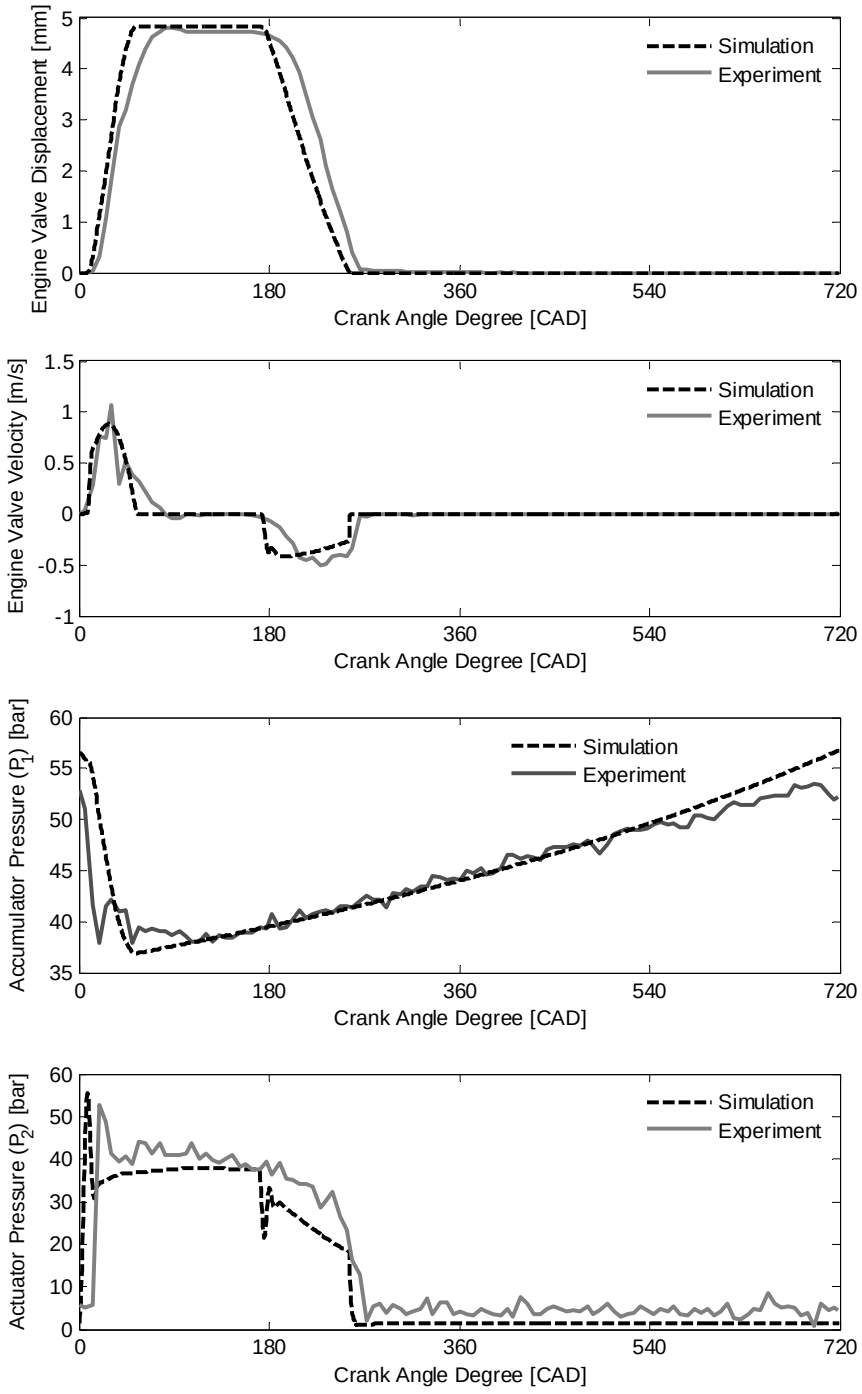

Figure 4-4: Comparison between simulation and experimental results at 1000rpm engine speed and 5mm lift

4.3 ENGINE VALVE SEATING VELOCITY

One of the main challenges in the variable engine valve actuation systems is controlling the valve seating velocity. Acceptable engine valve seating velocity (100 $mm.s^{-1}$ or lower) is essential to minimize the valvetrain noise, vibration and harshness (NVH) and maximize its durability [13], [12]. Many techniques have already been implemented by several researchers to ensure a very controlled seating velocity in camless valvetrains. Precise tracking control of the engine valve displacement by accurately controlling the proportional valve was used in [13] and [43] to achieve average seating velocities of about 12~70 $mm.s^{-1}$ at the range of engine speed of 1000~3000 rpm. In the electro-hydraulic valvetrain proposed by Lou et al. [44] , a portion of the kinetic energy during engine valve closing stage is absorbed by two spring system and the rest of the valve kinetic energy is dissipated through a geometrically fixed hydraulic damper. Using this technique, a valve seating velocity of 190 $mm.s^{-1}$ was achieved for the maximum valve lift of 8mm. In [45], an adjustable hydraulic cushion was used to keep the maximum engine valve contact velocity below 100 $mm.s^{-1}$.

In the proposed system prototype, since the engine valve actuator is not cushioned, a secondary cushioned cylinder, as shown in Figure 4-5, is coupled in series with the main hydraulic cylinder.

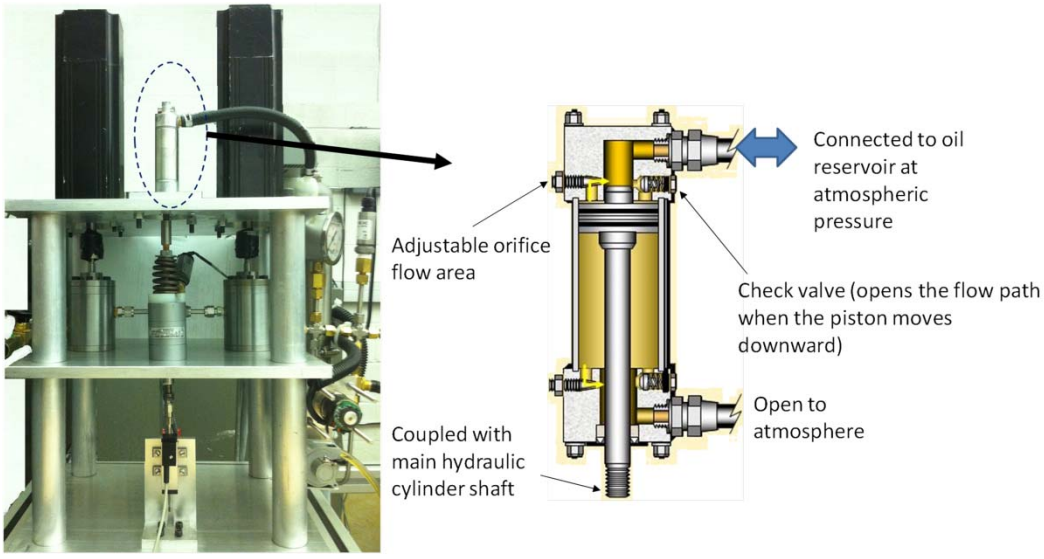

Figure 4-5: Hydraulic cushioning using a secondary cylinder

The upper port of the secondary cylinder is directly connected to the oil tank while its lower port is open to atmosphere. The valve seating velocity can be controlled by cushioning the final part of the piston stroke. During engine valve opening interval, the piston of the secondary cylinder is pulled downward and the upper chamber of the cylinder is filled with oil at atmospheric pressure through the main port, orifice and check valve flow areas; however, during the engine valve closing stage, the upward motion of the piston of the secondary hydraulic cylinder closes the main discharge port and check valve forces the oil to be discharged only through the adjustable orifice. This technique allows a fixed velocity control of the engine valve landing. The valve seating velocity is determined from the measured valve displacement versus time data when the engine valve touches the valve seat. For precise calculation of the valve seating velocity, high sampling rate is required. In this research our sampling frequency is limited to the maximum of 1kHz.

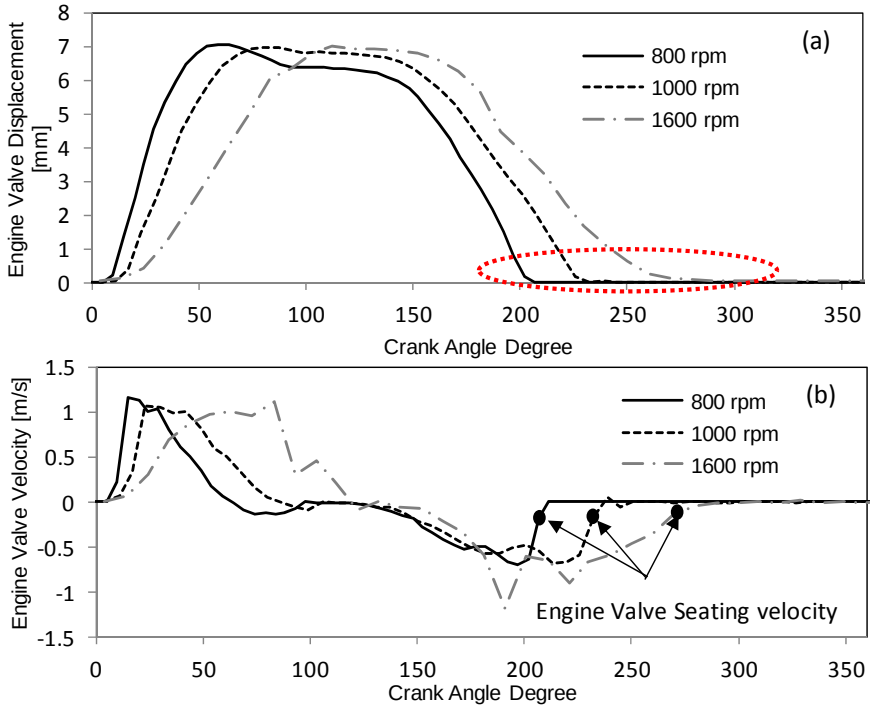

Figure 4-6: Evaluating the effectiveness of the actuator cushioning in reducing engine valve landing velocity at different engine speeds (Experiment)

Figure 4-6 shows the engine valve displacement and velocity at three different engine speeds of 800, 1000 and 1600 rpm and constant final valve lift of about 7mm. As shown in this figure, during engine valve closing stage at all three operating conditions, there is a variation in the engine valve velocity from the peak value of 700~1200 $mm.s^{-1}$ to zero. The engine valve velocity at one time step before it becomes zero can be used to determine the valve seating velocity. In Figure 4-6b, the engine valve seating velocities at three different engine speeds are specified with solid circles. As shown in this plot, the valve seating velocity is controlled around 150mm/s which is close to the desired threshold (100 $mm.s^{-1}$).

4.4 SUMMARY

In this chapter, different components of the new variable valve actuation system proposed in Chapter 3 were designed, prototyped and tested for a single engine valve actuation. In the prototype system, instead of a set of engine crankshaft and phase-shifter, a servo-motor was used to rotate each rotary spool valve. The results and conclusions achieved from numerical investigation of the proposed system were used to design and prototype the rotary spool valves and other components. A variable frequency drive was used to control the pump electric motor speed and consequently pump flowrate at different operating conditions as a way to control the supply pressure and final valve lift. Experimental data were used to identify some of the model parameters given in Section 3.3, such as coulomb friction, flow coefficient, total moving mass, spring stiffness and preload. The least square method was used to identify these parameters. Finally to verify the derived mathematical model of the system, both experimental setup and numerical model were run at an operating condition different than that the parameters identification was performed at. The comparison showed an excellent agreement between the experimental and numerical results. To improve engine valve durability, the system prototype was equipped with a valve seating velocity control mechanism comprising of a cushioned hydraulic cylinder. The experimental results showes engine valve seating velocity of about 150mm/s at different engine operating speeds.

Chapter 5

Engine Valve Timing Control with Constant Lift

So far, the mechanism dynamics, mathematical model and the experimental test bench were only discussed; however, without using controllers, a consistent and reliable valve motion cannot be guaranteed. Controlling the engine valve motion consists of achieving desired engine valve opening and closing angles and also reference valve lift. For this purpose, two control algorithms are introduced in the following sections. These algorithms are then implemented and tested experimentally to evaluate their performances.

5.1 CONTROLLER DEVELOPMENT

5.1.1 Engine valve timing Control

To control the engine valve timings and consequently its opening duration, the angular position of both rotary spool valves (HPSV and LPSV) should be controlled precisely with respect to crankshaft angle while rotating with half of the engine speed. As a result, the rotary spool valves are opened and closed in specific times within every engine cycle. Since the opening instant of the high pressure rotary valve (HPSV) determines the start of the engine valve opening event, to open the engine valve at $\theta_{Opening,ref}$ [CA°], the angular position of the spool port ($\theta_{S,HPSV}$) of HPSV with respect to the casing port ($\theta_{C,HPSV}$) when the crankshaft angle is zero, should be according to:

$$\theta_{C,HPSV} - \theta_{S,HPSV} \rightarrow \frac{\theta_{Opening,ref}}{2} + \frac{\varphi_{S,HPSV} + \varphi_{C,HPSV}}{2} \tag{5.1}$$

Although the engine valve opening time is determined by the opening instant of high pressure rotary valve, it may be delayed due to several factors such as high moving masses inertia and hydraulic fluid compressibility. This delay in the engine valve opening could be

compensated by advancing the HPSV opening instant based on the actual engine valve opening angle error measured in the previous engine cycle ($\theta_{Opening}$[k-1]- $\theta_{Opening,ref}$).

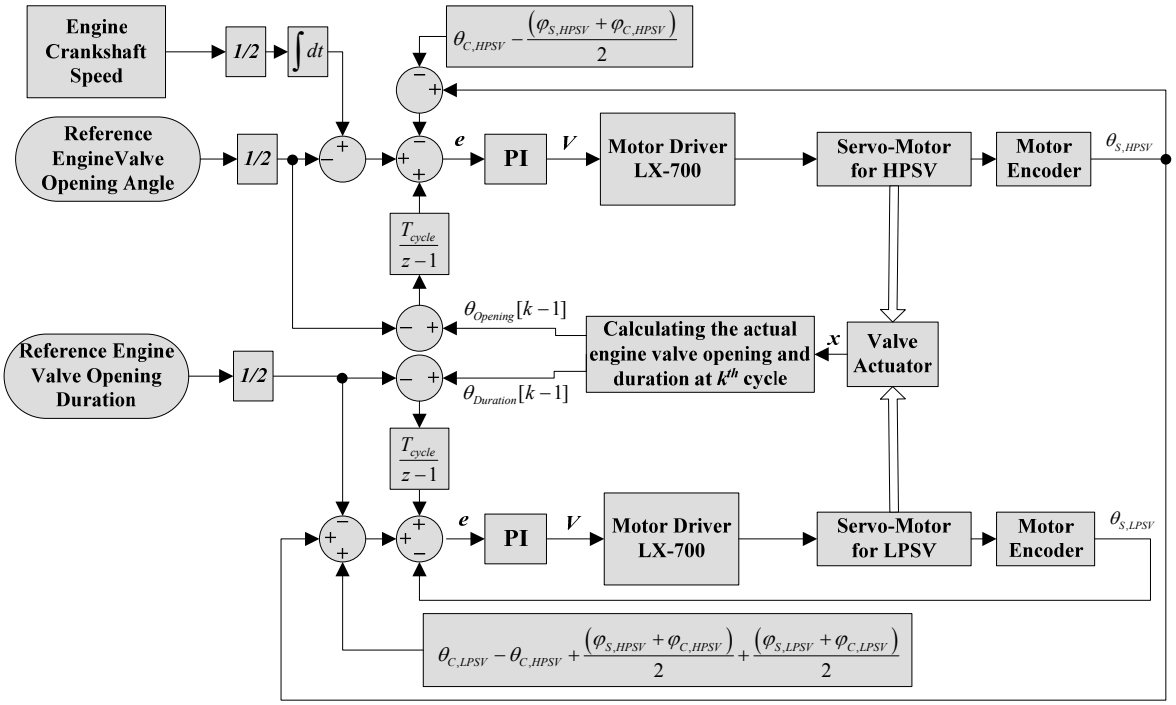

Figure 5-1: Valve opening and closing control algorithm used in the experiment

Similar to HPSV, the opening instant of the low pressure rotary valve (LPSV) determine the start of the engine valve closing events; however, unlike the opening event, the engine valve full closure does not coincide with the LPSV opening instant and it happens a few crank angle degrees after the low pressure rotary spool valve starts to open. The length of this interval depends on the engine valve return-spring force, the volume of the trapped oil in the hydraulic cylinder and also the hydraulic friction forces in the discharge line. Therefore, for a reference engine valve opening duration ($\theta_{Duration,ref}$), the spool position of the low pressure rotary valve ($\theta_{S,LPSV}$) is initially controlled such that the angular difference between the opening instances of high and low pressure rotary valves approaches to $\theta_{Duration,ref}$ and then it is corrected using the actual engine valve opening duration error measured in the previous engine cycle ($\theta_{Duration}$[k-1]- $\theta_{Duration,ref}$). Figure 5-1 illustrates the complete flowchart of the control logic used for timing of the engine valve opening and closing events. As shown in

this figure, two PI controllers are employed to control the angular positions of both rotary spool valves. The PI controllers' parameters (K_I and K_P) are fine tuned for optimum controller efficiency.

5.1.2 Constant Engine Valve Lift

Beside engine valve timing control, engine valve lift control is another critical issue which should be considered in the hydraulic valvetrains. There are two main reasons for lift control; first, to maintain the desired valve lift while the engine speed is varied and second, to vary the desired valve lift according to the engine requirements. In this section, the main objective of the engine valve lift control is to maintain a constant valve lift at all engine operating conditions.

As discussed in Section3.4, in the proposed valve actuation system, the final valve lift is very dependent on the hydraulic supply pressure and operating speed. In the proposed mechanism, the hydraulic fluid pressure and flowrate are provided by the variable speed positive displacement pump. When the high pressure rotary spool valve is closed, the pumped fluid is accumulated in the air-accumulator and the supply pressure increases. As the HPSV opens, the high pressure oil flows into the hydraulic cylinder opening the engine valve and the supply pressure drops (Figure 4-4). During steady operating condition (constant engine and pump speeds), the final engine valve lift (L_f) within every engine cycle is determined by:

$$L_f = \frac{120 Q_{pump}}{N_{engine} A_p} \tag{5.2}$$

By substituting (3.38) in (5.2), the required pump speed for a desired valve lift ($L_{f,ref}$) at various engine speeds can be determined as follows:

$$N_{pump} = \frac{L_{f,ref} A_p}{120 \eta_{volumetric} V_{disp}} N_{engine} = r_{pe} N_{engine} \tag{5.3}$$

In case of constant pump volumetric efficiency, there will be a constant r_{pe} for a specific valve lift at all operating conditions which eliminates the need for any lift controller for constant engine valve lift; however due to variable pump volumetric efficiency, the required

pump to engine speed ratio for constant valve lift is unpredictable. Figure 5-2 illustrates a comparison between the actual (measured) and the ideal ($\eta_{volumetric}$=100%) pump speed required for 7mm lift at various engine speeds. At each engine speed, the ratio between these two values implies the pump volumetric efficiency which is plotted in Figure 5-3. As shown in this figure, the pump volumetric efficiency is very low at lower engine speeds and it is gradually improved as the valve operating speed increases.

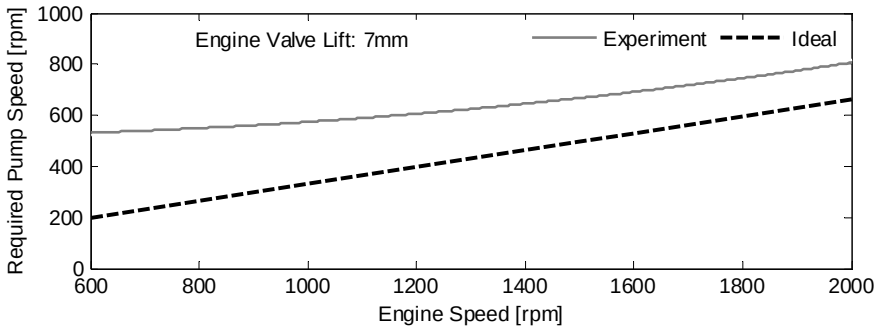

Figure 5-2: Comparison between the actual (experimental) and the ideal (100% volumetric efficiency) pump speeds at different engine speeds and fixed engine valve lift (7mm)

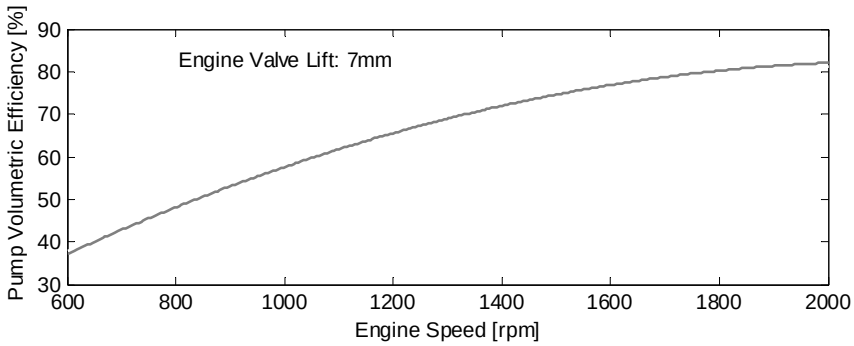

Figure 5-3: Volumetric efficiency of the positive displacement pump used in the test setup versus engine speed for the engine valve lift of 7mm

Due to high variation in pump volumetric efficiency, a feedback control system (Figure 5-4) is designed and implemented to maintain a desired valve lift at transient operation. In this control strategy, shown in Figure 5-4, the error between the desired and measured engine valve lift is used by a PI controller to correct the pump speed. The PI controller parameters are tuned for minimum control signal chattering and maximum tracking performance.

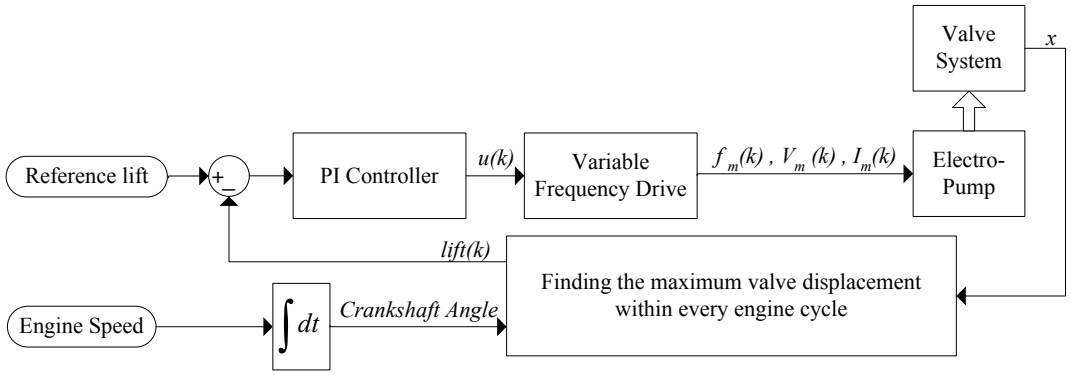

Figure 5-4: The control strategy to maintain constant engine valve lift at transient operation

5.2 RESULTS AND DISCUSSIONS

In this section the performance of the proposed system is evaluated experimentally. To evaluate the effectiveness of the proposed VVA system, several features of the system including the designed controllers performance and system repeatability are studied.

5.2.1 Engine Valve Timing Controller Performance

Figure 5-5 illustrates the flexibility of the proposed VVA system in achieving different engine valve opening and closing timings. As shown in this figure, the engine valve is first controlled to open at 0CA° (crank-angle degree) and close at 140CA°. By phase shifting the LPSV, the engine valve closing timing is then extended by 130CA°and the total valve opening duration becomes 270CA°. The third engine valve profile is achieved by phase shifting both HPSV and LPSV, simultaneously. In this figure, each valve profile consists of 16 consecutive engine cycles superimposed on each other to represent repeatability of the system.

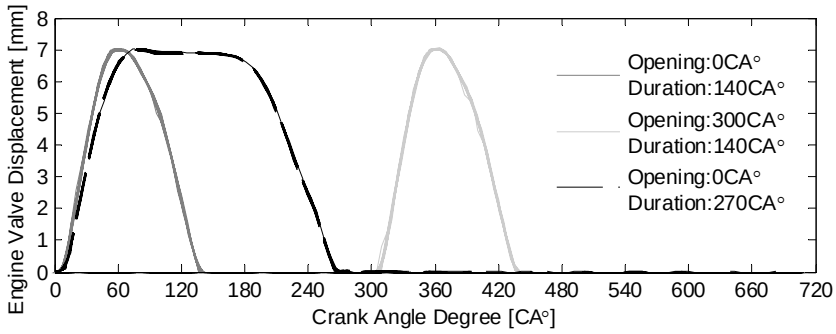

Figure 5-5: Variable engine valve timing (experimental)

Although the results, shown in Figure 5-5, corroborate the effectiveness of the valve timing control during steady operation, they do not show the precision of the designed control system during sudden changes in the reference valve opening or closing timing. For evaluation, the reference engine valve opening and closing timings are stepped up and down as shown in Figure 5-6a and Figure 5-7a. Figure 5-6b and Figure 5-7b show the tracking performance of the engine valve opening and closing timings respectively.

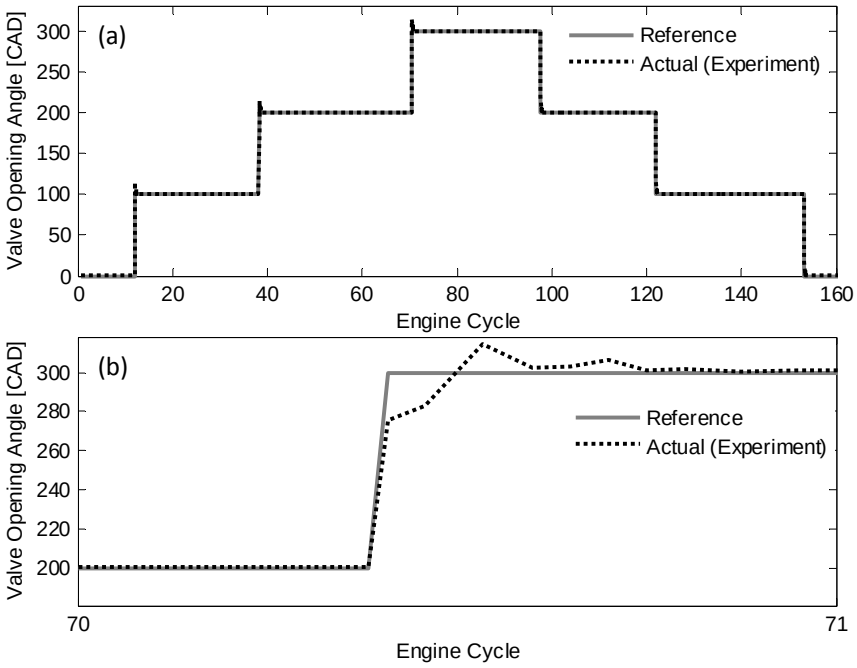

Figure 5-6: Proposed VVA system response to sudden changes in the reference engine valve opening angle (experiment)

As depicted in Figure 5-6b and Figure 5-7b, the proposed valve timing controller can reduce the tracking error resulted from the sudden changes in the reference input signals very quickly.

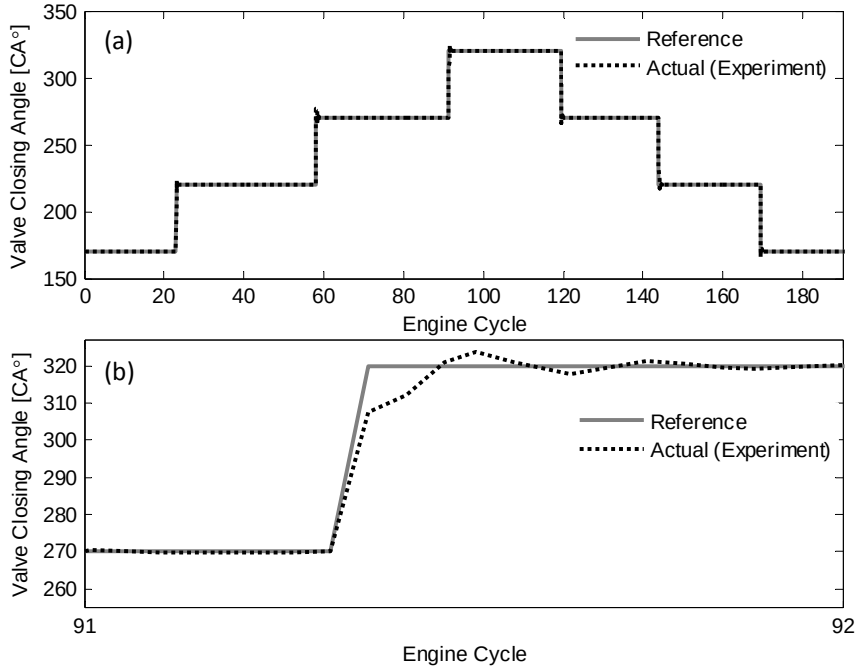

Figure 5-7: Proposed VVA system response to sudden changes in the reference engine valve closing angle (experiment)

5.2.2 Engine Valve Lift Controller Performance

As mentioned before, the main objective of the proposed valve lift controller is to maintain the engine valve lift during any change in the engine speed. To examine the performance of the developed lift control strategy, the engine speed is varied between 600rpm and 1600rpm while the reference valve lift is kept 7mm (Figure 5-8a). Figure 5-8a depicts the actual engine valve lift, achieved through the simulation and experiment, during transient and steady operations. As shown in this figure, during abrupt changes in the engine speed with the rate of 500rpm/s, the maximum valve lift deviation from the reference lift (7mm) does not exceed 0.7mm at all time.

The variation in the commanded speed signal to the hydraulic pump is also illustrated in Figure 5-8b. The volumetric efficiency of the pump estimated in Section5.1.2 was incorporated in the numerical simulation. As shown in this figure, although the engine speed increased by 166%, the pump speed increased by only 30%. This is due to very low pumping efficiency at lower operating speed.

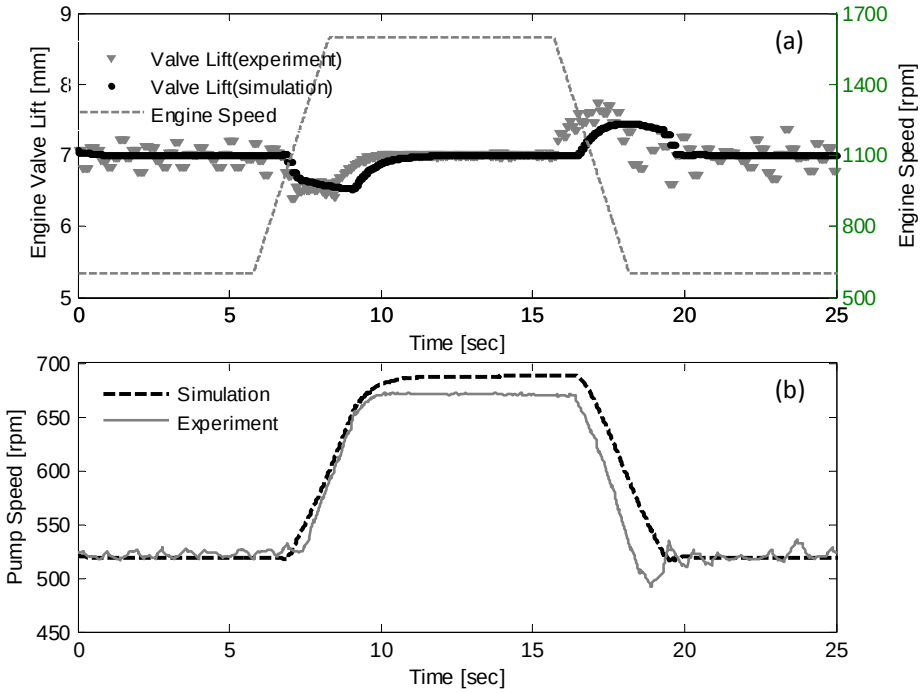

Figure 5-8: Lift controller performance in maintaining a constant valve lift at different operating conditions

Using this control method, it is also possible to vary the final engine valve lift at constant engine speed. Figure 5-9 shows the performance of the proposed controller in tracking the desired valve lift at 1000rpm engine speed. As shown in the magnified view of this figure, it takes about 1 second (~8 engine cycles) to change the engine valve lift from 9mm to 5mm. This delay is mostly due to the electric pump response time and also the time required for the accumulator pressure to be stabilized. Figure 5-10 shows the actual pump speed variation during this experiment and compares it with the theoretical value calculated based on 100% volumetric efficiency.

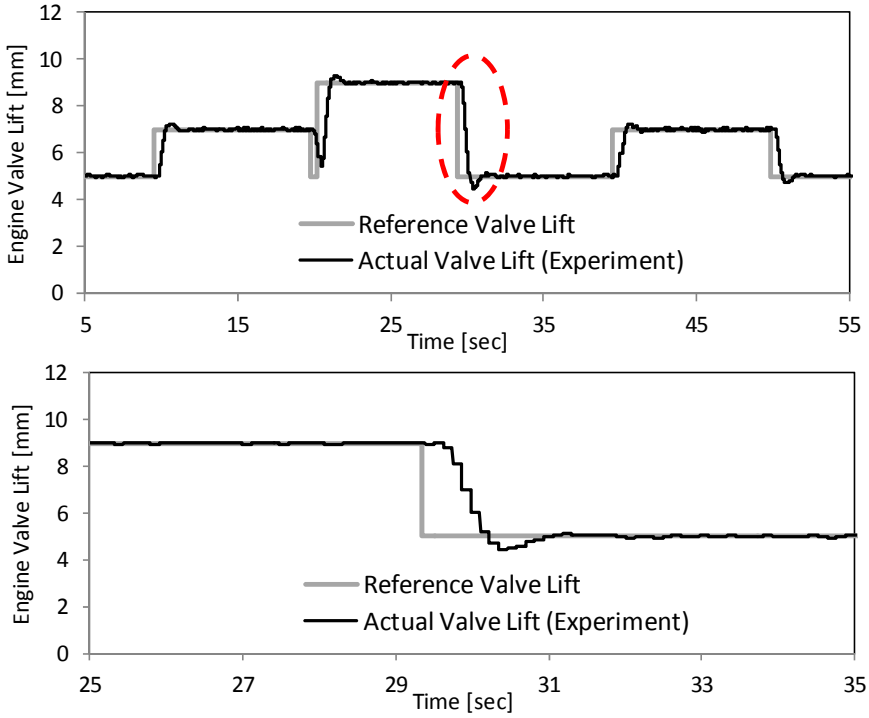

Figure 5-9: Lift controller performance in varying the final engine valve lift at constant engine speed (1000rpm)

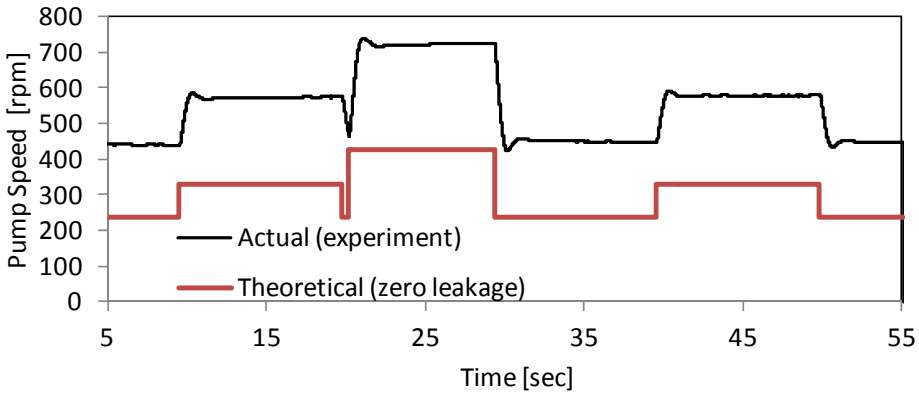

Figure 5-10: Comparison between the actual and theoretical pump speed required at different engine valve lift

5.2.3 System Repeatability

Besides controllability, the repeatability is another key measure which determines the performance of variable valve actuation system. To evaluate the system repeatability, the

experiment is performed at different engine speeds for constant engine valve lift of 7mm and desired engine valve opening and closing angles of 20 and 274 CA° for 80 consecutive valve events (at each engine speed) under steady operating conditions (Figure 5-11).

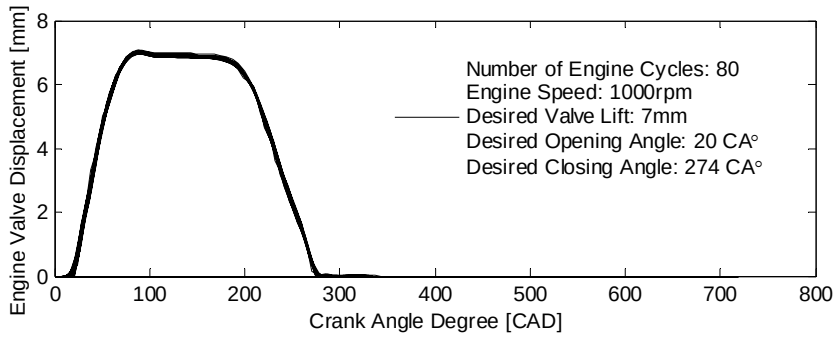

Figure 5-11: Engine valve displacement versus crankshaft angle for 80 consecutive engine cycles at 1000rpm engine speed (experiment)

In order to show the valve opening and closing variability, the crank angles at which the engine valve crosses the 0.5mm lift threshold during valve opening and closing intervals are recorded for 80 consecutive engine cycles and their deviations from their mean values are calculated. Figure 5-12 and Figure 5-13 illustrates the valve timings and lift variations from their average values at 1000rpm engine speed for 80 successive valve events. As show in Figure 5-12, the maximum deviation of the engine valve opening and closing events from their reference timings are about 1 and 2 crank angle degrees respectively.

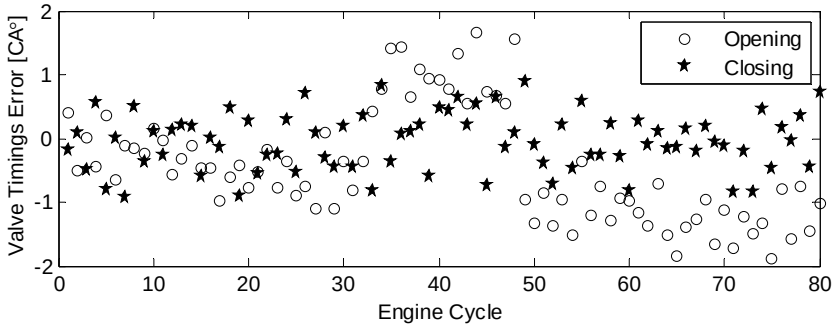

Figure 5-12: Deviations of the measured engine valve opening and closing angles from desired timings (experiment)

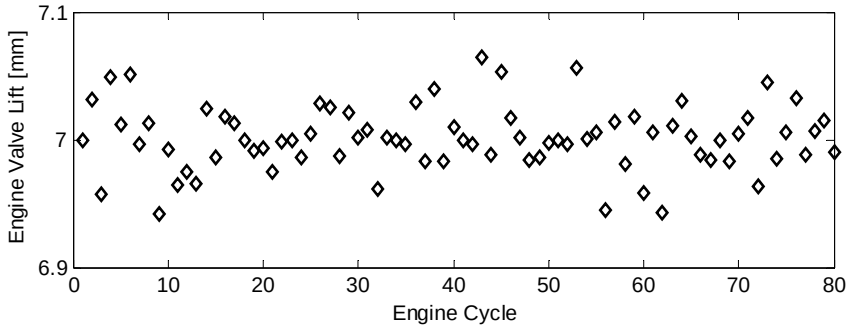

Figure 5-13: Variation of measured engine valve lift from reference lift (experiment)

As illustrated in Figure 5-13, using the proposed lift control strategy, the maximum variation of the engine valve lift from its reference value is less than 0.1mm. For more methodological analyses of the repeatability, the aforementioned variability tests were repeated at various engine speeds (800-2000rpm) and the standard deviations (σ) of the measured data were calculated and listed in Table 5-1.

Table 5-1: System repeatability

Engine Speed [rpm]	Valve Opening Repeatability (σ) [CA°]	Valve Closing Repeatability (σ) [CA°]	Valve Lift (σ) [mm]
800	0.5908	0.3168	0.0410
1000	0.8775	0.5249	0.0261
1200	0.7535	0.6097	0.0204
1400	0.9792	1.1037	0.0888
1600	1.1268	1.5255	0.0256
1800	1.1605	1.7098	0.0296
2000	2.0378	2.5268	0.0413

5.3 SUMMARY

In this chapter, two independent controllers were implemented and tested to precisely control the engine valve timing and also maintain a constant valve lift during transient operation. To evaluate the performance of the proposed VVA system, several aspects including control performance and repeatability were examined both numerically and experimentally. Following conclusions can be drawn from this chapter:

- Using the proposed system, it is possible to vary the engine valve opening/closing angles and valve opening duration from 0 to 720 CA°.

- The experimental results from valve timing control showed that 100CAº change in the engine valve opening and closing timing can be achieved in less than an engine cycle.
- Using the hydraulic power unit with the proposed hydraulic pump speed controller significantly reduces the sensitivity of the final engine valve lift to engine speed variation.
- The repeatability of the engine valve actuator was studied by running the system under steady conditions at different engine speeds. The variability of the engine valve opening and closing timings as well as engine valve lift was studied by calculating the standard deviation of the recorded data for minimum 80 consecutive engine cycles. The experimental results showed maximum standard deviation of 2.5CA° at 2000rpm engine speed. The repeatability test for engine valve lift also showed standard deviation of less than 90 microns.

Chapter 6

Variable Engine Valve Lift Control

6.1 Introduction

In addition to valve timing control, a precise engine valve lift control is crucial in hydraulic valve systems where the engine valve lift is highly influenced by the upstream pressure, engine speed, and other disturbances. This is to avoid unwanted valve closure or mechanical interference between the valve and engine piston at different operating conditions. Moreover, several advantages such as significant reduction in pumping losses through throttle-less control of intake air and valve deactivation are also gained by varying the engine valve lift especially during low load engine operation [46].

In electro-hydraulic camless valvetrain, control of the engine valve lift is usually achieved by precise control of the high pressure servo-valve within every engine cycle. Several studies have been conducted in designing a robust lift controller for these valvetrains [47]- [48]. However, in the proposed hydraulic VVA system, due to the absence of the electro-hydraulic servo valves, the desired engine valve lift is achieved using a different lift control technique. Controlling the supply pressure using a proportional bleed-valve is a lift control technique proposed for this valve system. To this end, a discrete sliding mode controller is designed using the average model of the system on the basis of a discrete Lyapunov function. The stability of the designed control system is proved and sufficient conditions of the controller gains to stabilize the system are given.

6.2 A Novel Engine Valve Lift Controller

Unlike electro-hydraulic camless valvetrains, in the proposed VVA system, the HPSV opening duration is proportional to engine speed and cannot be varied independently; thus, controlling the HPSV upstream pressure will be the only way of controlling the final engine

valve lift. Hence, the proposed VVA system is equipped with a novel lift control architecture, shown in Figure 6-1, consisting of a proportional bleed valve and a drain line. As the bleed valve opens, it drains a portion of the pumped fluid back to the oil reservoir and consequently reduces the pump downstream pressure. Using this technique it is possible to achieve smaller engine valve lift at various engine speeds.

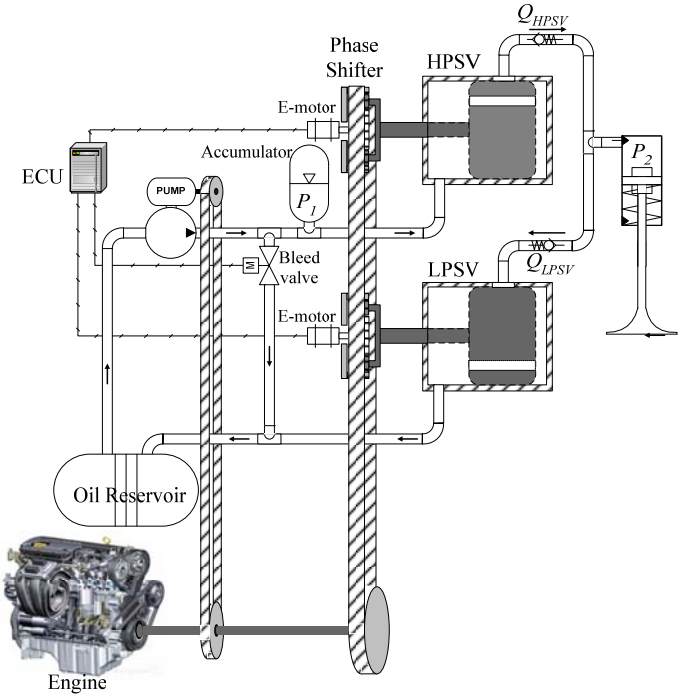

Figure 6-1: Implementation of the new engine valve lift controller on the proposed VVA system

In this system, the pump to engine speed ratio (r_{pe}) is constant and it is defined such that maximum desired engine valve lift ($L_{f,max}$) can be obtained at different engine speeds (N_{engine}) when the proportional bleed valve is fully closed. Hence, the pump to engine speed ratio is determined by:

$$r_{pe} = \frac{N_{pump}}{N_{engine}} = \frac{A_p L_{f,\max}}{2\eta_{volumetric,\min} V_{disp}} \tag{6.1}$$

where, A_p , $L_{f,max}$ and V_{disp} are hydraulic piston area, maximum engine valve lift, and pump volumetric displacement respectively. In (6.1), $\eta_{volumetric,min}$ is the minimum pump volumetric efficiency observed at worst operating condition. Figure 6-2 depicts the volumetric efficiency of the gear pump used in the current test setup at different downstream pressures and pump

speeds. As shown in this figure, the pump volumetric efficiency increases as the engine speed increases.

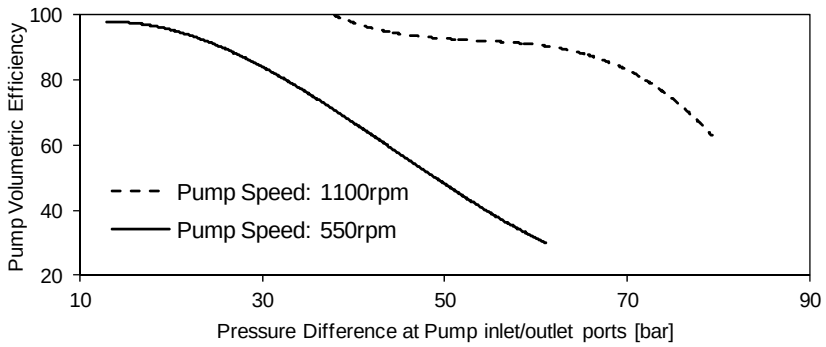

Figure 6-2: Volumetric efficiency of the gear pump used in the test setup versus pump downstream pressure and pump speed

6.3 SYSTEM MODEL

The mathematical model of the proposed VVA system equipped with the new valve lift control architecture is similar to the model developed in Section 3.3; however, the equations for accumulator air pressure gradient, (3.36), and volume, (3.37), are replaced with:

$$\frac{dV_1}{dt} = Q_{HPSV} + Q_{HPSV,leakage} + Q_{bleed} - Q_{pump} \tag{6.2}$$

$$\frac{dP_1}{dt} = -\frac{P_1^2}{P_0 V_0}\left(Q_{HPSV} + Q_{HPSV,leakage} + Q_{bleed} - Q_{pump}\right) \tag{6.3}$$

where, Q_{bleed}, is the oil flowrate through the proportional bleed valve and is approximated by:

$$Q_{bleed} = C_{v,bleed} A_{bleed} \sqrt{\frac{2\left(P_1 - P_{reservoir}\right)}{\rho}} \tag{6.4}$$

6.4 EXPERIMENTAL SETUP

To implement the proposed lift control system on the new valve actuation system, the current test setup is subjected to slight modifications. The engine valve lift control system consists of an integral bonnet needle valve (Swagelok B-1KS4) located in the oil supply line connecting the pump downstream to the oil reservoir. As shown in Figure 6-3, the needle valve is

connected to a dc planetary gear motor (Hennkwell HE372E) using a flexible coupling. The needle valve shaft angular position is measured using a string potentiometer (Celesco SP1-4). The gear motor input voltage is provided by a brush type PMW servo amplifier (Advanced Motion Control 12AB PMW Servo Drive). Figure 6-4 shows the electrical diagram of the proposed valve lift controller.

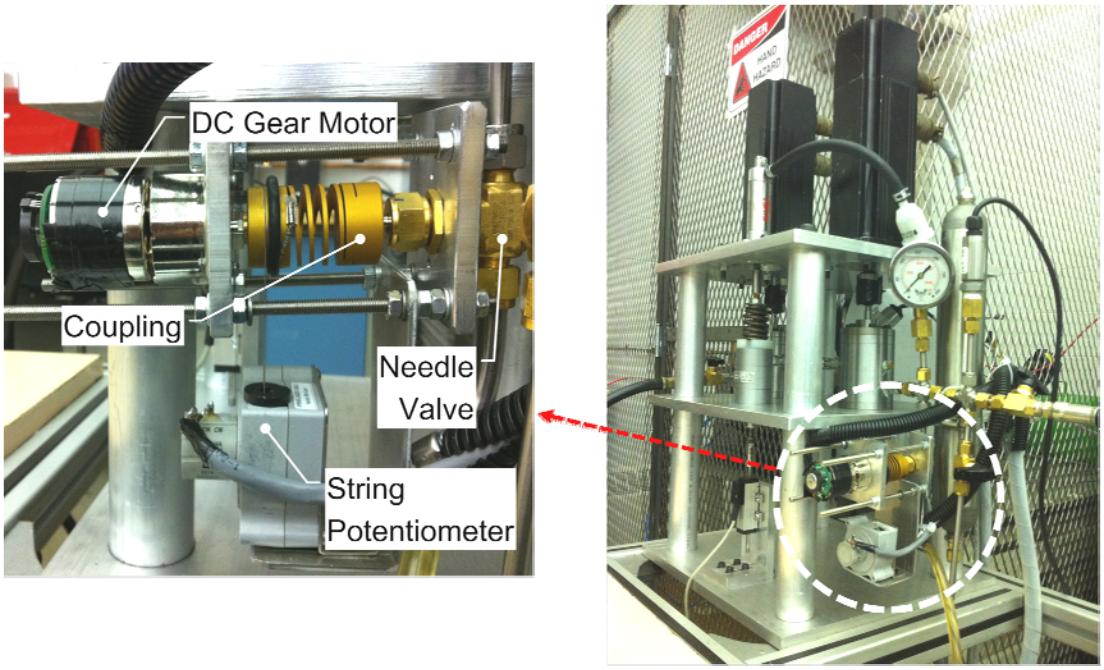

Figure 6-3: configuration of the proposed engine valve lift controller in the system test setup

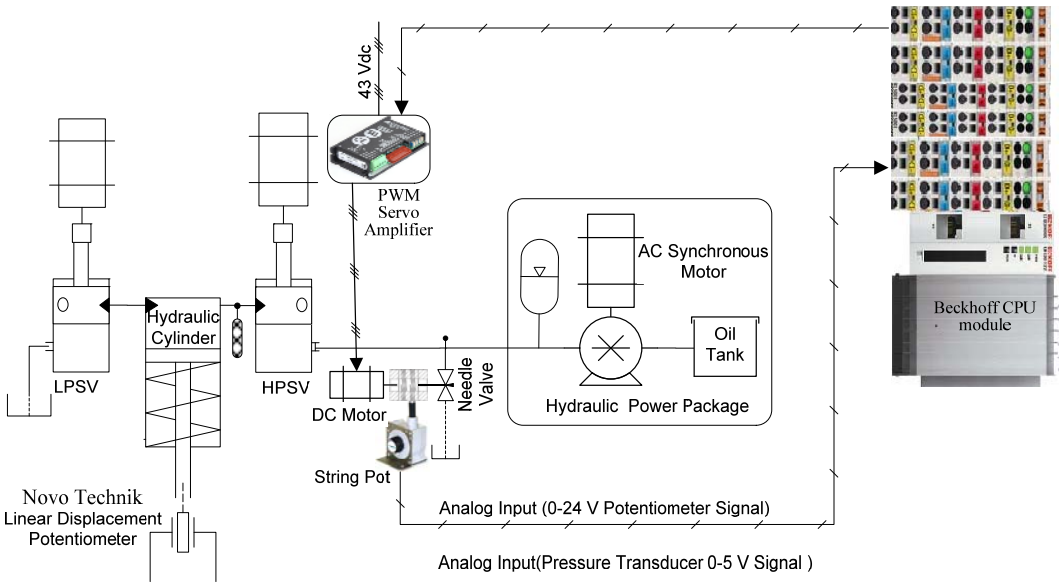

Figure 6-4: Engine valve lift controller electrical drawing

6.5 CONTROLLER DEVELOPMENT

There are two main reasons for controlling the maximum valve displacement; first, to maintain a constant lift during engine speed variation to avoid sudden increase or decrease in the final lift and secondly, to vary the final valve lift according to the engine requirements for improved performance. In the proposed lift control architecture, several control approaches can be used to determine the required bleed valve opening degree for the desired valve lift; however for fast and accurate valve response which is desired especially during mode transition operation, a model-based controller including feedback and feedforward laws is more appropriate. To develop a model-based controller, a mathematical model of the system must be used; however, if the complete model of the system, developed in Sections 3.3 and 6.3 , is used, the final control law will be highly complex and the control signal fluctuates significantly within every engine cycle. This is due to the severe fluctuation in the system pressure within every engine cycle and also due to the use of the actual valve displacement as the controlled parameter. Implementing the control system based on the complete model of the proposed VVA system requires a proportional bleed valve with an ultra fast actuator increasing the system's cost and complexity. Therefore, using an average model of the

system correlating the final valve lift of the next engine cycle to the mean values of system states (pressures and flowrates) at the current cycle will be extremely beneficial.

6.5.1 System Average Model

The average model of the system is based on the system energy and mass conservation principles. Based on the 1st law of thermodynamics, the input energy to the system is equal to the sum of the output energy from the system, irreversibilities and changes in the system internal energy.

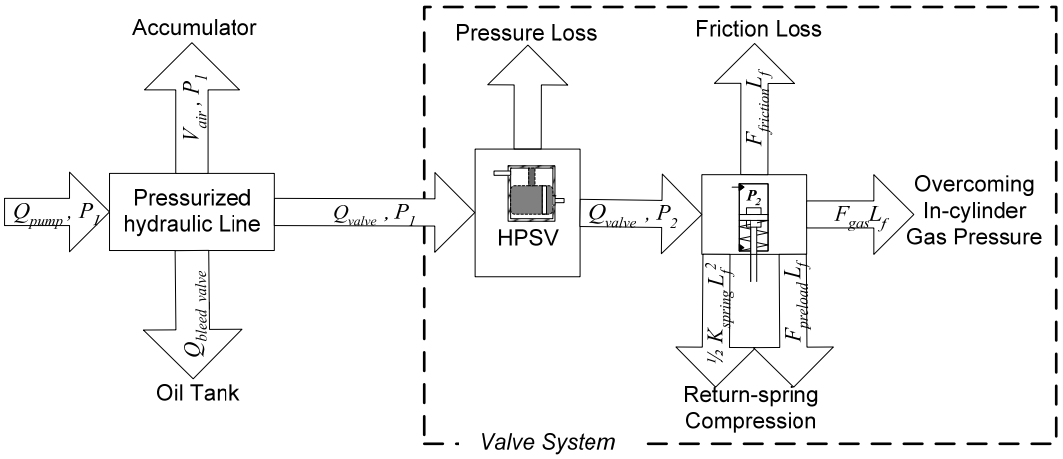

Figure 6-5: Energy flow in the proposed system

As shown in Figure 6-5, in the proposed VVA system it is assumed that the input energy is the hydraulic energy produced by the pump and the output energy is the energy consumed by the hydraulic cylinder to overcome the return spring and cylinder gas forces to actuate the engine valve. The system irreversibilities include energy losses at rotary spool valves and bleed valve ports and also those losses created due to the coulomb and viscose frictions in the hydraulic cylinder. The change in the system internal energy could be also considered as the change in the air-accumulator pressure.

As shown in Figure 6-5, the energy consumed by the valve system consists of energy losses at HPSV due to flow restriction and the energy used to overcome the hydraulic cylinder

friction and in-cylinder gas forces and also to compress the valve return-spring. Hence, the valve system energy consumption during a single engine cycle can be approximated by:

$$E_{valve-system}\Big|_{cycle} = \frac{1}{2}K_{spring}L_f^2 + F_{preload}L_f + F_{friction}L_f + \bar{F}_{gas}L_f + \int_{cycle}(P_1 - P_2)Q_{valve}dt \qquad (6.5)$$

where, L_f is the final engine valve lift within every engine cycle, $\bar{F}_{gas}$ is the average cylinder gas pressure during valve rise interval and Q_{valve} is the oil flowrate from HPSV into the hydraulic cylinder. In the above equation, the energy loss in the HPSV can be approximated using the 1st mean value theorem for integration:

$$\int_{cycle}(P_1 - P_2)Q_{valve}dt = \overline{\Delta P}\int_{cycle}Q_{valve}dt = \overline{\Delta P}A_pL_f \qquad (6.6)$$

where, $\overline{\Delta P}$ is the pressure difference across the high pressure rotary valve somewhere within the engine cycle. Based on the pressure and flowrate of the hydraulic oil passing through the HPSV, the valve system energy consumption can be also defined by:

$$E_{valve-system}\Big|_{cycle} = \int_{cycle}P_1Q_{valve}dt \qquad (6.7)$$

Again using 1st mean value theorem for integration, the above equation is written as:

$$E_{valve-system}\Big|_{cycle} = \bar{P}_1\int_{cycle}Q_{valve}dt = \bar{P}_1A_pL_f \qquad (6.8)$$

where, $\bar{P}_1$ is the accumulator pressure somewhere during the engine cycle which is approximated with the accumulator average pressure within that cycle. Substituting (6.8) and (6.6) in (6.5), the energy conservation equation for the valve system, (6.5), is reformulated as follows:

$$\bar{P}_1A_pL_f = \frac{1}{2}K_{spring}L_f^{\,2} + F_{preload}L_f + F_{friction}L_f + \bar{F}_{gas}L_f + \overline{\Delta P}A_pL_f \qquad (6.9)$$

Because $\overline{\Delta P}$ is less than $\bar{P}_1$, it can be approximated as follows:

$$\overline{\Delta P} = \left(\alpha + \tilde{\alpha}\right)\bar{P}_1 \qquad 0 \le \left(\alpha + \tilde{\alpha}\right) \le 1 \qquad (6.10)$$

In the above equation, α is approximated by a comparison between the results from the average model and the complete model of the system and is a compromise between different

system operating conditions. Also $\tilde{\alpha}$ compensates for the variation of α from one operating condition to another and is considered as model uncertainty. By substituting (6.10) in (6.9) and simplifying the final equation, the engine valve lift at k^{th} engine cycle is determined as:

$$L_f\left(k\right) = \frac{2\left(1-\alpha\right)\bar{P}_1(k)A_p - 2\left(F_{preload} + F_{friction} + \bar{F}_{gas}(k)\right) - 2\bar{P}_1(k)A_p\tilde{\alpha}(k)}{K_{spring}} \tag{6.11}$$

Using the above equation, the engine valve lift at $(k+1)^{th}$ cycle can be approximated by:

$$L_f\left(k+1\right) = \frac{2(1-\alpha)\bar{P}_1(k+1)A_p - 2\left(F_{preload} + F_{friction} + \bar{F}_{gas}(k+1)\right) - 2\bar{P}_1(k+1)A_p\tilde{\alpha}(k+1)}{K_{spring}} \tag{6.12}$$

Subtracting (6.11) from (6.12) results in:

$$L_f\left(k+1\right) - L_f(k) = \frac{2(1-\alpha)\left(\bar{P}_1(k+1) - \bar{P}_1(k)\right)A_p - 2\left(\bar{F}_{gas}(k+1) - \bar{F}_{gas}(k)\right)}{K_{spring}} + \underbrace{\frac{2\bar{P}_1(k+1)A_p\tilde{\alpha}(k+1) - 2\bar{P}_1(k)A_p\tilde{\alpha}(k)}{K_{spring}}}_{\tilde{f}_1(k)} \tag{6.13}$$

Assuming negligible cycle to cycle variation in the engine cylinder gas force during valve opening interval, equation (6.13) is simplified to:

$$L_f\left(k+1\right) = L_f(k) + \frac{2(1-\alpha)\left(\bar{P}_1(k+1) - \bar{P}_1(k)\right)A_p}{K_{spring}} + \tilde{f}_1(k) \tag{6.14}$$

Owing to high thermal mass of the accumulator body, the air compression and expansion processes happen at almost constant temperature and can be considered as isothermal and therefore, equation (6.14) can be rewritten as:

$$L_f\left(k+1\right) = L_f(k) + 2(1-\alpha)\left(\frac{P_{1,0}V_{1,0}\left(\bar{V}_1(k) - \bar{V}_1(k+1)\right)}{K_{spring}\bar{V}_1(k)\bar{V}_1(k+1)}\right)A_p + \tilde{f}_1(k) \tag{6.15}$$

where, $\bar{V}_1$ is the average accumulator gas volume during one cycle and $P_{1,0}$ and $V_{1,0}$ are accumulator precharge volume and pressure. Based on the mass conservation principle, the pumped fluid within every engine cycle is either stored in accumulator or drained through the bleed valve or flows into hydraulic cylinder. Therefore, at every engine cycle, the change in accumulator air volume can be approximated by:

$$\bar{V}_1(k)-\bar{V}_1(k+1)=\frac{120}{N_{engine}}\left(Q_{pump}(k)-C_{v,bleed}\left(k\right)A_{bleed}\sqrt{\frac{2\left(\bar{P}_1\left(k\right)-P_{reservoir}\right)}{\rho}}\right) \\ -A_pL_f\left(k\right)+\tilde{f}_2(k) \tag{6.16}$$

where, $\tilde{f}_2$compensates for the error existing in the above approximation. Substituting (6.16) in (6.15) and approximating $\bar{V}_1(k)\bar{V}_1(k+1)$ by $\bar{V}_1^2(k)$, the following non-linear dynamic system in a discrete time domain is achieved for the engine valve lift:

$$L_f(k+1)=f_k+g_ku_k+\tilde{f}_k \tag{6.17}$$

where,

$$f_k=L_f(k)\left(1-\frac{2(1-\alpha)\bar{P}_1^2(k)A_p^2}{K_{spring}P_{1,0}V_{1,0}}\right)+\frac{240\bar{P}_1^2(k)(1-\alpha)A_pQ_{pump}}{N_{engine}K_{spring}P_{1,0}V_{1,0}} \tag{6.18}$$

$$g_k=-\frac{240(1-\alpha)\bar{P}_1^2(k)A_pA_{bleed}}{N_{engine}P_{1,0}V_{1,0}K_{spring}}\sqrt{\frac{2\left(\bar{P}_1\left(k\right)-P_{reservoir}\right)}{\rho}} \tag{6.19}$$

$$\tilde{f}_k=\frac{2(1-\alpha)\bar{P}_1^2(k)A_p}{K_{spring}P_{1,0}V_{1,0}}\tilde{f}_2(k)+\tilde{f}_1(k) \tag{6.20}$$

$$u_k=C_{v,bleed}\left(k\right) \tag{6.21}$$

In (6.17), u_k and $\tilde{f}_k$are considered as the control signal and the model uncertainty at cycle k respectively. Here, it is assumed that the bleed valve flow coefficient ($C_{v,bleed}$) varies depending on the valve opening percentage and the bleed valve flow area (A_{bleed}) is assumed constant. Therefore, in the proposed engine valve lift controller, the control signal is considered to be the bleed valve flow coefficient ($C_{v,bleed}$). Since the bleed valve is an integral-bonnet needle valve, the valve opening and closing is realized by rotating the valve's stem clockwise or counter-clockwise. The relation between the valve flow coefficient ($C_{v,bleed}$) and valve's stem angular position (θ_{bleed}) is determined through experiment. Figure 6-6 shows the variation of the valve flow coefficient during the first 360° of bleed valve

opening. Using this graph, the bleed valve opening angle corresponding the calculated control signal ($C_{v,bleed}$) could be achieved.

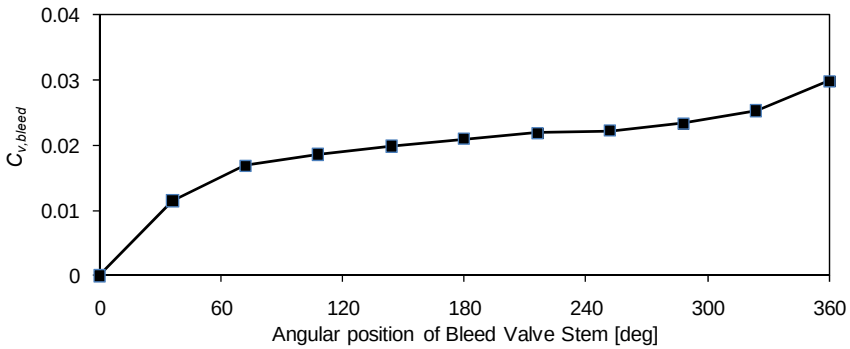

Figure 6-6: The bleed valve flow coefficient versus valve stem angle [deg]

In the real test setup, the bleed valve opening angle is controlled by a DC gear motor through input voltage control. The gear motor is equipped with a separate feedback controller (PID) to track the desired bleed valve opening angle (gearbox output shaft angle) calculated by the developed lift control law.

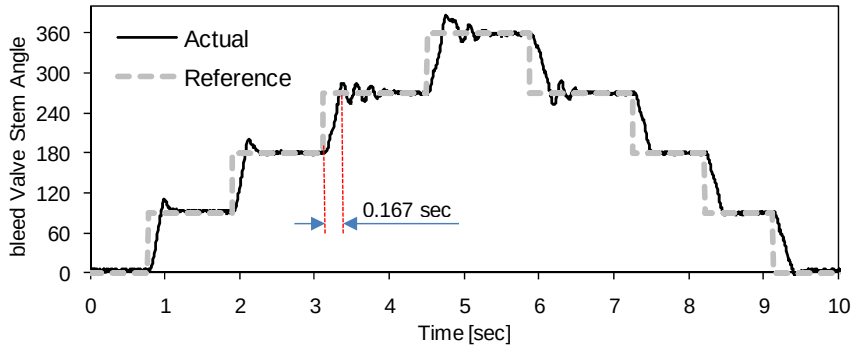

Figure 6-7: The proportional bleed valve controller tracking performance during sudden changes in the bleed valve opening degree (Proportional gain:70, Integral gain:50, Differential gain:80)

Figure 6-7 illustrates the tracking performance of the bleed valve actuator during sudden variation in the desired valve stem angle. As shown in this figure, the system including gear motor and its controller has a rise time of approximately 167ms as the reference valve stem angle varies 90 degrees. The slow bleed valve actuator response time is due to the choice of the DC motor and its gearbox which are not meant to be used in this application; however, as

it will be shown later, even with this slow actuator, accurate and fast lift control can be achieved.

6.5.2 System Average Model Validation

The complete mathematical model of the system, developed in Sections 3.3 and 6.3, is used to verify the accuracy and correctness of the system average model. To this end, both models are simulated in Matlab/Simulink for similar operating conditions (bleed valve opening level and engine speed) and the results for accumulator pressure and valve lift are compared. Figure 6-8 shows a comparison between the results for P_1 (accumulator pressure) and L_f (engine valve lift) achieved from complete and average models of the system at different engine speeds and bleed valve opening percentages. As shown in this figure, there is a good agreement between the results from both models at most of the operating conditions. The maximum error between the results obtained from the average model and those achieved from the complete model does not exceed 11%. These deviations are due to the existence of uncertainties in the average model and will be compensated by the control system. As shown in Figure 6-8, during the initial 10 seconds of the system operation, the engine valve stays closed due to low accumulator pressure. In fact, as the system is switched off for a long period of time, the whole system is depressurized due to leakage flow through the clearances that exist between the rotor and casing of both rotary spool valve and hydraulic pump. In the real application, this problem could be solved by pressurizing the accumulator before engine is switched on.

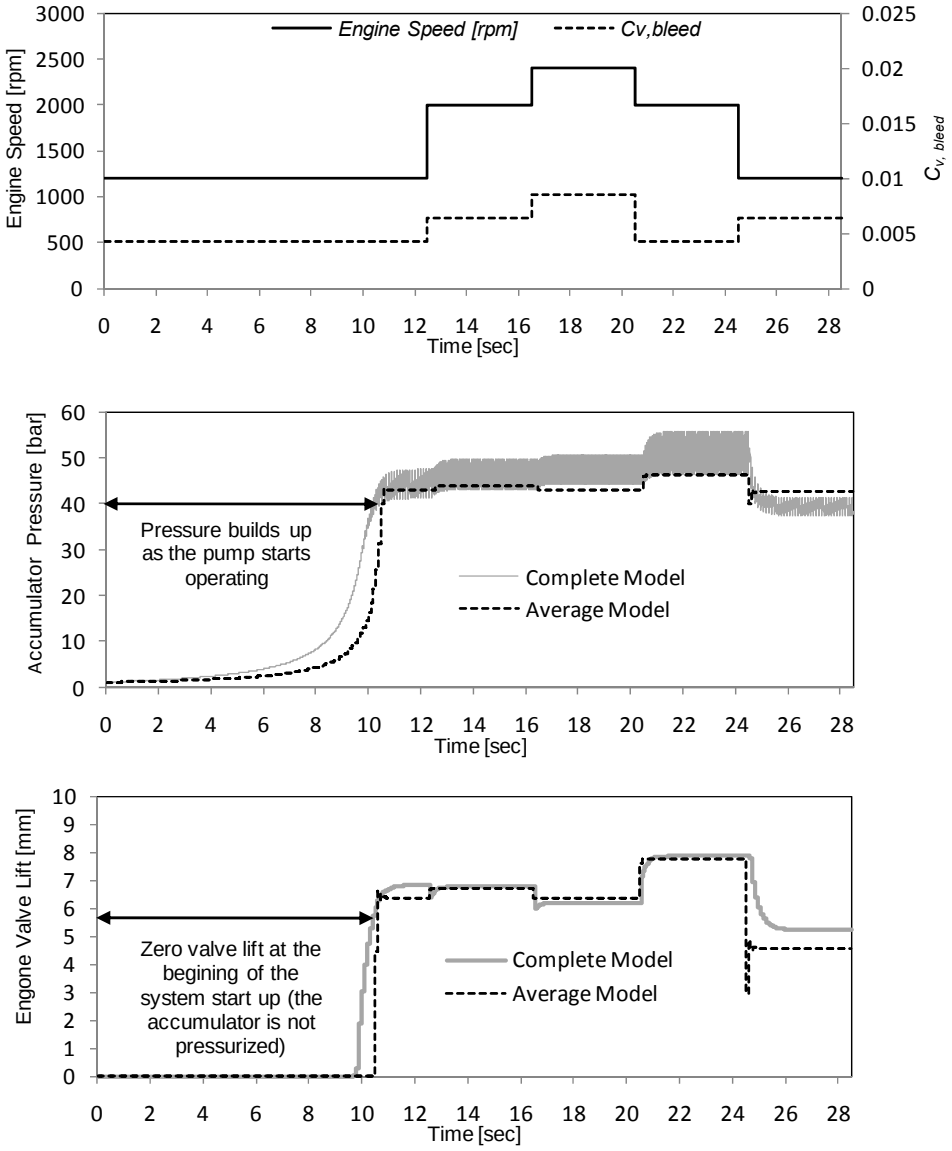

Figure 6-8: Comparison between the results for accumulator pressure and engine valve lift achieved from complete and average models at different engine speeds and bleed valve flow coefficients

6.5.3 Developing a Discrete Sliding Mode Controller

In this section, a discrete sliding mode controller is developed to control the non-linear discrete time system derived in Section 6.5.1. The sliding mode controller is known as the robust technique for controlling non-linear systems. Many studies have been performed on the stability of continuous sliding mode controllers [49], [50], [51]. In fact, with the invention

of ultra high speed processors, the need for using discrete time controllers have been diminished; however in this research, because the sampling rate is dictated by the engine cycle period, the use of a discrete controller with variable sampling time is inevitable. A few studies have been conducted on sliding mode control of discrete systems [52], [53], [54]. To design the lift controller based on the system average model given in (6.17), a sliding surface is defined by:

$$S_k = e_k + \lambda \sum_{i=1}^{k} e_i T_i \qquad ,\lambda > 0 \tag{6.22}$$

where, T_i is the sampling time (engine cycle period) and e_i is the lift tracking error at time step (engine cycle) i defined as:

$$e_i = L_f(i) - L_{f,ref}(i) \tag{6.23}$$

Here, the control problem is equivalent to that of reaching and remaining on the zero sliding surface $S^0 = \left\{ L_f \middle| S = 0 \right\}$.

Lemma 1. The lift tracking error e_k is asymptotically stable as the system rests on the plane S^0 for $k \geq k'$.

Proof. At the time steps $k' \ \ and \ \ \left(k'+1\right)$,

$$S_{k'} = 0 = e_{k'} + \lambda \sum_{i=1}^{k'} T_i e_i \tag{6.24}$$

$$S_{k'+1} = 0 = e_{k'+1} + \lambda \sum_{i=1}^{k'+1} T_i e_i \tag{6.25}$$

Subtracting (6.24) from (6.25) yields following relation between the lift tracking error at time steps k' and $k'+1$:

$$e_{k'+1} = \frac{e_{k'}}{\left(\lambda T_{k'+1} + 1\right)} \tag{6.26}$$

Similarly, at $\left(k'+2\right)^{th}$ time step, the tracking error is:

$$e_{k'+2} = \frac{e_{k'+1}}{\left(\lambda T_{k'+2} + 1\right)} = \frac{e_{k'}}{\left(\lambda T_{k'+2} + 1\right)\left(\lambda T_{k'+1} + 1\right)} \tag{6.27}$$

Subsequently, the tracking error at $\left(k'+n\right)^{th}$ time step is determined by:

$$e_{k'+n}=\frac{e_{k'}}{\left(\lambda T_{k'+n}+1\right)\left(\lambda T_{k'+n-1}+1\right)\cdots\left(\lambda T_{k'+1}+1\right)},n>0 \tag{6.28}$$

where,

$$\left(\lambda T_{k'+i}+1\right)>1 \qquad i=1,2,...,n \tag{6.29}$$

From (6.28) it is implied that as n increases, the tracking error approaches to zero asymptotically. The next step is to choose the control law u_k such that it guarantees the existence of the sliding mode. The control law consists of two distinct parts: equivalent and feedback control laws:

$$u_k=u_{fb}+u_{eq} \tag{6.30}$$

The equivalent control law (u_{eq}) is responsible for maintaining the system on the constant S plane while the feedback control law (u_{fb}) brings the system to the plane S^0.

Lemma 2. The equivalent control law for (6.17) such that the system rests on the plane of $\left\{S\middle|S_{k+1}=S_k\right\}$ for all k is given by:

$$u_{eq}=g_k^{-1}\left(L_{f,ref}(k)-f_k-\tilde{f}_k+\frac{e_k}{\lambda T_{k+1}+1}\right) \qquad ,g_k<0 \tag{6.31}$$

Proof. According to (6.22), the amount of S_{k+1} is determined by:

$$\begin{aligned}S_{k+1}&=e_{k+1}+\lambda\sum_{i=1}^{k+1}T_ie_i=\left(1+\lambda T_{k+1}\right)e_{k+1}+\lambda\sum_{i=1}^{k}T_ie_i\\&=\left(1+\lambda T_{k+1}\right)\left(L_f(k+1)-L_{f,ref}(k+1)\right)+\lambda\sum_{i=1}^{k}T_ie_i\end{aligned} \tag{6.32}$$

Using (6.17) and also assuming that on surface S^0 the system is only controlled by the equivalent control law, the above equation can be written as:

$$S_{k+1}=\left(1+\lambda T_{k+1}\right)\left(f_k+g_ku_{eq}+\tilde{f}_k-L_{f,ref}(k+1)\right)+\lambda\sum_{i=1}^{k}T_ie_i \tag{6.33}$$

Substituting (6.31) in (6.33) results in following equality:

$$S_{k+1} = e_k + \lambda \sum_{i=1}^{k} T_i e_i = S_k \tag{6.34}$$

Now, to determine the control law transferring the state to plane S^0, let V_k and ΔS_k be defined by:

$$V_k = \frac{1}{2} S_k^2 \tag{6.35}$$

$$\Delta S_{k+1} = S_{k+1} - S_k \tag{6.36}$$

where, V_k is a discrete Lyapunov function. Therefore, to transfer the system to the zero sliding surface, the control law should decrease V_k. In [53], it was proven that in order for V_{k+1} to be less than V_k, following inequality must be satisfied:

$$S_k \Delta S_{k+1} < -\frac{1}{2}\left(\Delta S_{k+1}\right)^2 \quad for \;\; S_k \neq 0 \tag{6.37}$$

The control law to satisfy (6.37) is given by the following lemma.

Lemma 3. The feedback controller (u_{fb}) for system (6.17) to transfer the states to plane of $S_k=0$ is given by:

$$u_{fb} = \frac{-K_{fb} g_k^{-1} S_k}{1 + \lambda T_{k+1}} \quad , \quad 0 < K_{fb} < 2 \tag{6.38}$$

Proof. As mentioned previously, in order for the system (6.17) to be stabilized on the plane S^0, the inequality (6.37) must be satisfied. Substituting (6.22) in (6.36), the following correlation is achieved for ΔS_{k+1}:

$$\Delta S_{k+1} = \left(1 + \lambda T_{k+1}\right) e_{k+1} - e_k \tag{6.39}$$

Using (6.17) and (6.23), the above equation can be reformulated to:

$$\Delta S_{k+1} = \left(1 + \lambda T_{k+1}\right)\left(f_k + g_k u_k + \tilde{f}_k - L_{f,ref}(k+1)\right) - e_k \tag{6.40}$$

where, control law u_k is determined by (6.30). Using (6.31), the above equation can be rewritten as:

$$\Delta S_{k+1} = \left(1+\lambda T_{k+1}\right)\left(f_k + g_k\left(u_{fb} + g_k^{-1}\left(L_{f,ref}(k+1) - f_k - \tilde{f}_k + \frac{e_k}{\lambda T_{k+1}+1}\right)\right) + \tilde{f}_k - L_{f,ref}(k+1)\right) - e_k \quad (6.41)$$

Simplifying (6.41), ΔS_{k+1} becomes:

$$\Delta S_{k+1} = \left(1+\lambda T_{k+1}\right) g_k u_{fb} \quad (6.42)$$

Substituting (6.42) in inequality (6.37) results in:

$$S_k\left(1+\lambda T_{k+1}\right) g_k u_{fb} < -\frac{1}{2}\left(1+\lambda T_{k+1}\right)^2 g_k^2 u_{fb}^2 \quad (6.43)$$

Since $\left(1+\lambda T_{k+1}\right) u_{fb}^2 \geq 0$, both sides of the inequality (6.43) can be divided by this term without changing the inequality sign:

$$\frac{S_k g_k}{u_{fb}} < -\frac{1}{2}\left(1+\lambda T_{k+1}\right) g_k^2 \quad (6.44)$$

According to (6.19), g_k is always negative; thus by dividing (6.44) by g_k, we have:

$$\frac{S_k}{u_{fb}} > -\frac{1}{2}\left(1+\lambda T_{k+1}\right) g_k \quad (6.45)$$

Since the term $-\frac{1}{2}\left(1+\lambda T_{k+1}\right) g_k$ is always positive, (6.45) can be written as:

$$\frac{S_k}{u_{fb}} = -K'_{fb}\frac{1}{2}\left(1+\lambda T_{k+1}\right) g_k \quad , \; K'_{fb} > 1 \quad (6.46)$$

where, K'_{fb} is the controller gain. Therefore, the feedback control law (u_{fb}) becomes:

$$u_{fb} = \frac{-2 g_k^{-1} S_k}{K'_{fb}\left(1+\lambda T_{k+1}\right)} \quad , \; K'_{fb} > 1 \quad (6.47)$$

Assuming $K_{fb} = 2 / K'_{fb}$, u_{fb} becomes:

$$u_{fb} = \frac{-K_{fb} g_k^{-1} S_k}{\left(1+\lambda T_{k+1}\right)} \quad , \quad 0 < K_{fb} < 2 \quad (6.48)$$

Now, by substituting (6.48) and (6.31) in (6.30), the final control law (u_k) is determined by:

$$u_k = g_k^{-1}\left(L_{ref}(k) - f_k - \tilde{f}_k + \frac{e_k}{\lambda T_{k+1} + 1} - \frac{K_{fb} S_k}{\left(1 + \lambda T_{k+1}\right)}\right) \quad , \quad \begin{cases} 0 < K_{fb} < 2 \\ \lambda > 0 \end{cases} \tag{6.49}$$

It should be noted that since $g_k < 0$ thus g_k^{-1} always exists. The above control law (u_k) is not realizable since computation of the equivalent control law (u_{eq}) requires complete information of the model uncertainty ($\tilde{f}_k$). To Solve this problem, one-step delayed uncertainty estimation has been used in [55], [56], [57]. Using this technique, the amount of uncertainty calculated at the end of the previous step is used as an approximation of the uncertainty for the current step.

$$\tilde{f}_k \approx \tilde{f}_{k-1} = L_f(k) - f_{k-1} - g_{k-1} L_f(k-1) \tag{6.50}$$

.

In (6.22), the summation of the tracking errors in the previous engine cycles is included to ensure zero steady state error; however in the presence of large initial error and also sudden changes in the reference valve lift, this integration process will lead to large error accumulation which may consequently cause large overshoots and actuator saturation. There are two approaches to solve this problem. In the first approach, a smaller value is chosen for the sliding surface gain (λ). This could severely diminish the controller performance in reducing the offset error. In the second method, which is more effective, the tracking error is accumulated only when the error is within a certain bound [51]. Using this method, the value of λ could be increased for better tracking performance.

6.6 ENGINE VALVE LIFT CONTROL PERFORMANCE

Figure 6-9 illustrates the implementation diagram of the lift control strategy for the proposed hydraulic valve actuation system. As shown in this figure, there are four inputs to and a single output from the lift controller. The inputs to the controller include the engine valve lift determined based on the complete valve profile at the end of cycle *k*, engine speed and desired valve lift signals coming from the ECU (engine control unit) and average accumulator pressure ($\bar{P}_1$) for the completed cycle. The controller output is the required bleed valve flow coefficient ($C_{v,bleed}$) which is calculated based on the correlation given in (6.49).

Using the map obtained for the bleed valve (Figure 6-6), the required bleed valve stem angle is estimated. To achieve the desired valve stem angle, a closed loop PID controller discussed in the previous section is used. The feedback signal to the PID controller is actual valve stem angle measured by a string potentiometer.

Based on the formulation derived for lift control, the control module of the experimental setup is programmed using structured text language and the system is run and tested for different inputs.

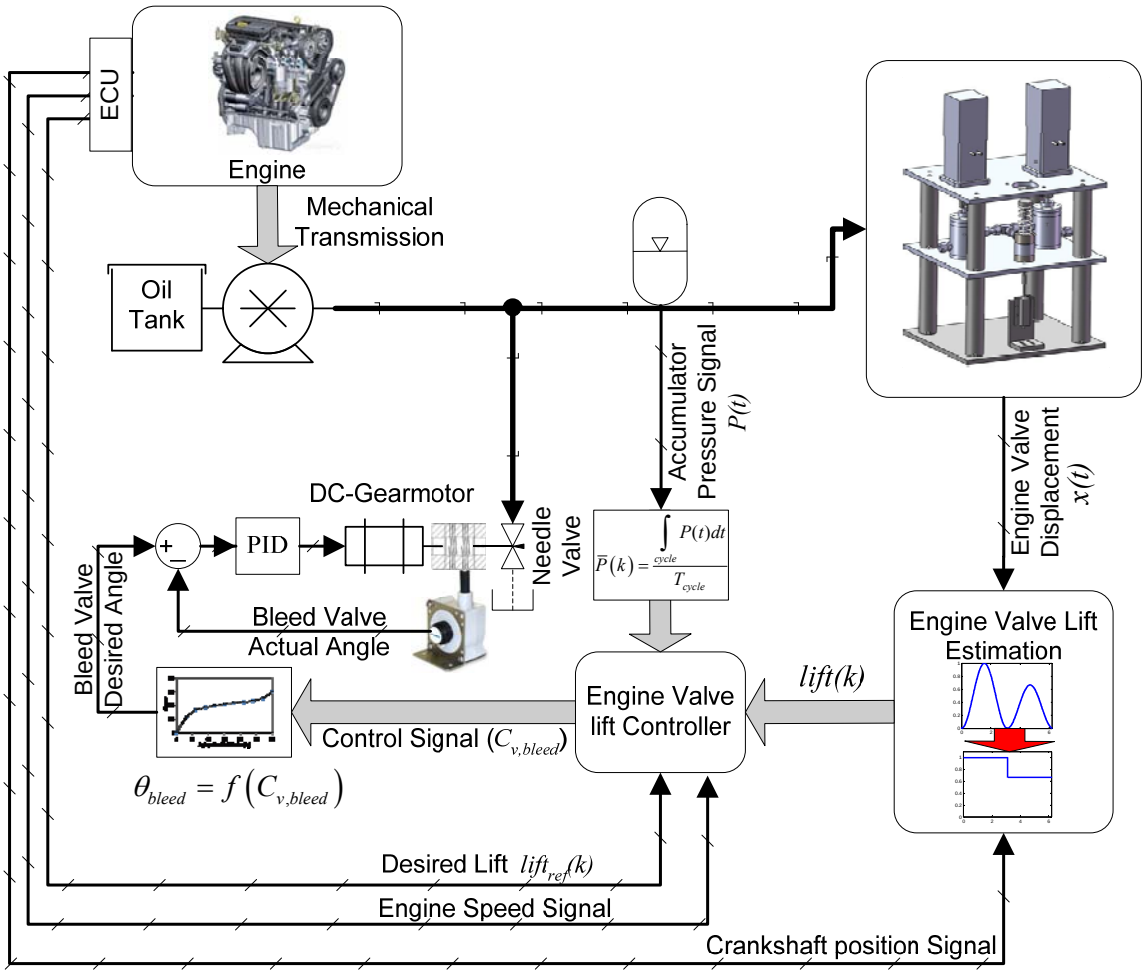

Figure 6-9: The implementation diagram of the designed lift controller in both simulation and experiment

Figure 6-10 shows the simulation and experimental results for the designed engine valve lift control system at constant engine and pump speeds (N_{engine}:1000rpm) and varying desired valve lift. The sliding mode controller parameters (λ and K_{fb}) along with model uncertainty factor (α) given in Table 6-1, are tuned through several experiments. Due to pump volumetric efficiency, the pump speed in the experiment is higher than that in the simulation ($N_{pump,exp}$:775rpm, $N_{pump,sim}$: 472rpm).

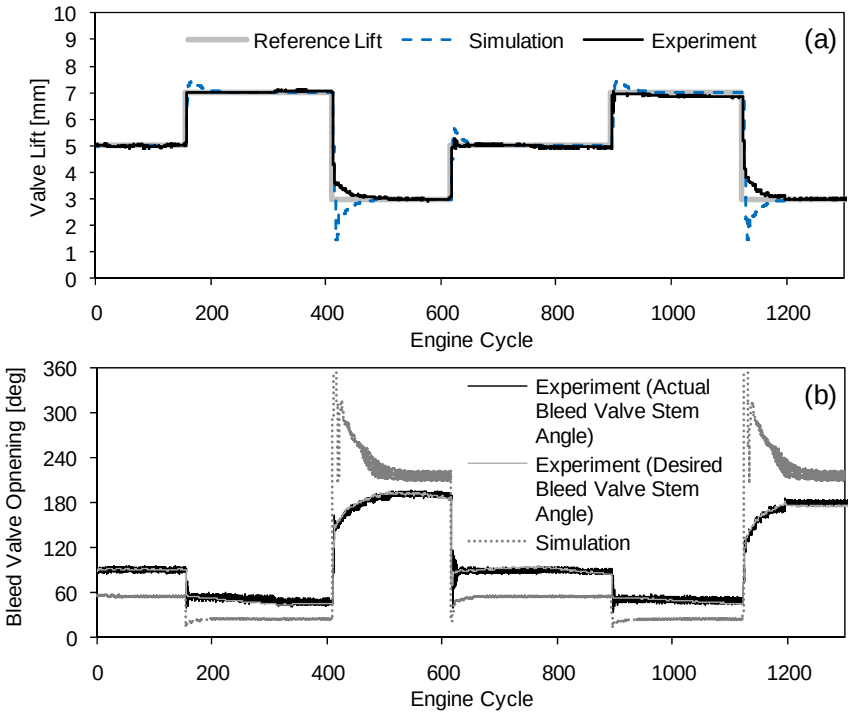

Figure 6-10: The tracking performance of the designed lift controller at constant engine speed (1000rpm)

As shown in Figure 6-10a, the designed model-based controller is capable of bringing the actual valve lift to the vicinity (within 0.5mm) of the desired lift in less than 5 engine cycles during sudden increase or decrease in the reference engine valve lift. The reason for the high overshoots observed in the simulation results is due to the fact that the values of λ and K_{fb} were tuned based on the experimental results for optimum system response. Figure 6-10b depicts the variation in the bleed valve opening stem angle to achieve the desired engine valve lift. The experimental results show that the bleed valve actual stem angular position

precisely follows the desired stem position computed by the controller. The considerable difference between the measured and simulated bleed valve stem angular positions is due to different pump speeds in experiment and simulation and also due to the absence of pump internal leakage in the simulation.

Table 6-1: The SMC parameters tuned through experiment

λ	K_{fb}	α
1/3	1.28	0.3

To evaluate the tracking performance of the proposed lift control strategy applied to the new VVA system, experimental data presented by Anderson et al [47] for an electro-hydraulic variable valve actuation (EHVVA) system is used. To this end, an experiment is run for identical conditions (similar engine speed and lift) and the results are compared. Figure 6-11 compares the engine valve lift control performance of the proposed VVA system with that of the existing EHVVA system. The comparison shows that the new VVA system with the proposed lift controller has a better settling time and smaller tracking error.

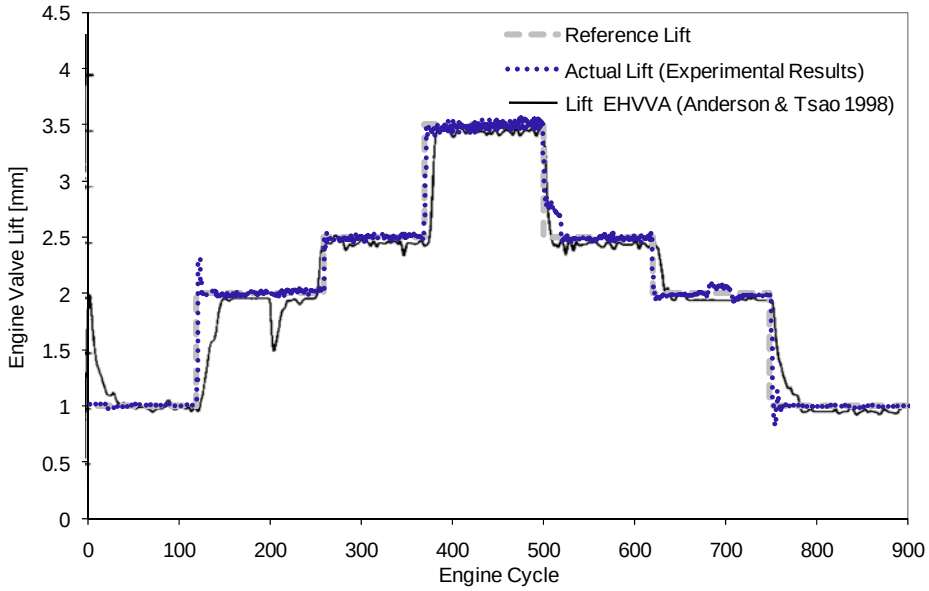

Figure 6-11: Comparison between the lift control performances of the proposed system and an existing EHVVA system at 2000 rpm

In both EHVVA system and proposed VVA system, maintaining the desired valve lift as the engine speed varies is another objective achieved by precise engine valve lift control. In fact, as the engine speed varies drastically, the valve opening frequency varies accordingly resulting in a sudden rise or drop in the final valve lift; therefore, in these valvetrains, the absence of a lift controller causes either an unwanted valve closure or mechanical interference between the valve and piston.

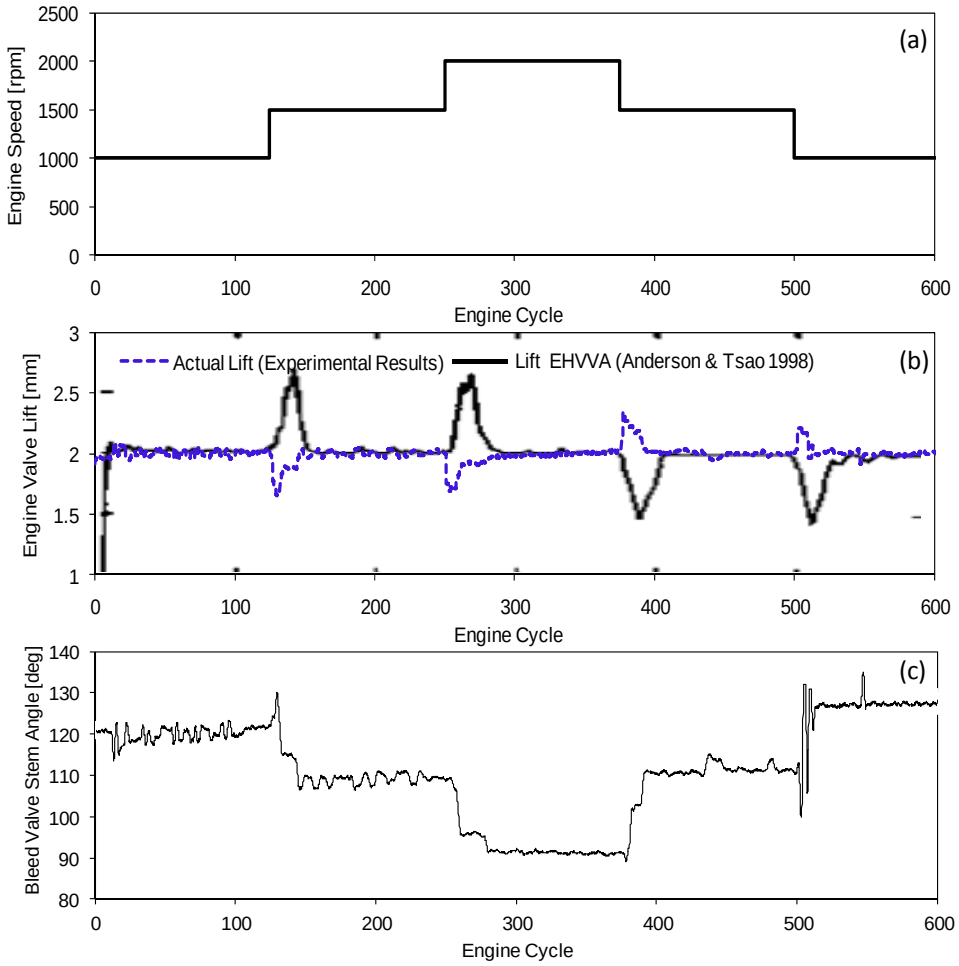

Figure 6-12: The efficacy of the designed lift controller in keeping the desired valve lift (2mm) during sudden variation in the engine speed (experiment)

In Figure 6-12b, the dashed line illustrates the variability of the final valve lift controlled by the proposed system during sudden changes in the engine speed shown in Figure 6-12a. Here,

the objective of the control problem is to maintain the final valve lift at 2mm at varying engine speed only by adjusting the bleed valve opening. Figure 6-12c shows the variations of the bleed valve stem angle determined by the developed valve lift controller. The experimental results achieved by the proposed VVA architecture show that during 500rpm step changes in the engine speed, the maximum lift deviation from its reference value does not exceed 0.4mm at all times. To investigate the quality of the achieved results, comparative data presented by Anderson et al in [47] for similar operating conditions are used (solid line in Figure 6-12b). The presented results from a conventional EHVVA system show that at similar changes in the engine speed, the maximum lift deviation exceeds 0.5mm.

6.7 SUMMARY

In this chapter, the proposed hydraulic variable valve actuation system was equipped with a novel valve lift control system. A more simplified and control-oriented dynamic model of the system was derived on the basis of energy and mass conservation principles and it was validated using the results obtained from the complete system model. Since the proposed average model is inherently in a discrete form (event-based), a discrete-time sliding mode controller insensitive to the sampling rate was designed using a discrete Lyapunov function. A sufficient condition for the controller gain to make the system stable was determined. The designed controller was incorporated into the complete model of the system and the entire system was studied numerically. The proposed lift control strategy was also implemented on the system experimental setup. The system control unit was then programmed with the developed discrete-time sliding mode control law and several experiments were performed to verify the performance of the proposed system. Following conclusions are made based on the experimental and numerical results:

- Using the proposed system it is possible to vary the engine valve lift from zero to its maximum allowable value at any operating condition.
- The experimental results showed that a desired engine valve lift is achieved in only few engine cycles with the proposed lift control strategy.

- Comparative data from an existing electro-hydraulic valvetrain were used to evaluate the competitiveness of the proposed system in tracking a desired valve lift and the comparison showed the excellence of the proposed system.

Chapter 7

Analysis of System Power Consumption and Robustness

So far, all the work done on the proposed VVA system was only to prove its feasibility, repeatability and precision; however, in order for the proposed valve actuation system to be considered as a substitute for conventional valvetrains, its power consumption and its robustness should be comparable with those in conventional cam-follower valvetrains. To this end, design parameters of the current system should be optimized for minimum power consumption and maximum robustness.

Several techniques including gradient or non-gradient methods can be used to optimize the design parameters of the system; however non-gradient methods are more robust in locating the global optima especially when the problem is not convex [58]. Another advantage of the non-gradient methods is that they do not require the derivative of the objective function to find the optimum point; therefore, these techniques are beneficial when the objective function is the result of complex computer simulation of highly non-linear mathematical models. Among different classes of non-gradient optimization methods, the genetic algorithm (GA), which was developed by Holland in early 70's [59], [60], is the one which is used in this work.

7.1 Improving System Power Efficiency and Robustness

In order for the new hydraulic VVA system to be applied to the production engines, its power efficiency and robustness should be maximized. For this purpose, design optimization has to be done to reduce the system power consumption while maintaining its performance in an

acceptable level. Several factors such as space limitation and costs are not considered in this optimization due to their high dependency to the engine requirement and size.

To optimize the proposed VVA system, the objective function and constraints of the optimization problem are initially formulated. In the next step, an optimization method is selected based on the type of the problem. The optimization problem is then solved numerically and the results are evaluated.

7.1.1 Optimization Parameters

Many design parameters affect the system performance; however the effects of some of the parameters on system optimization are trivial. For instance, increasing the size of the ports on the rotary spool valves or hydraulic cylinder will result in lower pressure drops and consequently lower power losses without violating the existing constraints; however, this increase is restricted by space availability. Moreover, increase in the opening angles of the rotary spool valves ports are also limited by the minimum required engine valve opening duration. Here in this study, the design parameters subjected to optimization are narrowed down to engine valve return-spring stiffness (K_{spring}) and preload ($F_{preload}$), hydraulic piston area (A_p) and accumulator precharge pressure ($P_{1,0}$) and volume ($V_{1,0}$); however, the proposed optimization structure can be easily expanded for more optimization parameters.

7.1.2 Objective function

In order for the new hydraulic VVA system to be applied on the production engines, its power consumption and robustness should be comparable with conventional valvetrain. In the proposed valve actuation system, the main portion of the input power is consumed in the hydraulic pump and the rest is used to actuate the rotary spool valves and phase-shifters; Owing to low friction between the rotary spool and its casing and also small flow forces, a small torque is required to rotate the spool shaft during valve operation. Also due to the intermittent operation of the phase shifters, their power consumption could be neglected. Thus, the objective function of the optimization problem could be estimated by the average power consumption of the hydraulic pump during one engine cycle:

$$J = \frac{\int_{cycle} P_1 Q_{pump} dt}{T_{cycle}} \tag{7.1}$$

There are two methods to calculate J at a certain engine operating condition. In the first method, the complete model of the system developed in Section 3.3 could be solved numerically over time using the initial conditions given below:

$$\begin{gathered} P_{1,t=0} = P_{1,0} \ , \ P_{2,t=0} = P_{1,0} \ , \ V_{1,t=0} = V_{1,0} \\ x_{t=0} = 0 \ , \ \dot{x}_{t=0} = 0 \end{gathered} \tag{7.2}$$

The simulation must be run until the accumulator pressure reaches to a certain level and a steady state condition is achieved (i.e. the values of the system states at one cycle become similar to those in the previous cycle). At this moment, the pump power consumption could be integrated and averaged through an engine cycle. In this method, because the initial accumulator pressure is far from the pressure required for the steady state operating condition, the simulation run time is relatively high resulting in high computational cost.

In the second method, the system operation during an engine cycle is divided into two time periods. The first time period starts as the high pressure rotary spool valve (HPSV) becomes fully closed (t_0) and it ends as the HPSV starts to open (t_1). The rest of the cycle (HPSV is open) is considered as the second time period (t_1 to t_2). Therefore, the objective function defined in (7.1) could be written as follows:

$$J = \frac{\int_{t_0}^{t_1} P_1 Q_{pump} dt}{T_{cycle}} + \frac{\int_{t_1}^{t_2} P_1 Q_{pump} dt}{T_{cycle}} = J_1 + J_2 \tag{7.3}$$

where,

$$\begin{bmatrix} t_0 & t_1 & t_2 \end{bmatrix} = \begin{bmatrix} 0 & \left(\frac{120}{N_{engine}} - \frac{\varphi_C + \varphi_S}{3N_{engine}} \right) & \frac{120}{N_{engine}} \end{bmatrix} \tag{7.4}$$

During the first time period, the input power to the pump is only used to increase the accumulator pressure which follows the equation below:

$$\frac{dP_1}{dt} = -k\frac{P_1^{\frac{k+1}{k}}}{P_{1,0}^{\ 1/k}V_{1,0}}\frac{dV_1}{dt} \tag{7.5}$$

Assuming zero bleed valve opening and negligible pump internal leakage, all the pumped fluid flows into the accumulator varying the trapped air volume:

$$\frac{dV_1}{dt} = -Q_{pump} \tag{7.6}$$

Substituting (7.5) and (7.6) in (7.3), the following relation is obtained for J_1:

$$J_1 = \frac{P_{1,0}V_{1,0}^k\left\{\left(\frac{1}{V_{1,t_0} - Q_{pump}\left(t_1 - t_0\right)}\right)^{k-1} - \left(\frac{1}{V_{1,t_0}}\right)^{k-1}\right\}}{\left(k-1\right)T_{cycle}} \quad , \; if \;\; k \neq 1 \tag{7.7}$$

$$J_1 = \frac{P_{1,0}V_{1,0}\ln\left(\frac{V_{1,t_0}}{V_{1,t_0} - Q_{pump}\left(t_1 - t_0\right)}\right)}{T_{cycle}} \quad , \; if\, k = 1 \tag{7.8}$$

where, $V_{1,t0}$ is the volume of the air trapped in the accumulator at the beginning of the first time interval (t_0). During the second time interval (t_1 to t_2), the following non-linear dynamic system must be solved numerically:

$$\dot{X} = f\left(X,t\right) \tag{7.9}$$

where,

$$X = \left[x, \dot{x}, P_1, P_2\right]^T \tag{7.10}$$

$$f\left(X,t\right) = \begin{bmatrix} \dot{x} \\ \dfrac{P_2A_pK_{spring}x - F_{preload} - F_{gas} - \text{sign}\left(\dot{x}\right)F_{friction}}{m} \\ k\dfrac{P_1^{\frac{k+1}{k}}}{P_{1,0}^{\ 1/k}V_{1,0}}\left(Q_{pump} - A_{HPSV}C_d\text{sign}\left(P_1 - P_2\right)\sqrt{\dfrac{2\left|P_1 - P_2\right|}{\rho}}\right) \\ \dfrac{\beta}{V_{2,0} + A_px}\left(A_{HPSV}C_d\text{sign}\left(P_1 - P_2\right)\sqrt{\dfrac{2\left|P_1 - P_2\right|}{\rho}} - A_p\dot{x}\right) \end{bmatrix} \tag{7.11}$$

$$A_{HPSV} = \begin{cases} \dfrac{2A_{HPSV,\max}\left(t - t_1\right)}{t_2 - t_1} & t_1 < t < \dfrac{t_1 + t_2}{2} \\ A_{HPSV,\max} - \dfrac{2A_{HPSV,\max}\left(t - (t_1 + t_2)/2\right)}{t_2 - t_1} & \dfrac{t_1 + t_2}{2} < t < t_2 \end{cases} \tag{7.12}$$

The initial conditions for the above differential equation are as:

$$[x, \dot{x}, P_1, P_2]^T_{@t_1} = \left[0, 0, P_{1,t_1}, P_{reservoir}\right]^T \tag{7.13}$$

where, P_{1,t_1} is the air accumulator pressure at the beginning of the second time interval and $P_{reservoir}$ is the oil reservoir pressure. Assuming constant pump flow and zero leakage, P_{1,t_1} could be determined by:

$$P_{1,t_1} = \frac{P_{1,0}V^k_{1,0}}{V^k_{1,t_1}} = \frac{P_{1,0}V^k_{1,0}}{\left(V_{1,t_0} - Q_{pump}\left(t_1 - t_0\right)\right)^k} \tag{7.14}$$

By solving the dynamic system given in (7.11), P_1 will be obtained for the time period (t_1 to t_2) and based on that J_2 will be estimated. However, calculating the amounts of both J_1 and J_2 necessitates approximation of $V_{1,t0}$. Using the fact that during the steady state condition, the accumulator pressure at a certain time instant within an engine cycle will be equal to that at the corresponding time instants in the previous or next engine cycles, the following sub-problem could be used to estimate $V_{1,t0}$:

$$find \;\; V_{1,t0} \;\; s.t. \;\; P_{1,t0} = P_{1,t2} \tag{7.15}$$

To this end, function $g(V_{1,t_0})$ is defined as follows:

$$g\left(V_{1,t_0}\right) = \frac{P_{1,0}V^k_{1,0}}{V^k_{1,t_0}} - \begin{bmatrix} 0 & 0 & 1 & 0 \end{bmatrix}\left(\int_{t_1}^{t_2} f\left(X,t\right)dt + i.c.\right) \tag{7.16}$$

where, the initial conditions for the above integration are:

$$i.c. = \begin{bmatrix} 0 & 0 & V_{1,t_0} & P_{reservoir} \end{bmatrix} \tag{7.17}$$

Therefore, the problem of finding $V_{1,t0}$ could be transformed into:

$$find \quad V_{1,t0} > 0 \quad s.t \quad g\left(V_{1,t0}\right) \to 0 \tag{7.18}$$

The above problem can be solved using Newton-Raphson method. Consequently, the accumulator pressure at the beginning of engine valve opening stage during steady operation is determined by:

$$P_{1,t0} = \frac{P_{1,0} V_{1,0}^{k}}{V_{1,t0}^{k}} \tag{7.19}$$

7.1.3 Constraints

In the minimization of the power consumption, several optimization constraints must be satisfied. Among these constraints, three of them have the highest degree of importance; first, full engine valve closure must be guaranteed at the end of valve closing stage; second, the system robustness should not be sacrificed for the sake of power minimization and third, the maximum upstream pressure should not exceeds the pump allowable pressure.

As the system is optimized for minimum power consumption, some of the design parameters such as hydraulic cylinder diameter, valve spring stiffness and preload might vary such that full engine valve closure could not be achieved at the end of valve closing stage especially at high engine speeds. This results in drastic reduction in the engine power which is not acceptable. The engine valve closing stage is modeled with:

$$\frac{d}{dt}\begin{bmatrix} x \\ \dot{x} \\ P_2 \end{bmatrix} = \underbrace{\begin{bmatrix} \dot{x} \\ \left(P_2 A_p - K_{spring} x - F_{preload} - F_{gas} - \text{sign}\left(\dot{x}\right) F_{friction}\right) / m \\ \dfrac{\beta}{V_{2,0} + A_p x}\left(A_{LPSV} C_d \sqrt{2\left(P_2 - P_{reservoir}\right) / \rho} - A_p \dot{x}\right) \end{bmatrix}}_{H} \tag{7.20}$$

Therefore, the first equality constraint of the optimization problem could be defined by:

$$c_1 : \begin{bmatrix} 1 & 0 & 0 \end{bmatrix} \left(\int_{0}^{\frac{\varphi_s + \varphi_c}{3N_{engine,\max}}} H\left(t\right) dt + i.c. \right) = 0 \tag{7.21}$$

where, the initial conditions are:

$$i.c. = \begin{bmatrix} L_f & 0 & \dfrac{F_{preload} + K_{spring} L_f}{A_p} \end{bmatrix} \tag{7.22}$$

The second optimization constraint is related to the system robustness. The aim of this constraint is to keep the sensitivity of the engine valve trajectory to external disturbances, such as engine cycle-to-cycle variations, at an acceptable level. In fact, due to variation in the engine peak cylinder pressure, the amount of combustion gases forces applied to the engine poppet valves during valve opening stage could vary significantly from one cycle to another. In the proposed VVA architecture, shown in Figure 3-1, this variation in the cylinder gas force can easily affect the final valve lift and deteriorate the system repeatability. In fact, if the engine cylinder pressure at the beginning of the exhaust stage at the current cycle is very different from that in the previous cycle, the final valve lift at the current cycle will be different from that in a previous cycle. This results in different trapped air volume in the accumulator and consequently different upstream pressure at the beginning of the next cycle. The fluctuation in the final valve lift continues until the cylinder gas force at the onset of engine valve rise interval becomes stable from one cycle to another. If the system designed based on the proposed architecture suffers from poor robustness, the engine cycle-to-cycle variation could either result in extremely high engine valve lift or cause unwanted valve closure through the whole cycle. To set a robustness constraint for the discussed optimization problem, it is assumed that there exists a possibility of 50% cycle-to-cycle variation in the engine cylinder pressure and its effect on the final valve lift is evaluated according to:

$$lift\ \ variation\,\% = 100 \frac{\left| \begin{bmatrix} 1 & 0 & 0 & 0 \end{bmatrix} \left(\int_{t_1}^{t_2} f\left(X,t\right)\Big|_{P_{cyl}} dt - \int_{t_1}^{t_2} f\left(X,t\right)\Big|_{(1\pm 0.5)P_{cyl}} dt \right) \right|}{\int_{t_1}^{t_2} f\left(X,t\right)\Big|_{P_{cyl}} dt} \tag{7.23}$$

Therefore, the second inequality constraint is defined by:

$$c_2 : \left(lift\ \ variation - \varepsilon \right) \leq 0 \tag{7.24}$$

where, ε is the maximum allowable variability of the engine valve lift as the engine cycle-to-cycle variation reaches up to 100%.

The final optimization constraint is the maximum system pressure. In fact as the system pressure increases, the chance of hydraulic leakage increases too. Moreover, due to mechanical limitations, the pump downstream pressure should be always below its maximum allowable working pressure (P_{max}):

$$c_3 : P_1\left(t\right) - P_{\max} \leq 0 \;\; , \;\; t_0 \leq t \leq t_2 \tag{7.25}$$

7.1.4 Optimization Technique

The optimization problem discussed in the previous section is a non-linear constrained optimization (NCO) in the form of:

$$\underset{z}{\text{minimize}} \;\; J\left(\vec{z}\right) \;\; \text{subject to} \;\; c : \begin{cases} c_1\left(\vec{z}\right) = 0 \\ c_2\left(\vec{z}\right) \leq 0 \\ c_3\left(\vec{z}\right) \leq 0 \end{cases} \;\; \text{and} \;\; \vec{z} \geq 0 \tag{7.26}$$

$$\vec{z} = \begin{bmatrix} A_p & K_{spring} & F_{preload} & V_{1,0} & P_{1,0} \end{bmatrix}^T \tag{7.27}$$

where, the objective function $J : \mathbb{R}^{4+} \rightarrow \mathbb{R}^{+}$, and the constraint functions $c : \mathbb{R}^{4+} \rightarrow \mathbb{R}^{3}$ are all continuous functions. Since there are no closed form expressions for the objective and the constraint functions, there will be no derivative of the objective function available in a straightforward manner. Thus, using a derivative-based optimization method to solve (7.26) will be computationally expensive and does not always guarantee finding the global minimum. There are several non-derivative optimization techniques for solving non-linear constrained optimization problems. These methods include but not limited to complex method [61], Rosenbrock algorithm [62], pattern search method, Simplex method [63] and genetic algorithm [58]. However, among the non-derivative methods, genetic algorithm (GA) is the most robust technique in locating the global optimum. Here in this study, the genetic algorithm method is used to globally minimize the objective function (J) while satisfying all the constraints (c_i).

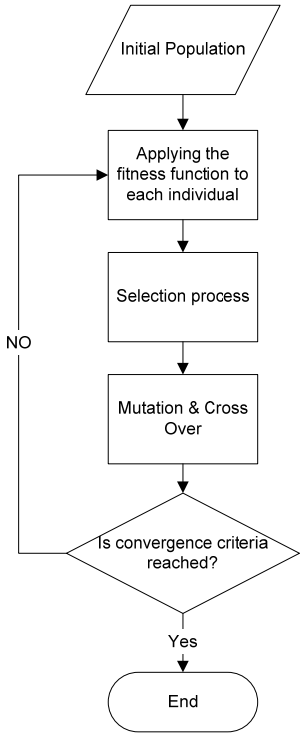

Figure 7-1: The schematic flowchart of the GA optimization

In the genetic algorithm developed for this optimization problem, each chromosome is created based on a combination of different values of optimization parameters discussed in Section7.1.1. The fitness value of each chromosome is determined based on the values of the corresponding objective function and constraints. A set of chromosomes forms a population where the fittest ones are selected to reproduce a new set of chromosomes and consequently a new population. The process of mating between selected parents consists of two main processes: crossover and mutation. In the crossover process, the parents from the mating pool give rise to two off-springs through exchanging some of their genes. During mutation, some of the chromosomes are changed by changing some of their genes in a random way. Although the mutation process deteriorates the convergence of the optimization process, it significantly improves the diversity of the population and consequently the possibility of finding the global optimum. Figure 7-1 illustrates the different stages of the genetic algorithm optimization. The detail discussion of the genetic algorithm is not in the scope of this dissertation.

7.1.4.1 Encoding

In genetic algorithm, each optimization parameter must be encoded by gene using an appropriate representation such as a real number or a string of bits (binary) [58]. Although the values of optimization parameters described in Section 7.1.1 are all positive real numbers, to meet the fabrication limitations and tolerances and also to reduce the computational costs, it is assumed that the minimum allowable variation in each design parameter during the optimization process is limited by a certain value providing this limitation does not significantly affect the optimization performance. Hence, in this problem, instead of real encoding, a binary encoding is used to generate genes. Moreover, it is possible to choose a lower/upper bounds for each design parameters; however, if the optimization is converged at parameters upper/lower bounds, then these bounds should be further relaxed. Table 7-1 presents the values of the upper/lower bounds and also minimum allowable variations selected for each optimization parameters.

Table 7-1: The optimization parameters bounds and minimum allowable variations

	K_{spring} [kN/m]	$F_{preload}$ [N]	A_p [mm2]	$P_{1,0}$ [kPa]	$V_{1,0}$[cc]
Min	1	0	10	100	1
Minimum Variation	4	15	7	10	7
Max	125	465	227	1000	218

Based on the maximum and minimum bounds and also minimum allowable variation of the design parameter z_i, an n-bit binary code is used as a representative of the design parameter value, where n is determined as follows:

$$n(z_i) = \log_2 \left(\frac{\max(z_i) - \min(z_i)}{\text{minimum allowable variation}(z_i)} + 1 \right) \tag{7.28}$$

The corresponding genes for the design parameters could form an m-bit chromosome which describes an individual design solution (z).

$$m = \sum_{i=1}^{r} n(z_i) \tag{7.29}$$

7.1.4.2 Fitness Function (FF)

The initial population is generated using a set of chromosomes each contains binary encoded design parameters with random value. The next step is to apply a fitness function to each one of these chromosomes to measure the quality of the solution encoded by each chromosome. The fitness of each chromosome is a value that reflects its performance and is usually determined by evaluating the optimization objective function (J) while considering all the constraints (c_i). During the last few years, several methods have been proposed for handling the non-linear constraints when using genetic algorithm for an optimization problems; however, most of the proposed constraint-handling methods have been based on the concept of penalty function. In this method, the fitness function is arranged such that the infeasible solutions ($\vec{z} \notin \mathbb{F}$) are penalized as follows:

$$FF\left(\vec{z}\right) = \begin{cases} J\left(\vec{z}\right) & if \quad \vec{z} \in \mathbb{F} \\ J\left(\vec{z}\right) + penalty\left(\vec{z}\right) & otherwise \end{cases} \tag{7.30}$$

Using this method, the constrained optimization problem is converted into an unconstrained problem. Usually the value of the penalty function is based on the distance of the solution $\vec{z}$ from the feasible region $\mathbb{F}$ and the effort to repair the solution. There are several methods to define the penalty function. These methods include static penalties [64], dynamic penalties [65], annealing penalties [66] and adaptive penalties [67]. In this study, the second method is used as a base to define the penalty function. Based on the method of dynamic penalties, the fitness function is formulated as follows:

$$FF\left(\vec{z}\right) = \begin{cases} J\left(\vec{z}\right) & if \quad \vec{z} \in \mathbb{F} \\ J\left(\vec{z}\right) + \iota^{\alpha_1} \sum_{j=1}^{m} R_j c_j^{\alpha_2} & otherwise \end{cases} \tag{7.31}$$

Where, α_1 and α_2 are constants and R_j is a constant multiplier for j^{th} constraint. In the above equation, ι is the optimization iteration number. By using the dynamic penalty method, the constraints are initially relaxed and the forces on the infeasible solutions are increased as the optimization proceeds. This increases the chance of finding the global minimum when it is located close to the constraint boundaries.

7.1.4.3 Selection and Recombination

Knowing the fitness of the individuals at each generation, a selection process can take place to choose the fittest individuals which will be the parents of the succeeding generation. There are several selection methods proposed for the genetic algorithm; however the most commonly used selection schemes are as follows:

- Proportional selection (roulette wheel, stochastic remainder and stochastic universal)
- Ranking selection (linear or exponential)
- Tournament selection
- Truncated selection

In this optimization problem, the proportional method is used to select the parents of the next generation. This method is the original selection method proposed for genetic algorithm by Holland [59]. The next step to generate a next population is recombination. The recombination step includes crossover and mutation processes. After the parents being selected, crossover takes place. During this stage, some of the genes of a pair of individuals are exchanged to create the new offspring. Mutation is another important genetic operator that randomly changes the genetic structure of the individuals. This operator allows the introduction of new individual to the population and consequently reduces the loss of diversity. The Matlab GA command is used to solve the optimization problem discussed in this study. Table 7-2 shows the settings used in the genetic algorithm optimization.

Table 7-2: The GA optimization setting

Population Type	***Selection Method***	***Mutation Method***	***Crossover Method***	***Ratio of crossover to mutation***
Binary	stochastic universal	Gaussian	Scattered	0.6

7.1.4.4 Generalized Optimization

Due to wide range of engine speed, the optimization should be performed for different valve operating speeds. Since the objective function and the constraints, developed in the previous sections, are functions of engine speed, consequently this will result in a few sets of optimal

solutions instead of a unique one. To solve this problem, a generalized form of the fitness function independent of the engine speed is introduced as follows:

$$FF_{gen}(\vec{z}) = \sum_{i=1}^{n} \omega_i FF_i\left(\vec{z}\right) \tag{7.32}$$

where,

$$\Delta N_{engine} = \frac{N_{engine,\max}}{n} \quad , \; n > 1 \tag{7.33}$$

$$FF_i\left(\vec{z}\right) = \begin{cases} J\left(\vec{z}, i \times \Delta N_{engine}\right) & if \quad \vec{z} \in \mathbb{F} \\ J\left(\vec{z}, i \times \Delta N_{engine}\right) + \iota^{\alpha_1} \sum_{j=1}^{m} R_j c_j^{\alpha_2}(\vec{z}, i \times \Delta N_{engine}) & otherwise \end{cases} \tag{7.34}$$

In (7.32), ω_i is the fitness function multiplier corresponding to the i^{th} engine speed and its value varies from one drive cycle to another.

7.2 Accuracy of the Objective Function and Constraint Approximations

In this section, the simplified models proposed to approximate the objective function and constraints are verified using the results from the complete model of the system given in Section 3.3. These models and correlations include the governing equations given for engine valve opening stage (7.11), engine valve closing stage (7.20), and also the model given for approximating the accumulator pressure right before the engine valve opening stage ($P_{1,t0}$) during steady state operation (7.18). To this end, the complete model of the system is run for an arbitrary operating condition (1500rpm, 10mm lift, and zero in-cylinder gas force) using the design parameters given in Table 4-1 and the results are compared with those achieved from the models used in the optimization.

To verify the correctness of the correlation given for the accumulator pressure at the beginning of the engine valve opening interval ($P_{1,t0}$), the complete model of the system is run from the initial system condition ($P_{1,0}$=*1bar* , $V_{1,0}$= *200cc*) until the steady operating condition is achieved (i.e. the final valve lift is unchanged from one cycle to another). At this time, the value of $P_{1,t0}$ is recorded and it is compared with that achieved through solving

(7.18). Figure 7-2 shows the comparison between results from both models at wide range of engine speeds (1000-5000rpm).

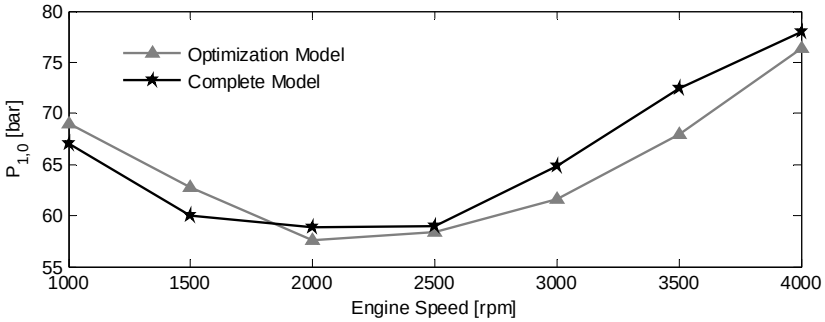

Figure 7-2: Comparison between $P_{1,t0}$ achieved from the system complete model and that approximated using (7.18) at wide range of engine speeds (1000-5000rpm)

As shown in this figure the difference between the two set of results does not exceed 7% at all engine speeds. The accuracy of the mathematical model used for the optimization problem is further investigated by comparing the engine valve profile and accumulator pressure achieved from the simplified model with those resulted from the complete model at steady operating condition (1500rpm). As shown in Figure 7-3 and Figure 7-4, there is a good agreement between the results achieved from both models.

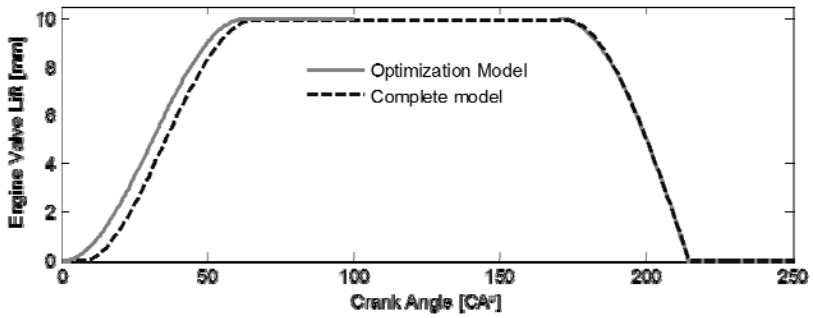

Figure 7-3: Comparison between the engine valve trajectory achieved from the complete model of the system during steady operation and that obtained from (7.11) and (7.20) at 1500rpm

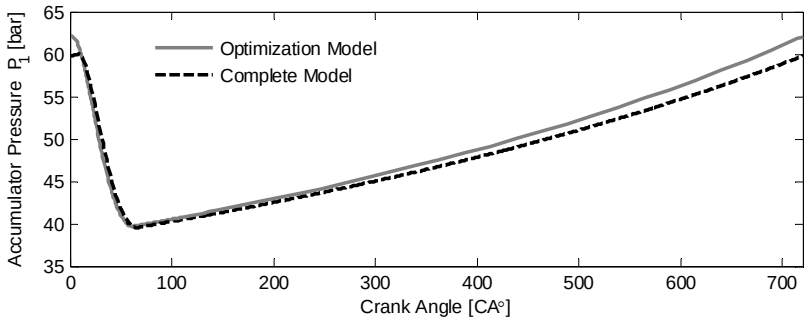

Figure 7-4: Comparison between the accumulator pressure achieved from the complete model of the system during steady operation and that obtained from (7.11) and (7.20) at 1500rpm

7.3 SYSTEM OPTIMIZATION RESULTS

The optimization problem discussed in Section 7.1 is initially solved at different engine speeds (1000 to 5000rpm) using the objective function given in (7.31) and the results are compared with those obtained from the optimization with the generalized objective function given in (7.32).

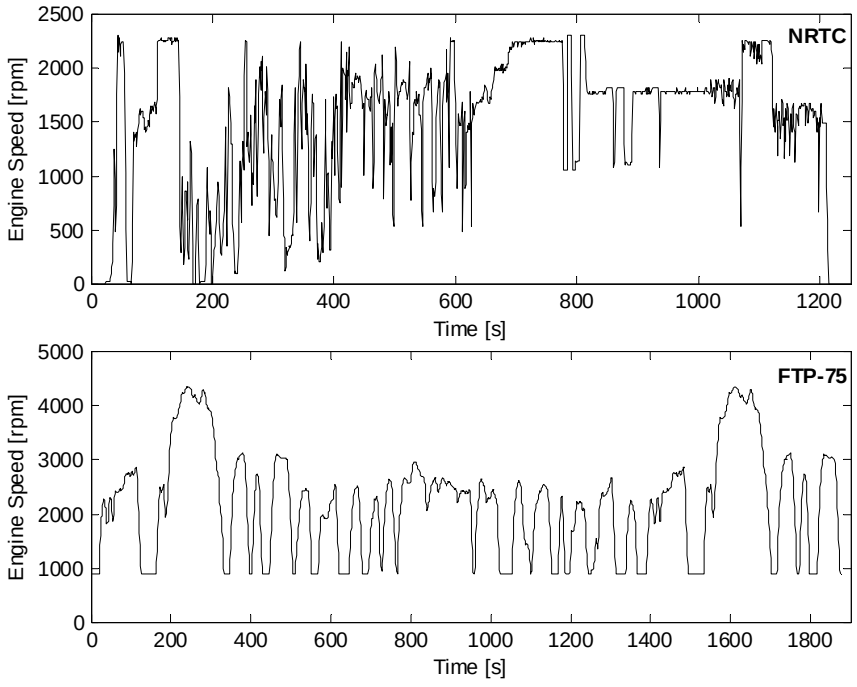

Figure 7-5: Engine speed trend in NRTC (heavy duty engines) and FTP-75 (light duty engines) cycles

In the optimization with generalized form of objective function, the values of ω_i (engine speed weight factor) at different engine speeds can be determined using an engine test cycle most fitted to the valve system application (e.g. NRTC, FTP-75, etc). Figure 7-5 shows the engine speed trend during NRTC and FTP-75 cycles. To determine ω_i at different engine speeds, the probability distribution of the engine speed is plotted for each test cycle (Figure 7-6). Here in this study, the FTP-75 test cycle is chosen to be used for valve system optimization.

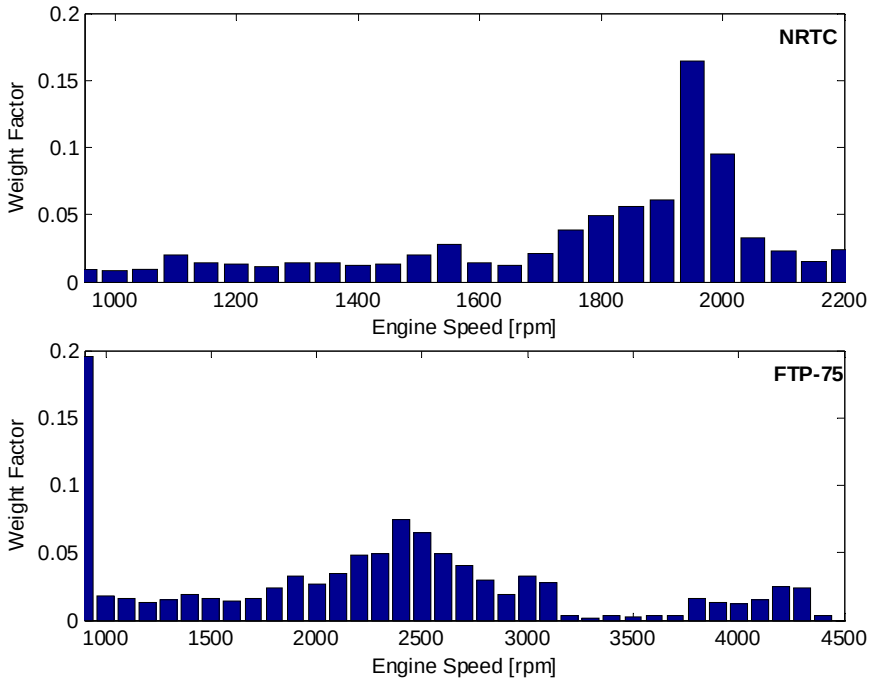

Figure 7-6: Weight factor (ω_i) for different engine speeds in NRTC and FTP-75 cycles

In the proposed valve system, improving the system robustness is crucial especially for the exhaust valve actuators where the effect of engine cycle-to-cycle variation on the valve operation is significant. Due to the trade-off existing between the valve system robustness and its power consumption, the system optimum design is a compromise between these two factors. To model the engine cycle-to-cycle variation, the cylinder gas force model presented in [44] is used. This model was obtained based on the peak cylinder pressure of 6 bar at the beginning of the exhaust stage for a 29 mm diameter poppet valve [68]. Figure 7-7 shows the value of the in-cylinder gas force on the engine valve at different valve displacement levels

during opening interval. It is assumed that at worst condition, the in-cylinder gas force could fluctuate up to 100% (400 to 0 N) from one cycle to another.

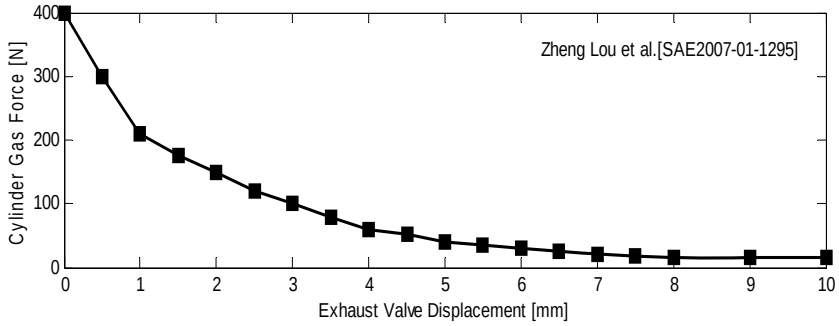

Figure 7-7: In-cylinder gas force versus engine valve displacement during exhaust valve opening stage [44]

In this optimization, the maximum sensitivity of the engine valve lift to cycle-to-cycle variation in in-cylinder gas pressure is set to 30% of the desired lift (10 mm), the maximum engine speed at which full valve closure must be guaranteed is set to 5000rpm and the maximum system upstream pressure is set to 200 bar. Due to the dependency of the piston friction forces including coulomb and viscose frictions on the type of the hydraulic cylinder and its sealing, the effect of these forces are not considered in this optimization problem.

The optimum design parameters resulted from system optimization at different engine speeds are given in Table 7-3. As it is seen in this table, the system optimized parameters changes with the engine speed. In fact, during the system optimization at a specific engine speed, the optimization only tries to minimize the power consumption while satisfying the sensitivity and pressure constraint at that engine speed. As shown in Figure 7-8 and Figure 7-9, for those optimizations performed at individual engine speed, the optimum parameters always satisfies the constraints at that engine speed but not at all engine speeds. Among all set of optimum parameters, only those achieved for a range of engine speed (optimum 6) satisfies the constraints at all engine operating conditions; however, as illustrated in Figure 7-10, this set of optimized parameters will lead to a higher power consumption compared with others. In fact, in the last optimization, the power efficiency of the system is scarified for its robustness and durability.

Table 7-3: The optimized design parameters at different engine speed settings

Optimization	Engine Speed [rpm]	Optimized Parameters			
		K [N/m]	$F_{preload}$ [N]	A_p [mm^2]	$V_{1\,@1bar}$ [cc]
Optimum (1)	1000	53000	0	164	73
Optimum (2)	2000	77000	0	66	38
Optimum (3)	3000	81000	0	136	115
Optimum (4)	4000	45000	0	206	31
Optimum (5)	5000	65000	0	164	66
Optimum (6)	1000-5000	113000	0	52	171

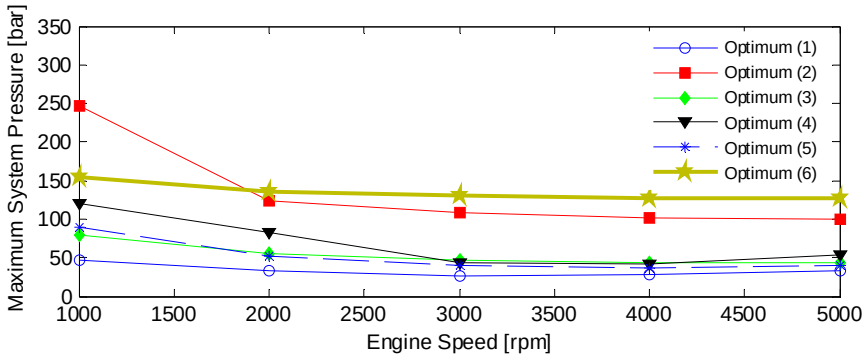

Figure 7-8: Maximum accumulator pressure at different engine speeds for different sets of optimum design parameters

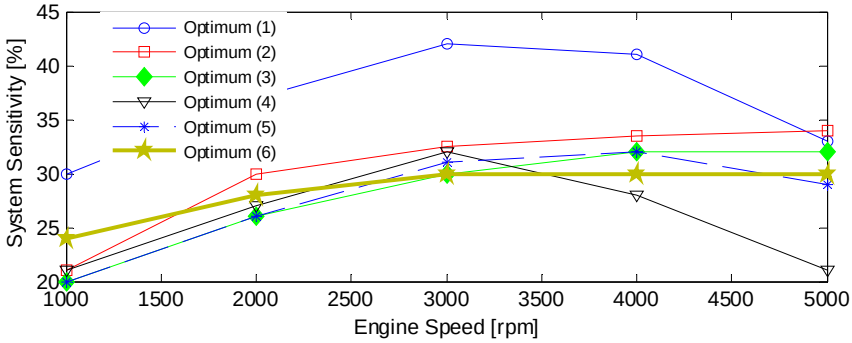

Figure 7-9: The engine valve lift sensitivity at different engine speeds for different sets of optimum parameters

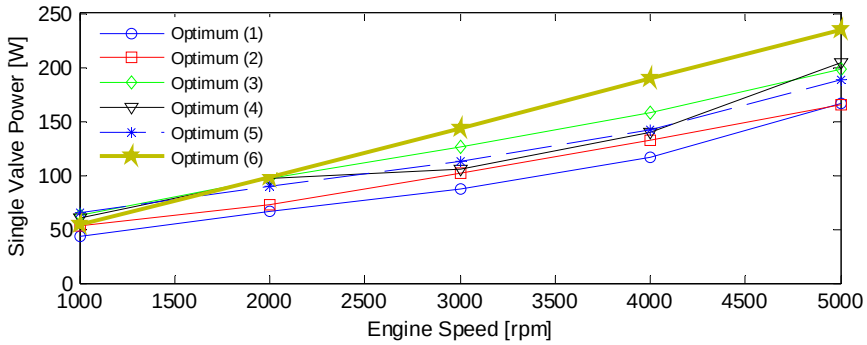

Figure 7-10: Power consumption of a single valve actuator at different engine speeds for different set of optimized design parameters

To study the effect of system robustness on power consumption, the optimization is solved for various levels of system's sensitivity (ε). Figure 7-11 shows the tradeoff between power consumption and valve lift sensitivity of the system optimized at 3000rpm engine speed. As shown in this figure, reducing the proposed VVA system sensitivity from 50% to 20% will raise the system power consumption by more than 2.3 times.

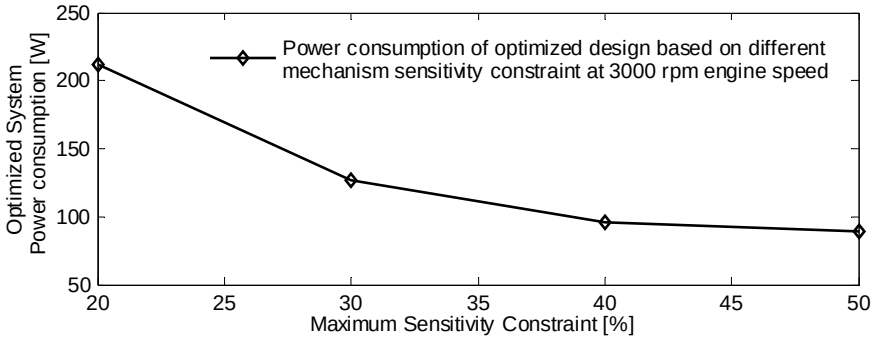

Figure 7-11: Power consumption of the optimized system (optimum 3) versus system sensitivity

To quantify the improvement in the system power efficiency as the result of optimization, the power consumption of the valve system prototype is measured at hydraulic pump outlet and it is compared with the simulation results for the optimized system. For more realistic comparison, the hydraulic piston-cylinder friction force identified in Section 4.2 is included in the simulation. In Figure 7-12, the hydraulic power of the original system is compared with that in the optimized system. As shown in this figure, the power efficiency of the optimized system is minimum 33% higher than that in the original system. Moreover, the optimized system was designed to operate up to 5000 rpm engine speed while in the

prototype system, due to the low return spring stiffness, the maximum operating engine speed is 2500 rpm.

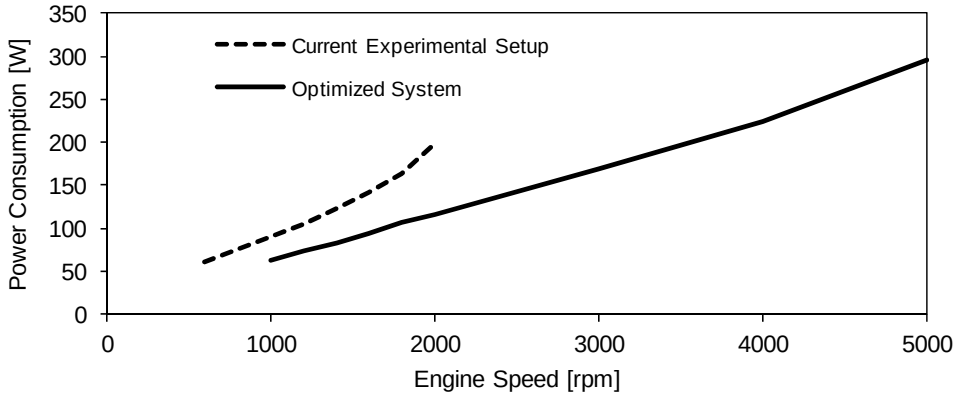

Figure 7-12: Comparison between the power consumptions of the prototype and optimized system (optimum 6)

7.3.1 Effect of HPSV opening angle on power consumption

In the proposed VVA system, the maximum engine valve rise duration depends on the HPSV opening angle which is limited to the minimum required engine valve opening duration over wide range of engine operating conditions. As the HPSV port angle becomes larger, the engine valve has more time to reach the desired lift and consequently the hydraulic pressure required to open the engine valve is reduced especially at higher engine speeds. Figure 7-13 shows the effect of increasing the HPSV port angle on the pump downstream pressure in the optimized VVA system (optimum 6) at different engine speeds. As depicted in this figure, at lower engine speeds (below 2500 rpm), shortening the HPSV opening interval does not increase the pumping pressure; however, at higher engine speeds, since the total time available for the engine valve to fully open is extremely limited, any small decrease in HPSV opening interval will lead to drastic increase in pumping pressure and consequently system power consumption.

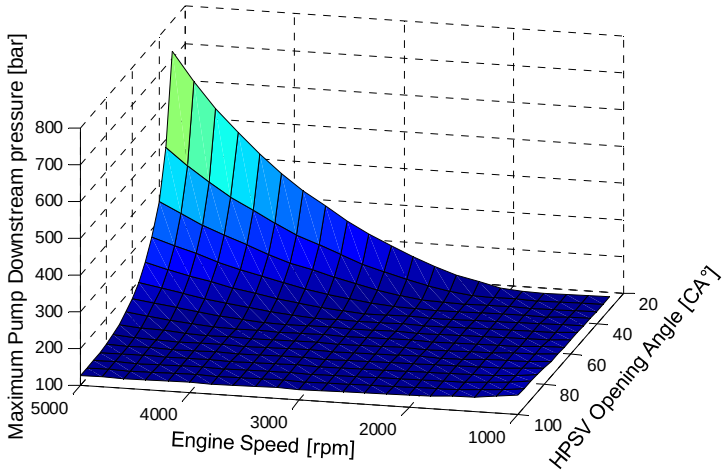

Figure 7-13: Effect of decrease in HPSV opening angle on the pumping pressure at different engine speeds

As shown in Figure 7-14, the energy efficiency of the optimized VVA system (optimum 6) is drastically deteriorated at higher engine speeds as the high pressure spool valve opening angle drops below 70 CA°. On the contrary, increasing the HPSV opening angle above 70 CA° does not reduce the system power consumption and only increases the minimum allowable engine valve opening duration (since HPSV must be fully closed before LPSV starts to open).

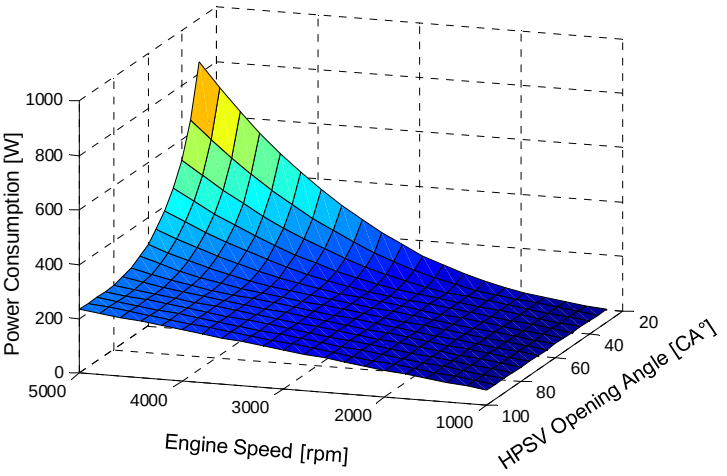

Figure 7-14: Effect of decrease in HPSV opening angle on power consumption at different engine speeds

Since, in the proposed VVA system, increase in the minimum allowable engine valve opening duration reduces the system flexibility, opening angle of 70 degree is the optimum design for the high pressure spool valve.

7.4 ENERGY RECOVERY SYSTEM

In addition to design optimization, many studies have been conducted by several researchers to reduce the power consumption of the hydraulic valvetrains using different techniques. In many developed electro-hydraulic valvetrains, [69], [33], the entire engine valve return stroke is performed at the pressure of the low pressure tank and the energy used to compress the return spring is lost. In [45] and [70], the hydraulic oil is wasted into the low pressure tank only during the last part of the closing stage and a large part of the engine valve return stroke is performed at the supply pressure pumping the oil into the supply line. This is possible because the valve spring compression at maximum valve lift is higher than that statically obtainable with the available supply pressure due to moving masses' inertia. In this technique, controlling the timings of the two intervals in the closing stage is performed with the aid of solenoid actuated spool valves. A combination of two-spring pendulum and bypass design was used in [44] to reduce the required fluid flow and pressure during most of the engine valve travel. This results in actuator power consumption comparable to that of a conventional cam-follower valvetrains. In [38], it was also shown that the power consumption of the hydraulically returned electro-hydraulic valvetrain would be 30% lower in average, compared to a similar spring returned system.

As seen in the previous section, the system sensitivity to engine cycle-to-cycle variation can be reduced by increasing the spring stiffness or hydraulic piston area. However, increase in the values of these design parameters results in increase in system power consumption. To eliminate the tradeoff between system power consumption and robustness, an energy recovery system is introduced in this section.

Due to constant hydraulic piston area, LPSV opening angle, spring stiffness and preload, the engine valve full closure angle depends only on the engine speed. Thus in the proposed VVA system, early valve closure is occurred at lower engine speeds. In fact, during engine valve closing stage at lower engine speeds, only a portion of the available spring potential energy is

used to discharge oil from the hydraulic cylinder and the rest is wasted through the impact between the valve and its seat or through the heat dissipation at hydraulic cushion which is used to control the engine valve seating velocity. To conserve the surplus spring potential energy during valve closing stage, the hydraulic power unit is equipped with a novel energy recovery system shown in Figure 7-15. Using this system, the main pump upstream pressure (hydraulic cylinder downstream pressure) can be varied using a secondary hydraulic pump coupled to the main pump shaft along with two on/off valves. In fact, the engine valve actuator downstream pressure is regulated such that the surplus spring energy is used to maintain the main pump upstream pressure during engine valve operation. This will reduce the main pump power consumption considerably. To this end, the pressure of the accumulator (b) is increased by closing the digital valve (a) and (b). This increase in the main pump upstream pressure continues as far as full engine valve closure is guaranteed. As the main pump upstream pressure is reached to a certain value, the digital valve (b) is opened. At this time, the pressure of accumulator (b) remains almost constant due to existence of unidirectional valve. Valve (a) is opened as soon as the return spring potential energy is not enough any longer for completely closing the engine valve.

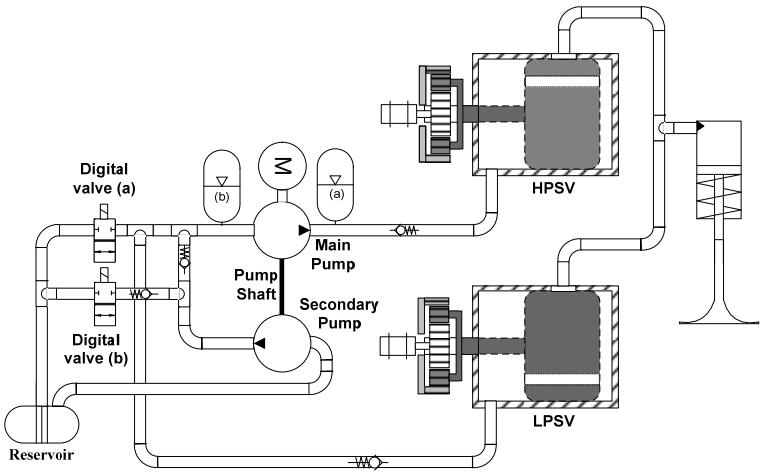

Figure 7-15: The proposed energy recovery system for the new flexible valve system

To study the performance of the proposed energy recovery system, all the hydraulic, electrical and mechanical components of the system are simulated in AMESim8.b© software. As shown in Figure 7-16, the model consists of several sub-model including gear pumps,

hydraulic cylinder, air accumulators, high and low pressure rotary spool valves (HPSV, LPSV), friction model, in-cylinder gas force model, unidirectional valves (check valves) and solenoid on-off valves. To obtain 10mm engine valve lift at all engine speeds, the pump to engine speed ratio is selected based on:

$$\frac{N_{pump}}{N_{engine}} = \frac{A_p}{200V_{disp}} \tag{7.35}$$

The high/low pressure rotary spool valves are modeled by variable hydraulic restrictors which are controlled through a Simulink interface block. The solenoid on-off valves are modeled using electronically controlled 2-positions-2-ports valves. The air compression and expansion processes in the air accumulators are considered as polytropic processes (k=1.3). The hydraulic cylinder is modeled with a single-acting spring-return hydraulic actuator. For the sake of simplicity, the engine valve and hydraulic piston masses are lumped into a single linear mass. The friction force between piston and cylinder of the hydraulic actuator is modeled using a constant coulomb friction during the piston motion. In this model, the design parameters are set based on their optimum values achieved in Section 7.3 (optimum 6).

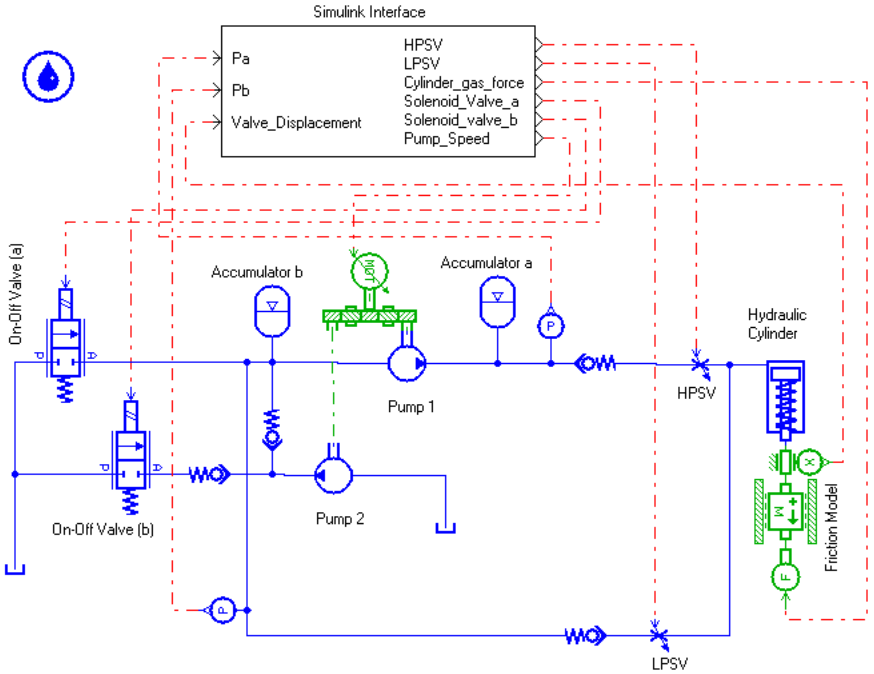

Figure 7-16: AMESim model of the proposed energy recovery configuration

To estimate the maximum power saving achieved by the proposed energy recovery system, the maximum LPSV downstream pressure, at which full engine valve closure is guaranteed at the end of the engine valve closing stage, is determined at different engine speeds and LPSV opening angles.

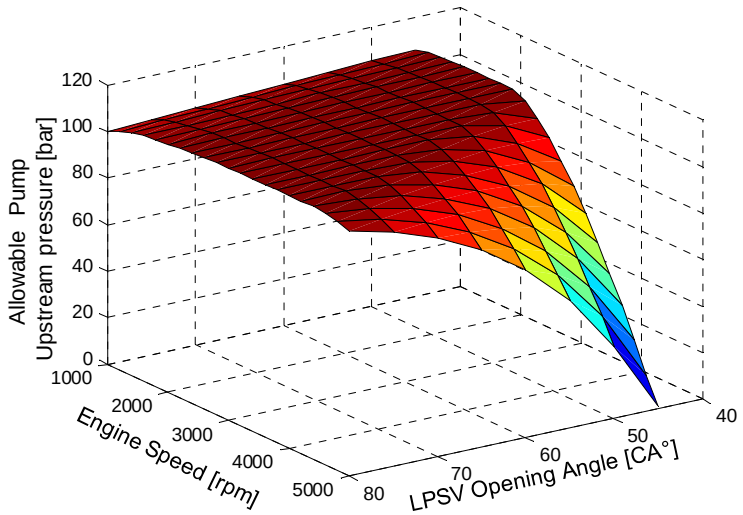

Figure 7-17: The maximum allowable pump upstream pressure for maximum energy recovery at different engine speeds and LPSV opening angle

As shown in Figure 7-17, at 80 degree opening angle for the LPSV, the LPSV downstream pressure can be kept around 100bar at all engine speeds; however, as the LPSV opening angle becomes smaller, this pressure must be controlled as the engine speed varies. Figure 7-18 illustrates the engine valve profile produced by the optimized VVA system with and without energy recovery system. As presented in this figure, in the optimized VVA system with 80CA° LPSV opening angle and maximum sensitivity of 30% to engine cycle-to-cycle variations, the actuator return-spring is such stiff that even at 5000rpm, full engine valve closure is occurred 30CA° before the LPSV is fully closed. The results also show that by increasing the LPSV downstream pressure from 1 to 100 bar, full engine valve closure is still feasible with almost 30CA° delay. Comparing two engine valve profiles in Figure 7-18 shows that higher LPSV downstream pressure will lead to a lower engine valve seating velocity.

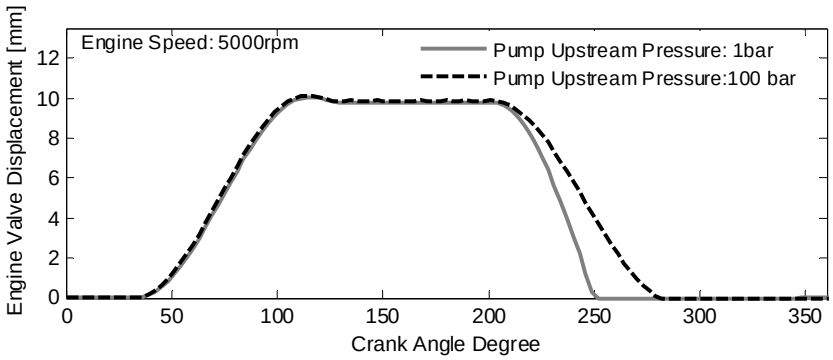

Figure 7-18: Engine valve opening profile with and w/o energy recovery system (LPSV opening angle: 80CA°)

Figure 7-19 shows the power consumption of the proposed VVA architecture with optimum design parameters (optimum 6) for a single engine valve with and without the proposed energy recovery system at a variety of LPSV opening angles and a range of engine speeds. As depicted in this figure, using the proposed energy recovery system, the power consumption of the optimized VVA system with LPSV opening angle of 80 CA° can be theoretically reduced by 87%. The results show that as the LPSV opening angles becomes smaller, the maximum amount of energy saving becomes restricted at higher engine speeds.

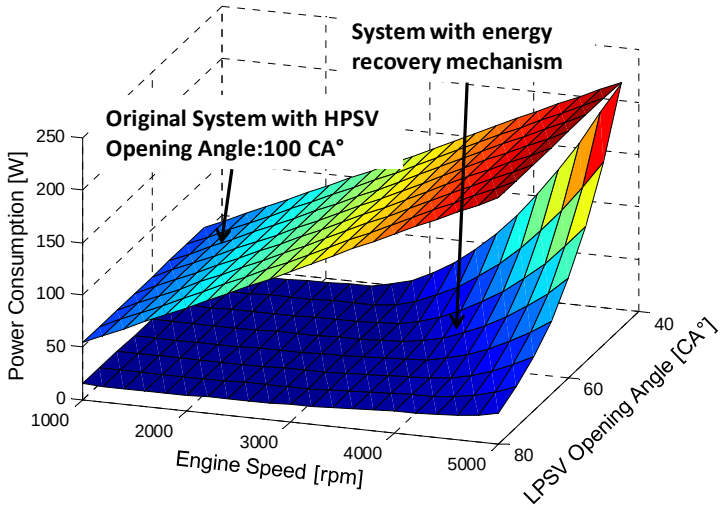

Figure 7-19: Improvement in system power consumption at wide range of engine speeds and different LPSV opening angles with the aid of energy recovery mechanism

7.5 IMPROVED SYSTEM POWER CONSUMPTION AND ROBUSTNESS

In this section the improvement in the performance of the optimized system is verified by looking at its power consumption and robustness. To evaluate the proposed system energy efficiency, we use comparative power consumption data, provided by Turner et al., for a 16 valve cam driven valvetrain and two-stage electro-hydraulic variable valve actuation system (EHVVA) [38]. The presented data for the two-stage EHVVA is the power measured at pump outlet (only at high pressure side) for full load operating points listed in Table 7-5. Similarly, the pump power data presented does not take account of volumetric efficiency.

Table 7-4: The optimized design parameters for the intake valve actuation system

K [N/m]	$F_{preload}$ [N]	A_p [mm2]	$V1_{@1bar}$ [cc]
31000	0	10	129

Due to different robustness requirements, the optimum design for the intake valves is different from that for the exhaust valves. In fact, cycle-to-cycle variation in the engine cylinder gas force which is the main cause of variability in the engine valve trajectory is negligible for intake valves. Therefore, the sensitivity constraint could be relaxed in optimization of the proposed VVA system for intake valves. Table 7-4 lists the optimum design parameters approximated for the intake valves actuation system for a range of engine speeds (1000-5000rpm). Table 7-5 shows the optimum power consumptions for the intake and exhaust valves as well as the total power consumption for a 16-valve engine at full load condition.

Table 7-5: Power consumption of the proposed VVA system for 16-valves engine at full load operation (simulation results) [38]

Full Load Operating Points		Power consumption [kW]		
Engine Speed [rpm]	Valve Lift [mm]	8 Intake Valves	8 Exhaust Valves (w/o recovery system)	8 Exhaust Valves (w. recovery system)
5000	9.2	0.816	1.76	0.3996
4000	9.2	0.515	1.39	0.2584
3000	9.2	0.315	1.05	0.2052
2000	5.2	0.114	0.41	0.0970
1000	5	0.055	0.22	0.0811

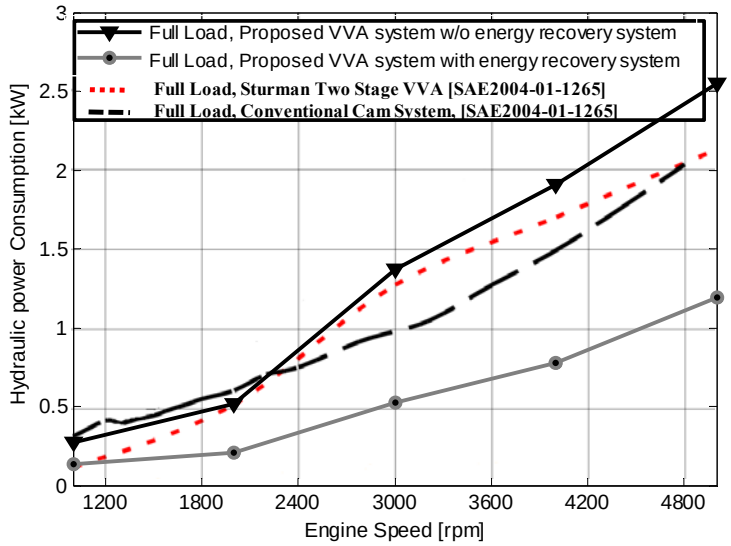

Figure 7-20: Comparison between the power consumption of different valvetrains

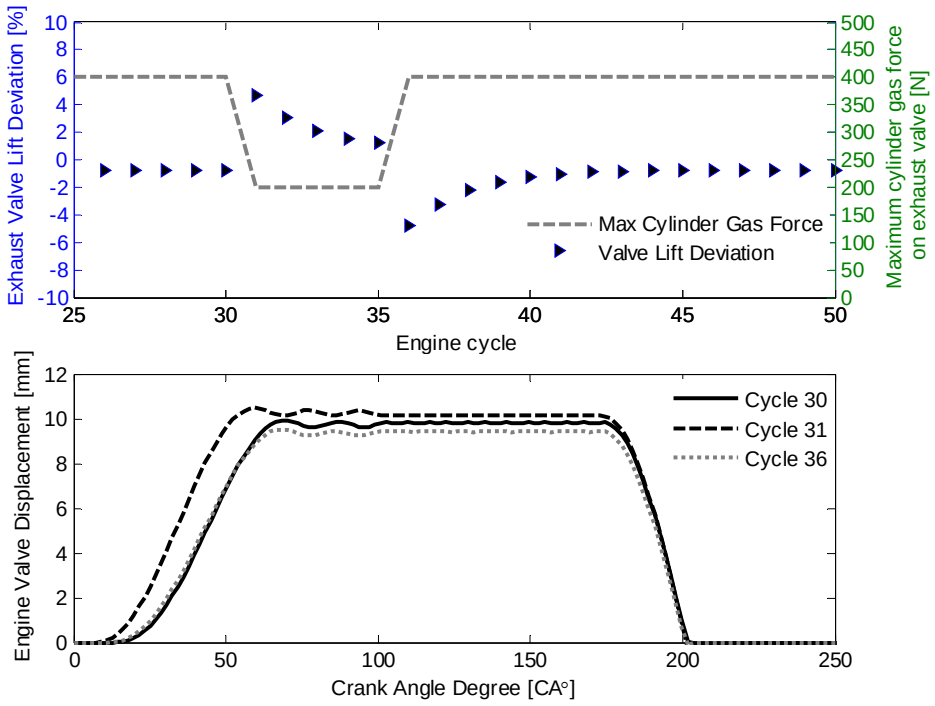

Figure 7-21: The engine valve lift variability due to in-cylinder pressure cycle-to-cycle variation

As shown in Figure 7-20, the power consumption of the proposed variable valve actuation system with optimized parameters and without energy recovery system is comparable with

those of the conventional cam driven valvetrains and existing electro-hydraulic VVA systems at engine speeds blow 2500rpm and it is slightly greater at higher engine speeds. However, as the proposed VVA design is equipped with the proposed energy recovery system, its power consumption becomes much lower (~58%) than that of other valvetrains at wide range of engine speeds.

The robustness of the optimized VVA system is also investigated using the AMESim model. To this end, the model parameters are set to their optimum values (optimum 6) and the in-cylinder gas force model given in Section 7.3 is used. The model is run for 3000rpm engine speed and the engine cylinder gas force is deliberately dropped to 50% of its original value at random engine cycles. Figure 7-21 illustrates the engine valve lift variability due to cycle-to-cycle variation in the engine cylinder pressure. As presented in this figure, the engine valve lift deviation from its desired value (10mm) does not exceed 5% (500 μm) of the desired lift as the maximum engine cylinder gas fore on the exhaust valve varies by 200N/cycle.

7.6 SUMMARY

In this chapter, to improve the competitiveness of a newly developed fully flexible variable valve actuation system, its power consumption and robustness were subject to an optimization. To this end, an optimization problem was developed in which its objective function (system power consumption) and constraints (system sensitivity and full engine valve closure) were set up based on a simplified formulation whose accuracy was verified later. The advantage of the proposed mathematical model over the complete model of the systems is that systems behavior during steady operating condition can be approximated a head of time. This in fact reduces the computational cost significantly. In this study, the system parameters subjected to optimization included engine valve return-spring stiffness and preload, hydraulic piston area, accumulator precharge pressure and volume. The optimization problem was initially run for every specific engine speeds and finally it was solved for a range of engine speed and the results were compared. The effects of HPSV opening angle and maximum allowable system sensitivity on the power consumption were also investigated. In the proposed VVA system, due to a tradeoff between system power

consumption and its robustness, the optimized system is a compromise between these two factors. Consequently, the optimized system power consumption was still higher than that of the conventional valvetrain. To solve this issue, the system was equipped with a novel energy recovery technique allowing the proposed VVA system to have minimum power consumption and maximum robustness simultaneously. Finally, the performance of the optimized system was evaluated and considerable improvement in system energy efficiency and its robustness was observed.

Chapter 8

Summary, Conclusions and Future Work

After a brief introduction and a literature survey on different types of flexible engine valve systems in the first two chapters and understanding some of their limitations and drawbacks including high mechanism and control complexity, low repeatability, reliability and robustness and high power consumption, a new valve actuation system with almost similar degree of flexibility as camless valvetrains and high degree of repeatability and reliability as cam-based valvetrain was proposed in the third chapter. The main difference between the proposed valve actuation system and electro-hydraulic camless valvetrain is that two solenoid actuated servo-valves are replaced with two rotary spool valves. This, in fact, eliminates the problem caused by the solenoid valve response time at higher engine speeds. Each rotary spool valve can be either actuated by the engine crankshaft through an electric or a hydraulic phase shifter mechanism or directly by servo motors. The numerical model of the system was developed using the governing differential equations of the system. Using the developed mathematical model, the proposed VVA system was studied numerically. The simulation results showed that in the developed actuation system, the engine valve lift is highly dependent on the engine speed and oil supply pressure. This highlighted the need for a controllable hydraulic power unit. The effect of the clearance between the spool and casing of the rotary spool valves on the leakage flowrate and consequently on the valve actuator performance was also studied. It was observed that increase in this clearance would quadratically increase the leakage and result in unwanted engine valve opening or closing. Using the developed engine cylinder gas dynamic model, the effect of cylinder gas pressure on the engine valve actuation and also the effect of engine valve timing and lift on the engine gas exchange process were evaluated. The results showed that in this system, the variation in cylinder gas pressure could influence the valve actuation system precision. It was also

observed that the engine gas exchange process is affected by both engine valve timing and engine valve lift.

Using the results obtained from the system numerical study, the prototype of the proposed VVA system was designed, fabricated and instrumented for single engine valve actuation. An engine valve timing controller and a preliminary lift controller were designed and incorporated in the system prototype. Experiments were conducted to study the repeatability, accuracy, robustness and power consumption of the system. It was shown experimentally that using the designed VVA system, it is possible to change the engine valve opening and closing timings by 100CA° within an engine cycle. It was also shown that the preliminary lift controller can maintain the final valve lift within ±0.5mm of the desired lift during sudden changes in the operating speed. Testing the system repeatability in the speed range of 800 to 2000rpm confirmed the maximum standard deviation of 2.5CA° for engine valve timing and 0.08mm for engine valve lift.

For fast engine valve lift variation in engine mode transition control such as HCCI (homogenous charge compression ignition) and air hybrid and also throttle-less engine control (throttle tip-in), a new engine valve lift controller was proposed, designed and implemented. The original idea was based on controlling the valve system hydraulic supply pressure using a proportional bleed valve. To reduce the controller complexity and computational cost, an average model of the system was developed based on the energy and mass conservation principles. A discrete time non-linear sliding mode controller was designed using discrete Lyapunov function and its stability was proved. The measured and desired engine valve lift, system upstream pressure and engine speed are the inputs to the designed controller and the proportional bleed valve flow coefficient is the only output from the control law. It was experimentally illustrated that using the designed lift controller, the engine valve lift can be precisely varied by 4mm within maximum 5 engine cycles with steady state error of less than 0.1mm. The proposed lift controller has also the capability to be applied on the existing electro-hydraulic camless valvetrain. Comparing the performance of the proposed lift controller with that of the existing techniques used in electro-hydraulic camless valve systems, the superiority of the proposed control system was proved.

To improve the system effectiveness, its power consumption and robustness were studied. To this end, a constraint non-convex optimization problem was set up whose objective function and constraints were developed using the simplified model of the system to reduce computational cost. Genetic algorithm with dynamic penalty method was employed to find the optimum system parameters while satisfying the problem constraints. Comparison between the power consumption of the optimized and original system for a single engine valve actuation showed an improvement of about 33% at 2000rpm. Moreover, the optimized system is able to operate at engine speed of 5000 rpm while the original system was designed only for maximum engine speed of 2000rpm. Due to the existing tradeoff between the system power consumption and robustness in hydraulic or pneumatic valvetrains, the power efficiency is always sacrificed to reduce system sensitivity to external disturbances. For the first time, in this thesis, a new energy recovery system was proposed to recover a portion of the energy wasted for enhancing system robustness. This idea is extendable to any electro-hydraulic valve system and can reduce the average power consumption by almost 42%.

In general, this research project advances the state of knowledge in hydraulic variable valve actuation systems, contributing to related areas such as engine valve lift control, event based sliding mode control and hydraulic VVA systems design optimization. So far, this research has resulted in following academic publications and patent:

P1- Amir Khajepour and Mohammad Pournazeri, Fully Flexible Variable Valve Actuation System with Rotary Spool Valve, *US Provisional Patent,* No. 61/573,025, August 9, 2011.

J1- Mohammad Pournazeri, Amir Khajepour, Amir Fazeli, An Efficient Lift Control Technique in Electro-hydraulic Camless Valvetrain Using variable Speed Hydraulic Pump, *SAE International Journal of Engines*, June 2011 vol. 4 no. 1 1247-1259.

J2- Mohammad Pournazeri, Amir Khajepour, Amir Fazeli, A New Electro-hydraulic Valvetrain Configuration with Improved Lift Controllability, *International Journal of powertrain*, In press

J3- Mohammad Pournazeri, Amir Khajepour, Development of a new fully flexible hydraulic variable valve actuation system using rotary spool valves, *Journal of Dynamic Systems, Measurement and Control*, (Under Review)

J4- Mohammad Pournazeri, Amir Khajepour, Precise Lift Control in a New Variable Valve Actuation System Using Discrete-Time Sliding Mode Control, *Journal of Mechanism and Machine Theory* (Submitted)

C1- Mohammad Pournazeri, Amir Fazeli, Amir Khajepour, A cam-based Electro-hydraulic Variable Valve Timing System for Pneumatic hybrid Engines, *Proceedings of ASME International Mechanical Engineering Congress and Exposition*, Florida, November 13-19, 2009, Lake Buena Vista, Florida, USA, IMECE2009-10531

C2- Mohammad Pournazeri, Amir Khajepour, Amir Fazeli, A New Valve Lift Control technique in Electro-hydraulic Variable Valve Actuation System, *Proceedings of ASME 2010 Internal Combustion Engine Division*, September 12-15, 2010, San Antonio, Texas, USA, ICEF2010-35050

C3- Mohammad Pournazeri, Amir Fazeli, Amir Khajepour, A Robust lift control technique in Electro-hydraulic Camless Valves Using System Average Model, *Proceedings of ASME 2010 International Mechanical Engineering Congress & Exposition*, November 12-18, 2010, Vancouver, British Columbia, Canada, IMECE2010-38691

C4- Mohammad Pournazeri, Amir Khajepour, Amir Fazeli, An Efficient Lift Control Technique in Electro-hydraulic Camless Valvetrain Using variable Speed Hydraulic Pump, *SAE 2011-01-0940*, Detroit

C5- Mohammad Pournazeri, Amir Khajepour, A Robust Variable Valve Actuation System with Energy Recovery mechanism, *Proceedings of the Internal Combustion Engine Division Spring Technical Conference*, May 6-9, 2012, Torino, Italy, ICES2012-81173

8.1 FUTURE WORK

Based on the completed work on new hydraulic variable valve actuation system, the following future activities are recommended:

- In this research project, the focus of both experimental and analytical work was only on a single engine valve actuation system; however, the configuration and control strategy of the proposed system when applied to a multi-engine valve application was not covered. It is suggested that a comprehensive numerical study to be done to find the optimum configuration of the proposed system for multi poppet valve engine and repeatability, accuracy and robustness of that system to be evaluated.
- Since the VVA system prototype was not installed on the engine cylinder, the effect of in-cylinder gas forces on its performance was not studied experimentally and it was only investigated numerically. It is recommended that the cylinder head of a single cylinder engine is modified such that it accommodates the existing valve system prototype and the system performance is studied during engine operation.
- It was numerically observed that the spool valve flow coefficient and friction has high influence on the total system power consumption; however, in this research project, the design of the rotary spool valves was not studied in depth. As a part of future work, computational fluid dynamics and finite element modeling could be employed to improve the spool valve flow characteristic while minimizing the friction forces and valve size.
- The effect of oil temperature on the hydraulic fluid viscosity (Appendix B) and consequently system performance and power consumption has not been studied in this research work and could be investigated in future.
- As discussed in the introduction section of this dissertation, one of the applications of the fully flexible valvetrains is for air hybrid engines to realize different modes of operation. In fact, this project was a part of a new air hybrid engine project proposed by Khajepour et al. utilizing two air tanks whose pressures are controlled by the engine valvetrains. In the existing test setup for the proposed hybrid engine, both regenerative braking and air motor modes were realized using servo-pneumatic valves; however, due to servo-valves temperature and response limitations, the setup could not be operated in the combustion mode or at high engine speeds. Therefore,

equipping the existing air hybrid engine setup with the designed hydraulic valvetrain will lead to full verification of both systems and is strongly suggested as a potential future work.

References

[1] L Mianzo, "Output feedback H∞ preview control of an electromechanical valve actuator," *IEEE Transaction on Control Systems Technology*, vol. 15, no. 3, May 2007.

[2] X. Ai, M. Wilmer, D. Remboski, "Electrical variable cam phase shifter for internal combustion engine," in *SAE 2008-01-1351*, 2008.

[3] R. R. Henry, B. Lequesne, "A novel, fully flexible, electro-mechanical engine valve actuation system," in *SAE 970249*, 1997.

[4] Thomas Dresner and Philip Barkan, "A review and classification of variable valve timing mechanisms ," in *SAE 890674*, 1989.

[5] H Hong, G B Parvate Patil, and B Gordon, "Review and analysis of variable valve timing strategies—eight ways to approach," *Journal of Automobile Engineering*, vol. 218, no. 10, pp. 1179-1200, October 2004.

[6] T M Lancefield, R J Gayler, and Chattopadhay, "The application of variable event valve timing to a modern diesel engine," in *SAE 2000-01-1229*, 2000.

[7] John Schwoerer, Sotir Dodi, Marty Fox, Shengqiang Huang, and Zhou Yang, "Internal EGR Systems for NOx Emission Reduction in Heavy-Duty Diesel Engines," in *SAE international*, Detroit, MI, pp. 2004-01-1315.

[8] M Pournazeri, A Fazeli, and A Khajepour, "A cam-based electro-hydraulic variable valve timing system for pneumatic hybrid engines," in *Proceedings of ASME International Mechanical Engineering Congress and Exposition, IMECE*, 2009.

[9] C Gray, "A review of variable engine valve timing," in *SAE 880386*, Detroit, 1988.

[10] Chun Tai, Modeling and control of cmless engine valvetrain systems, 2002, PhD Dissertation.

[11] Kiangrong Shen, Jianlong Zhang, Eric J Barth, and Michael Goldfarb, "Non-linear model-based control of pulse width modulated pneumatic servo system," *Journal of Dynamic Systems, Measurement and Control*, vol. 128, Sep 2006.

[12] Jeff Allen and Dow Law, "Production electro-hydraulic variable valvetrain for a new generation of I.C. Engines," in *SAE 2002-01-1109*.

[13] Zongxuan Sun and David Cleary, "Dynamics and control of an electro-hydraulic fully flexible

valve actuation system," in *Proceedings of the American Control Conference*, 2003.

[14] IJB TA. (2007, April) Wikipedia.com. [Online]. http://en.wikipedia.org/wiki/File:Pushrod2.PNG

[15] Stahlkocher. (2005, July) Wikipedia.com. [Online]. http://en.wikipedia.org/wiki/File:DOHC-Zylinderkopf-Schnitt.jpg

[16] Robert L Norton, *Cam design and manufacturing handbook*.: Industrial Press Inc, 2002.

[17] G B Parvate-Patil, H Hong, and B Gordon, "An assessment of intake and exhaust philosophies for variable valve timing," in *SAE 2003-32-0078*, Madison, WI, 2003.

[18] Tim Lancefield, "The influence of variable valve actuation on the part load fuel economy of a modern light-duty diesel engine," in *SAE2003-01-0028*, 2003.

[19] Jens Schafer and Jeff Balko, "High performance electric camshaft phasing system," in *SAE 2007-01-1294*, 2007.

[20] (2008) Delphi Variable Cam phasers. [Online]. http://delphi.com/manufacturers/auto/powertrain/gas/valvetrain

[21] (2008) VTEC mechanism by Honda. [Online]. www. world.honda.com/automobile-technology/VTEC/

[22] K nagaya, H Kobayashi, and K Koike, "Valve timing and valve lift control mechanism for engines," *Journal of Mechatronics*, vol. 16, pp. 121-129, September 2005.

[23] Lucio Bernard, Andrea Ferrarl, and Rinaldo Rinolf, "Fuel economy improvement potential of UNIAIR throttleless technology," *ATA*, vol. 56, 2003.

[24] Jong-Cheol Lee, Chun Woo Lee, and James A Nitkiewicz, "The application of a lost motion VVT system to a DOHC SI engine," in *SAE 950816*, 1995.

[25] Haoran Hu, Joseph M Vorih, and Mark A Israel, "The integrated lost motion VVT diesel engine retarder," in *SAE 973180*, 1997.

[26] Harald Fessler and Marco Genova, "An electro-hydraulic lost motion VVA system for a 3.0 liter diesel engine," in *SAE 2004-01-3018*, 2004.

[27] Peter Kreuter, Peter Heuser, and Joachim Reinicke-Murm, "The Meta VVH System-The advantages of continuously mechanical variable valve timing," in *SAE 1999-01-0329*, 1999.

[28] L Gould, W Richeson, and F Erickson, "Performance evaluation of a camless engine using

valve actuation with programmable timing," in *SAE 910450*, 1991.

[29] V Giglio, B Iorio, G Police, and A Gaeta, "Analysis of advantages and of problems of electromechanical valve actuators," in *SAE 2002-01-1105*, 2002.

[30] Y Wang et al., "Modeling and control of electromechanical valve actuator," in *SAE 2002-01-1106*.

[31] Mark D Anderson, Tsu Chin Tsao, and Michael B Levin, "Adaptive Lift Control for a Camless Electrohydraulic Valvetrain," in *SAE 981029*, Detroit, MI, 1998.

[32] J S Brader and D N Rocheleau, "Development of a piezo electrically-controlled hydraulic actuator for a camless engine," *Journal of Automotive Engineering, IMechE*, vol. 218, 2004.

[33] CW Turner, GR Babbitt, CS Balton, MA Raimao, and DD Giordano, "Design and control of a two-stage electro-hydraulic valve actuation system," in *SAE 2004-01-1265*, 2004.

[34] J Ma, H Schock, U Carlson, A Hoglund, and M Hedma, "Analysis and modeling of an electronically controlled pneumatic hydraulic valve for an automotive engine," in *SAE 2006-01-0042*, 2006.

[35] S Trajkovic, P Tunestal, and B Johansson, "Introductory Study of Variable Valve Actuation for Pneumatic Hybridization," in *SAE2007-01- 0288*, 2007.

[36] J Ma, H Schock, G Zhu, and J Winkelman, "Model refence adaptive control of a pneumatic valve actuator for infinitely variable valve timing and lif," in *SAE 2007-01-1297*, 2007.

[37] Jia Ma, Guoming Zhu, Andrew Hartsig, and Harold Sc, "Model-based predictive control of an electro-pneumatic exhaust valve for internal combustion engine," in *American Control Conference*, 2008.

[38] Christopher W Turner, Guy R Babbitt, Christopher S Balton, Miguel A Raimao, and Daniel D Giordano, "Design and control of a two-stage electro-hydraulic valve actuation system," in *SAE 2004-01-1265*, 2004.

[39] D McCloy and H Martin, *Control of Fluid Power: Analysis and Design*, 2nd ed.: Ellis Horwood Ltd., 1980.

[40] Al-Ghathian, M Faisal, Tarawneh, and S Maufag, "Friction forces in o-ring sealing," *American Journal of Applied Sciences*, vol. 2, no. 3, pp. 626-632, 2005.

[41] Noah D Manring, *Hydraulic Control Systems*.: John Wiley and Sons, Inc., 2005.

[42] Bridget A Baran, "Engine Lubrication Oil Aeration," Massachusetts Institute of Technology, Boston, MSc Thesis 2007.

[43] Zongxuan Sun and Tang-Wei Kuo, "Transient control of electro-hydraulic fully flexible engine valve actuation system," *IEEE Transactions on Control Systems Technology*, vol. 18, no. 3, August 2009.

[44] Zheng Lou, "Camless variable valve actuation designs with two-spring pendulum and electrohydraulic latching," in *SAE 2007-01-1295*, 2007.

[45] M Battistoni, L Foschini, L Postrioti, and M Christiani, "Development of an electro-hydraulic camless VVA system," in *SAE 2007-24-0088*, Capri (Naples), Italy, 2007.

[46] G B Parvate-Patil, H Hong, and B Gordon, "An assessment of intake and exhaust philosophies for variable valve timing," in *SAE 2003-32-0078*, 2003.

[47] Mark D Anderson, Tsu-Chin Tsao, and Michael B Levin, "Adaptive Lift Control for a Camless Electrohydraulic Valvetrain," in *SAE 981029*, 1998.

[48] Zongxuan Sun, "Electrohydraulic fully flexible valve actuation system with internal feedback ," *Journal of Dynamic Systems, Measurement and Control*, vol. 131, March 2009.

[49] H K Khalil, *Nonlinear Systems*, 3rd ed.: Prentice-Hall Inc, 2002.

[50] J J Slotine and W Li, *Applied non-linear control*.: Prentice-Hall Inc, 1991.

[51] Meysar Zeinali and Leila Notash, "Adaptive sliding mode control with uncertainty estimator for robot manipulator," *Mechanism and Machine Theory*, vol. 45, no. 1, pp. 80-90, January 2009.

[52] C Y Chan, "Robust discrete-time sliding mode controller," *System & Control Letters*, vol. 23, pp. 371-374, 1994.

[53] Katsuhisa Furuta, "Sliding mode control of a discrete system," *System & Control Letters*, vol. 14, pp. 145-152, 1990.

[54] S Z Sarpturk, Y Istefanopulos, and O Kaynak, "On the stability of discrete-time sliding mode control systems," *IEEE Transaction Automatic Control*, vol. 32, pp. 930-932, 1987.

[55] M Jalili-Kharaajoo and R Fazaie, "Discrete-Time Sliding Mode Conttrol of Permanent Magnet Linear Synchronous Motro in High-Performance Motion with Large Parameter Uncertainty," in *SICE Annual Conference*, Fukui, 2003.

[56] W C Su, S V Drakunov, and U Ozguner, "An O(T2) boundary layer in sliding mode for

sampled data system," *IEEE Transaction, Automatic Control*, vol. 45, no. 3, pp. 482-485, 2000.

[57] W C Su, S V Drakunov, and K D Young, "Sliding Mode with Chattering Reduction in Sampled Data Systems," in *32th Conference on Decision and Control*, 1993.

[58] David E Goldberg, *Genetic Algorithms in Search, Optimization, and Machine Learning*, 1st ed. Boston, MA, USA: Addison-Wesley Longman Publishing Co., Inc. , 1989.

[59] John H Holland, *Adaptation in natural and artificial systems: An Introductory Analysis with Applications to Biology, Control, and Artificial Intelligence*. Cambridge, MA, USA : MIT Press, 1992.

[60] Colin R Reeves and E Jonathan Rowe, *genetic Algorithms - Pronciples and Perspectives: A Guide to GA Theory*.: Kluwer Academic Publishers Group, 2003.

[61] M J Box, "A new method of constrained optimization and a comparison with other methods," *The Computer Journal*, vol. 8, no. 1, pp. 42-52, January 1965.

[62] H H ROSENBROCK, "An Automatic Method for finding the Greatest or Least Value of a Function," vol. 3, no. 175, 1960.

[63] J A NELDER and R MEAD, "A simplex method for function minimization," *The Computer Journal*, vol. 7, p. 308, 1965.

[64] A Homaifar, S H Y Lai, and X Qi, "Constrained optimization via genetic algorithm," *Simulation*, vol. 62, no. 4, pp. 242-252, 1994.

[65] J Joines and C Houck, "On the use of non-stationary penalty functions to solve non-linear constrained optimization problem with GAs," in *IEEE World Congress on Computational Intelligence*, Orlando, FL , 1994, pp. 579 - 584.

[66] Z Michalwicz and N Attia, "Evolutionary optimization of constrained problems," in *3rd Annual Conference on Evolutionary programming*, River Edge, NJ, 1994, pp. 98-108.

[67] A B Hadj-Alouane and J C Bean, "A genetic algorithm for a multiple-choice integer program," The University of Michigan, Technical TR 92-50, 1992.

[68] A Warburton, L Fleming, J Scott, N Butler, and W Wyganski, "Inteligent Valve Actuation (IVA) System for Gasoline and Diesel Engines," in *SAE 2005-01-0772*, Detroit, MI, 2005.

[69] D Denger and K Mischker, "The electro-hydraulic valvetrain system EHVS-system and potential," in *SAE 2005-01-0774*, 2005.

[70] Michael M Schechter and Michael B Levin, "Camless Engine," in *SAE960581*, 1996.

[71] Arthur Akers and Richard Smith, *Hydraulic power System Analysis*.: Taylor and Francis, 2006.

[72] J J Slotine and W Li, *Applied non-linear control*. Toronto : Prentice-Hall Inc, 1991.

[73] M. Schechter, "Operating a vehicle with braking energy recovery," 7231998, 2007.

[74] M. Schechter, "New Cycle for Automobile Engines," in *SAE1999-01-0623*, 1999.

[75] Jurgen R., *Automobile Electronics Handbook*. New York: McGrraw-Hill , 1995.

[76] M Pournazeri, A Khajepour, and A Fazeli, "A new valve lift control technique in electrohydraulic variable valve actuation systems," in *ASME International Combustion Engine Division ICEF2010*, San Antonio, 2010.

[77] K M Misovec, B G Johnson, G Mansouri, O E Sturman, and S Massey, "Digital Valve Technology Applied to the Control of a Hydraulic Valve Actuator," in *SAE 1999-01-0825*, Detroit, MI, 1999.

[78] J R Liu, B Jin, Y J Xie, Y Chen, and Z T Weng, "Research on the electro-hydraulic variable valve actuation system based on three-way proportional reducing valve," *International Journal of Automotive Technology*, vol. 10, no. 1, pp. 27-36, 2009.

[79] Hsein-Hsin Liao, Mathew J Roelle, and Christian Gerdes, "repetitive control of an electro-hydraulic engine valve actuation system," in *AMerican Control Conference*, 2008.

[80] Miroslav Krstic, Ioannis Kanellakopoulos, and Petar V Kokotovic, *Nonlinear and Adaptive Control Design By Miroslav Krstic*.: Wiley-Interscience , 1995.

[81] M F Khandaker, H Hong, and L Rodrigues, "Modeling and controller design for a voice coil actuated engine valve," in *IEEE Conference on Control Applications*, Toronto, 2005.

[82] H K Khalil, *Nonlinear Systems*, 3rd ed. Upper Saddle River, New Jersey: Prentice-Hall Inc, 2002.

[83] A. Stefanopoulou, Y. Wang K. Peterson, "Control of electromechanical actuators: Valves tapping in rhythm, Multidiciplinary research in control," in *LNCIS 289*, 2003.

[84] P A Ioannou and B Fidan, *Adaptive Control Tutorial*.: Society for Industrial and Applied Mathematics, 2006.

[85] Vasile I., Charlet A. and Chamaillard Y. Higelin P., "Parametric optimization of a new hybrid pneumatic combustion engine concept," *Int. J. Engine Res.*, no. 5, pp. 205–217, 2004.

[86] Vasile L.,Onder C. and Guzzella L. Donitz C., "Realizing a Concept for High Efficiency and Excellent Drivability: The Downsized and Supercharged Hybrid Pneumatic Engine," in *SAE2009-01-1326*, 2009.

[87] Siew Hwa Chan and J Zhu, "Modeling of engine in-cylinder thermodynamics under high values of ignition retard," *International Journal of Thermal Sciences*, vol. 40, no. 1, pp. 94-103, 2001.

[88] Tai C.,Tsao T. C. ,Levin M. B. ,Barta G. and Schechter M. , "Using Camless Valvetrain for Air Hybrid Optimization," in *SAE2003-01-0038.*, 2003.

[89] J. P. Watson, R. J. Wakeman, "Simulation of a pneumatic valve actuation system for internal combustion engine," in *SAE 2005-01-0771*.

[90] S. Butzmann, J. Melbert, "Sensorless Control of Electromagnetic Actuator for Variable Valve Train," in *SAE 2000—01-1225*, 2000.

[91] Donitz C., Vasile I., Onder C. and Guzzella L., "Modelling and optimizing two- and four-stroke hybrid pneumatic engines," *Journal of Automobile Engineering*, vol. 223, no. 2, 2009.

[92] S. Trajkovic, A. Milosavljevic, P. Tunestal, B. Johanssonm, "FPGA Controlled Pneumatic Variable Valve Actuation," in *SAE 2006-01-0041*, 2006.

[93] "Energy Efficiency Trends in Canada 1990 to 2007," 2009.

[94] J. S. Brader, D. N. Rocheleau, "Development of a piezoelectrically controlled hydraulic actuator for a camless engine," *Automobile Engineering*, vol. 218, 2004.

[95] T. A. Parlikar, W. S. Change, Y. H. Qiu, M. D. Seeman, D. J. Perreault, J. G. Kassakian, T. A. Keim , "Design and experimental implementation of an electromagnetic engine valve drive," *IEEE/ASME Transactions on Mechatronics*, vol. 10, no. 5, October 2005.

[96] Lee C., Zhao H. and Ma T., "Analysis of a Cost Effective Air Hybrid Concept," , SAE2009-01-1111, 2009.

[97] Mohammad Pournazeri, Amir Fazeli, Amir Khajepour, "A robust lift control technique in electro-hydraulic camless valves using system average model," in *IMECE2010*, Vancouver, 2010.

[98] Fazeli A., Khajepour A., Devaud C. and Lashgarian N., "A New Air Hybrid Engine Using Throttle Control," in *SAE2009-01-1319*, 2009.

[99] K M Misovec, B G Johnson, G Mansouri, O E Sturman, and S Massey, "Digital Valve

Technology Applied to the Control of a Hydraulic Valve Actuator," in *SAE 1999-01-0825*, 1999.

[100] Zongxuan Sun and Tang-Wei Kuo, "Transient control of electro-hydraulic fully flexible engine valve actuation system," *IEEE Transactions on Control Systems Technology*, 2009.

[101] Mohammad Pournazeri and Amir Khajepour, "Fully Flexible Variable Valve Actuation System with Rotary Spool Valve," US Provisional Patent 61/573,025, August 9, 2011.

[102] Mohammad Pournazeri, Amir Khajepour, and Amir Fazeli, "A New Electro-hydraulic Valvetrain Configuration with Improved Lift Controllability," *International Journal of Powertrain*, 2011.

[103] J Ziegler and N Nichols, "Optimum Settings for Automatic Controllers," *ASME*, vol. 64, pp. 759-768, 1942.

[104] E Sher and T Bar-Kohany, "Optimization of variable valve timing for maximizing performance of an unthrottled SI engine—a theoretical study," *Energy*, vol. 23, pp. 757–775, April 2002.

Appendix A

An Introduction to Cam-Follower Mechanisms

The most common application of cam and follower mechanisms is valve actuation in internal combustion engines. As discussed in Section 2.1, in fixed timing valvetrains, the valve actuation is performed either by cam follower directly or through pushrods or rocker arms. However, in most of the cam-based VVT systems, usually there is an intermediate mechanism, which transfers the motion of the cam follower to the engine valve. This mechanism enables the system to slightly change the valve timings, lift or duration with respect to the cam profile. In these VVT systems, according to the system requirements, the cam and follower design may differ from those in fixed timing systems.

A.1 Cam-Follower System Classification

The cam-follower systems can be classified based on the follower motion, cam and follower type and their joint closure. In engine application, the follower motion is translational.

A.1.1 Cam and follower joint closure

In general there are two types of joint closures between cam and follower: force closure and form closure. In the force closure mechanism, an external force is required to keep the cam and follower physically in contact. This force is usually provided by a compression spring and is not allowed to be negative during system operation to avoid contact loss between cam and follower. However, in the form closure mechanism, the cam and follower are kept in contact only by cam geometry. In this design, a groove cam captures a roller follower which follows groove profile. Using, form joint closure mechanism, the force applied on the follower can be either negative or positive [16]. One of the advantages of the form joint follower compared with force joint follower is that the contact between cam and follower is maintained at any operational conditions.

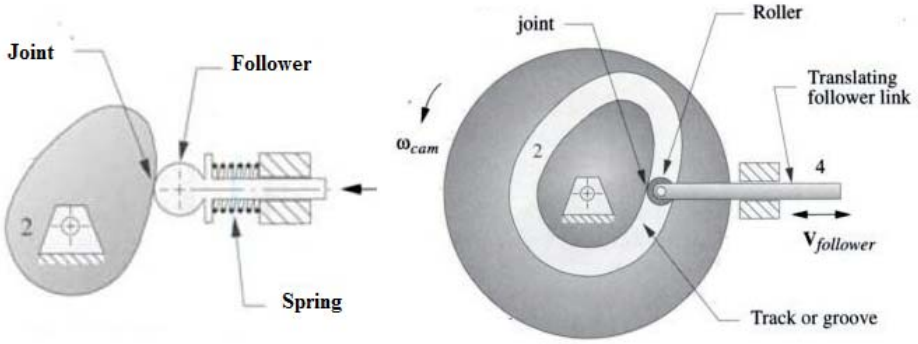

Figure A- 1: Force (left) and form (right) joint closure types [16]

A.1.2 Followers Classification

As shown in Figure A-2, there are three types of cam followers: flat-faced, curved and roller follower. The main advantage of the roller followers over other two types of followers is their less rolling friction. However, due to simplicity and lower cost, flat faced followers are usually employed in the conventional valve systems. Many modern automotive engines have started using roller follower instead of flat faced followers for their lower friction. In groove cam mechanisms (form closure type), the use of roller follower is inevitable. The mushroom followers are usually used in 3d-cam mechanisms.

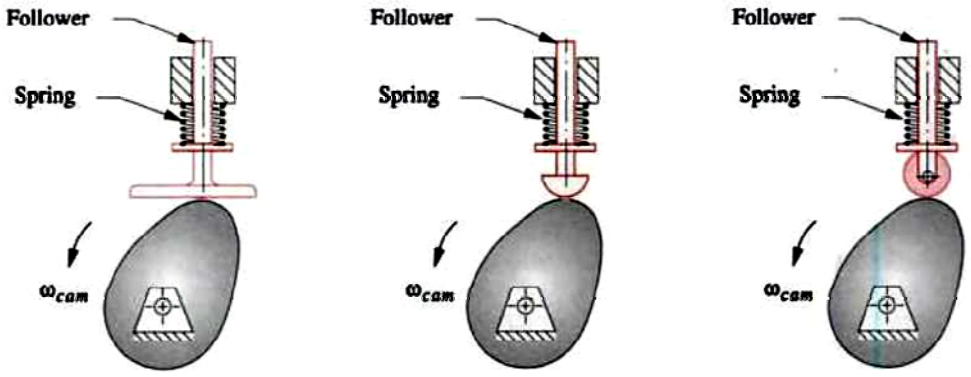

Figure A-2: Flat Faced (left), curved (middle) and roller followers (right) [16]

The direction of the follower's motion with respect to cam rotation axis determines whether the cam is radial or axial. However, in engine applications, radial cams are mostly used and are classified into "plate cams" (force closed) and "grooved cam" (form closed). Three-dimensional cam or Camoid is a combination of radial and axial cams. Using this type of

cam, it is possible to vary valve timings, duration and lift continuously by applying both rotational and axial displacement to the cam.

A.2 Acceptable Cam-Follower Profiles

A.2.1 S V A J Functions

For better system dynamics, the cam-follower displacement function (*S*) must have third-order continuity, which means it shall be continuous through the first and second derivatives of the displacement (*V*elocity and *A*cceleration) across the entire cam interval. In another word, the "*J*erk" function which is the third derivative of the displacement must be finite across the entire cam interval.

A.2.2 Different Cam Profiles

Several profiles have been proposed for cam-follower displacement, but only a few of them fully satisfy the *SVAJ* law. The primary profile for cam-follower displacement is simple harmonic motion:

$$\begin{cases} s = \dfrac{h}{2}\left[1 - \cos\left(\pi\dfrac{\theta}{\beta}\right)\right] \\ v = \dfrac{\pi}{\beta}\dfrac{h}{2}\sin\left(\pi\dfrac{\theta}{\beta}\right) \\ a = \dfrac{\pi^2}{\beta^2}\dfrac{h}{2}\cos\left(\pi\dfrac{\theta}{\beta}\right) \\ j = \dfrac{\pi^3}{\beta^3}\dfrac{h}{2}\sin\left(\pi\dfrac{\theta}{\beta}\right) \end{cases} \tag{A.1}$$

where, h is maximum valve lift, β is valve opening or closing interval and θ is cam angular position. The drawback of this design is that there are discontinuities in acceleration at both ends of each interval. This results in existence of infinite spikes of jerk at the interval start and end points. One of the cam profile functions which is acceptable at moderate to high speeds is "cycloidal" displacement. In this profile, the displacement function is in fact a sum of straight line of slope h and negative sine wave:

$$\begin{cases} s = h\left[\dfrac{\theta}{\beta} - \dfrac{1}{2\pi}\sin\left(2\pi\dfrac{\theta}{\beta}\right)\right] \\ v = \dfrac{h}{\beta}\left[1 - \cos\left(2\pi\dfrac{\theta}{\beta}\right)\right] \\ a = 2\pi\dfrac{h}{\beta^2}\sin\left(2\pi\dfrac{\theta}{\beta}\right) \\ j = 4\pi^2\dfrac{h}{\beta^3}\cos\left(2\pi\dfrac{\theta}{\beta}\right) \end{cases} \tag{A.2}$$

Moreover, there are several other cam profiles such as "trapezoidal acceleration", "sine-constant-cosine-acceleration (SCCA)" and "polynomial" which have finite jerks across the entire cam interval.

A.3 Cam Size Determination

In addition to *SVAJ* criteria, there are two other important factors that affect cam size and its profile. These factors are pressure angle and radius of curvature.

A.3.1 Pressure Angle in Cam with Roller Follower

As shown in Figure A-3, in cam mechanisms with roller follower, the force is transmitted from the cam to follower along the direction which is perpendicular to the common tangent or axis of slip. This direction is called axis of transmission. The pressure angle is defined as the angle between the direction of follower motion and axis of transmission and could be determined across the entire cam interval using following equation:

$$\varphi = \arctan\frac{v - \varepsilon}{s + \sqrt{R_P^2 - \varepsilon^2}} \tag{A.3}$$

Where s, v, R_P and ε are follower displacement, follower velocity (length/rad), prime circle radius and cam eccentricity. As the pressure angle decreases, most of the transmitted force goes into motion of the follower and not into slip. However, if the pressure angle increases, it leads to higher follower sliding frictions and it may damage the follower. As a rule of thumb, the pressure angle, which determines the torque applied by the cam surface on the follower, is desired to be between zero and ±30º [16]. In order to control the pressure angle, the cam prime circle radius and eccentricity shall be optimized. If changing prime circle radius and

eccentricity does not lead to an acceptable pressure angle, the cam-follower displacement and velocity curves shall be modified. In the cam with roller follower, the relation between the normal force (N) and follower force (F) can be written as follows [16]:

$$\frac{N}{F + m_{follower}\ddot{s}} = \frac{b}{b\cos\varphi - (2\mu a + \mu b - \mu^2 d)\sin\varphi} \tag{A.4}$$

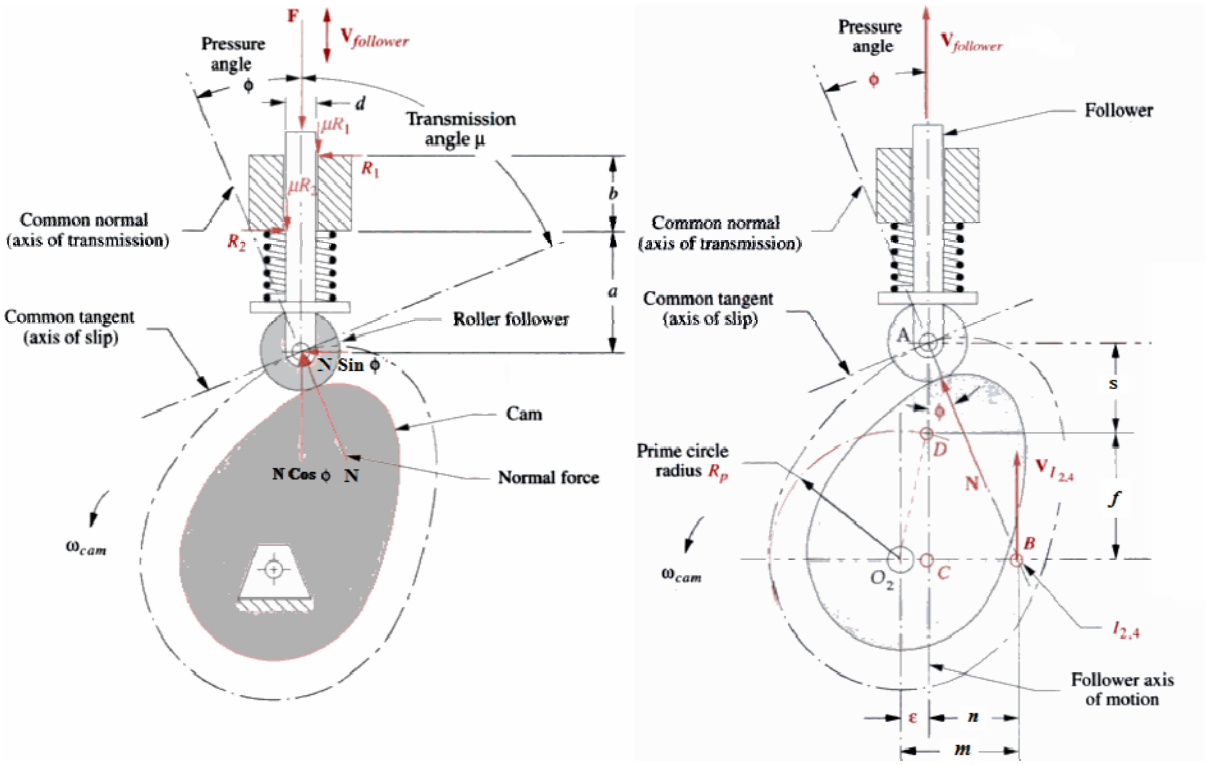

Figure A- 3: Cam with roller follower [16]

The results from analysis of the cam with roller follower (Figure A-4) show that increase in cam opening interval reduces the pressure angle significantly. In addition to, however, enlarging the cam size (R_P) will lead to further decrease in pressure angle; however, this solution is not desired in engine applications due to space limitation. Thus for a regular cam with roller follower, the minimum cam opening or closing interval is about 50 degree. Thus the minimum valve opening duration that a cam with roller follower mechanism can provide is about 100 degree.

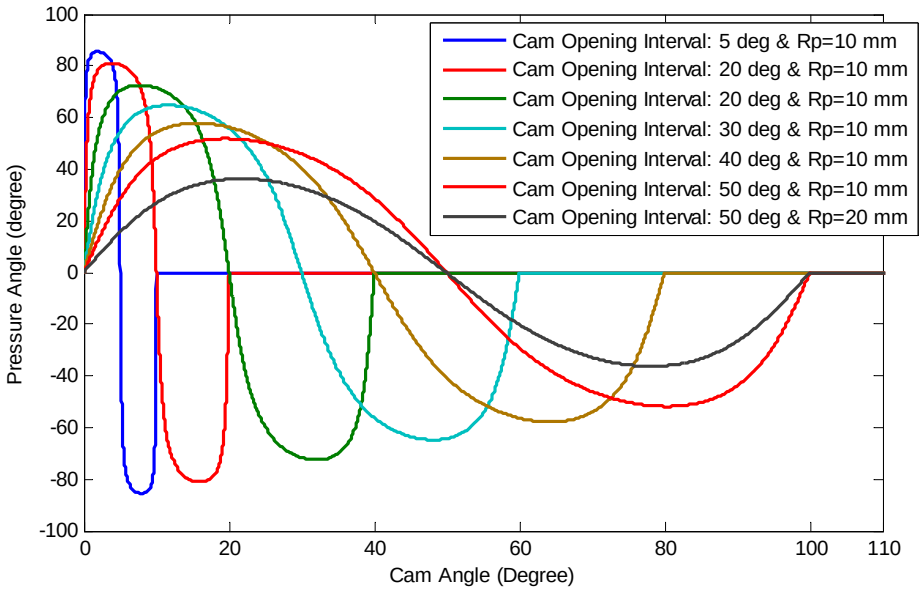

Figure A-4: Effects of cam opening/closing interval as well as cam size on pressure angle

A.3.2 Radius of Curvature in Cam with Flat-Faced Follower

The radius of curvature of the finished cam is of concern regardless of the follower type. In cam mechanism with roller follower, the limitation on the curvature radius does not affect the cam follower rise or fall intervals. However, in cam with flat faced follower, the situation is different. In this cam-follower mechanism, a negative radius of curvature on the cam cannot be accommodated [16] and this limits cam rise or fall intervals for the specified cam size. The following correlation can be used to determine the minimum rise/fall angle interval (β) that can be obtained from the cam with flat faced follower and specified size:

$$\beta = Cos^{-1}\left(\frac{R_b}{R_b + h}\right) = Cos^{-1}\left(\frac{R_b}{R_b + h}\right) \tag{A.5}$$

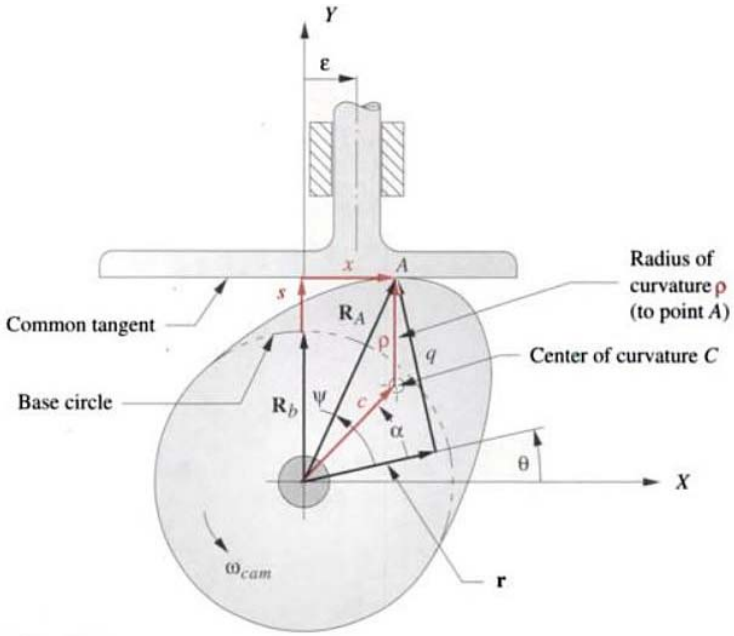

Figure A- 5: Cam with Flat Faced Follower [16]

A.4 **Conclusion**

In fact, using the cam-follower mechanism does not allow total valve opening duration of lower than 100 degrees. This is one of the drawbacks of the cam-follower systems. Therefore, in most of the cam-based VVT systems, either they are not able to open and close the engine valve in less than 100 cam degrees (200 CA°) or they must employ an intermediate mechanism to do this.

Appendix B

An Introduction to Hydraulic Power Systems

B.1 Advantages of Fluid Power Systems

There are several advantages in using hydraulic systems rather than mechanical or electrical systems. These advantages are:

- High power to weight ratio
- Wide speed range of operating conditions
- Simpler design with fewer moving parts in comparison with mechanical or electrical machines
- Possibility of power transmission to remote locations
- Lubrication and cooling capability of hydraulic fluid

B.2 Basic Properties of Hydraulic Fluid

Physical properties of the hydraulic fluid are determinant factors in fluid power systems performance. The main properties include oil density (ρ), absolute and kinematic viscosity (μ and ν), liquid compressibility (Bulk Modulus) and vapor pressure.

B.2.1 Fluid Viscosity

The fluid viscosity (μ) is a measure of the resistance to motion imposed by the fluid caused by the shear stress over the wetted area. In fact, the resistance force is proportional to the fluid velocity as well as contact area and inversely proportional to fluid thickness.

$$F = \mu A \frac{dV}{dy} \tag{B.1}$$

One of the disadvantages of hydraulic systems compared with other systems is their susceptibility to the oil pressure and temperature changes. In fact the fluid viscosity tends to

decrease as the temperature increases and increase as the oil pressure increases. Due to the rapid change of absolute viscosity with temperature especially at low temperatures, the performance of the hydraulic systems can be highly affected during system cold-start. The dependency of the fluid viscosity to the temperature and pressure can be illustrated using following exponential function [71]:

$$\mu(T,P) = \mu_0 \exp\left[a(P-P_0) - b(T-T_0)\right] \tag{B.2}$$

where a and b are constant for particular fluid and μ_0, P_0 and T_0 are the fluid properties at the reference condition. Regardless of the hydraulic fluid type, it is usually recommended that the oil viscosity remain within 7.8 to 95.7cP. However, for the cold-start the maximum viscosity shall be less than 1390cP and the minimum viscosity shall be greater than 5.0 cP.

B.2.2 Fluid Compressibility

Liquid compressibility has significant effect on the frequency of hydraulic power systems. This effect influences the system response time and dynamics especially during high speed operation [24].

B.2.2.1 Liquid Bulk Modulus

As the liquid pressure and temperature change, the density of the fluid changes slightly. This small variation in the fluid density can be described by a first order Taylor series approximation as follow [41]:

$$\rho = \rho_0 + \left.\frac{\partial \rho}{\partial P}\right|_0 (P-P_0) + \left.\frac{\partial \rho}{\partial T}\right|_0 (T-T_0) \tag{B.3}$$

where, ρ_0, P_0 and T_0 are fluid properties at reference condition. When a change is applied on the hydraulic fluid temperature or pressure, the density of the fluid varies. This change in fluid density can be determined using two constants called isothermal fluid bulk modulus (β) and isobar fluid coefficient of thermal expansion (α). The relation between these quantities can be written as following equations [41]:

$$\frac{1}{\beta} = \frac{1}{\rho}\frac{\partial \rho}{\partial P} = -\frac{1}{V}\frac{dV}{dP} \tag{B.4}$$

$$\alpha = -\frac{1}{\rho}\frac{\partial \rho}{\partial T} = -\frac{1}{V}\frac{dV}{dT} \tag{B.5}$$

Substituting these two equations in the fluid density equation yields the following equation of state for the hydraulic fluid [23]:

$$\rho = \rho_0 \left[1 + \frac{1}{\beta_0}(P - P_0) - \alpha_0 (T - T_0)\right] \tag{B.6}$$

B.2.2.2 Effective Bulk Modulus

In hydraulic systems, due to the existence of un-dissolved air in the hydraulic fluid, the bulk modulus of the system reduces significantly. Therefore in these systems the effective bulk modulus shall be used [71].

$$\frac{1}{\beta_e} = \frac{1}{\beta_{Oil}} + \psi \frac{1}{\beta_{Air}} \tag{B.7}$$

where,

$$\psi = \frac{V_{Air}}{V_{Oil}} \tag{B.8}$$

As it is seen in the above equations, reducing the un-dissolved air volume in the oil volume increases the effective bulk modulus. This can be done by increasing the system working pressure. On the other hand, if the system pressure reduces, the volume of the air trapped in the system increases adiabatically and deteriorates the oil effective modulus [71].

B.2.3 Vapor Pressure

Vapor pressure is the pressure at which a liquid tends to vaporize at the specific temperature. If the liquid pressure drops below the vapor pressure the liquid starts vaporizing. At this instant, the vapor bubbles do not tend to dissolve in the liquid like air and rather they collapse with ultra high frequency and create large transient pressure. When these vapor bubbles collapse near the hydraulic components surface, they cause extreme erosion and damage. This phenomenon is called cavitation and must be strictly avoided during system operation.

B.3 **Orifice Equation**

One of the most important equations which are useful for modeling a hydraulic system is orifice equation. This equation is based on the Bernoulli equation and it is applicable for incompressible flow with high Reynolds number.

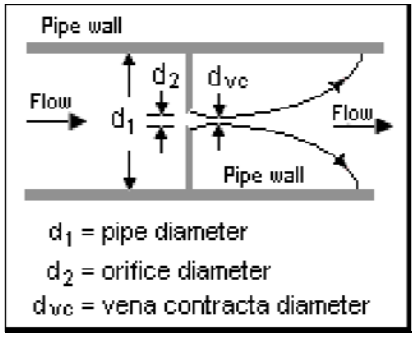

Figure B- 1: Flow through orifice

In the orifice, the ratio of the vena-contracta area to the area of the orifice is called the contraction coefficient. The contraction coefficient is determined experimentally for different orifices.

$$C_C = \frac{A_{VC}}{A_2} = \frac{d_{VC}^2}{d_2^2} \tag{B.9}$$

Using Bernoulli equation, the relation between flow velocities before and after orifice plate can be written as follow:

$$u_{out}^2 - u_{in}^2 = \frac{2(P_{in} - P_{out})}{\rho} \tag{B.10}$$

Using mass conservation, we have:

$$u_{in}A_1 = u_{out}A_{VC} = u_{out}A_2C_C \Rightarrow u_{in} = \frac{u_{out}A_2C_C}{A_1} \tag{B.11}$$

Substituting this equation in Bernoulli equation yields following correlation for flowrate through orifice:

$$Q = A_2C_d\sqrt{\frac{2(P_{in} - P_{out})}{\rho}} \tag{B.12}$$

where C_d is called orifice discharge coefficient and can be determined by:

$$C_d = \frac{C_C}{\left(1 - C_C \frac{A_2}{A_1}\right)} \tag{B.13}$$

B.4 **Pressure Dynamics in Hydraulic Conduits**

In hydraulic systems, significant pressure transitions are introduced due to compressibility and inertia of oil. This transient phenomenon can result in severe system vibration and also pressure waves which can damage the hydraulic components. Close-coupling i.e. locating the components close to each other, is often used to minimize the effects of transmission line dynamics on the components [43]. However, in those cases where close-coupling is not feasible the effects of pressure transition can be analyzed using the mass and momentum conservation equations.

B.4.1 Continuity Equation

Considering an infinitesimal control volume within the cylindrical pipe with the length of *dx* and cross section area of *A*, the total rate of mass flow within the system can be written as follow [41]:

$$\frac{dM}{dt} = \frac{\partial}{\partial t} \underbrace{\int_{CV} \rho A\, dx}_{\substack{\text{Rate of change} \\ \text{of the mass withing CV}}} + \underbrace{\int_{CS} \rho u dA}_{\text{Boundary Flow}} \tag{B.14}$$

Recognizing that the cross section area of the pipe is constant along the control volume (*dA=0*) and also assuming linear variation of pressure, density and velocity along the small control volume, the above equation can be written as below [41]:

$$\frac{dM}{dt} = \left(\rho + \frac{\partial \rho}{\partial x}\delta x\right)\left(u + \frac{\partial u}{\partial x}\delta x\right)A - u\rho A = \frac{\partial}{\partial t}\int_0^{\delta x} (\rho + \frac{\partial \rho}{\partial x}x)A\, dx \tag{B.15}$$

By neglecting the terms that are quadratically small, the continuity equation will be:

$$\frac{\partial \rho}{\partial t} + \frac{\partial (u\rho)}{\partial x} = 0 \tag{B.16}$$

B.4.2 Momentum Conservation Equation

Reynolds transport theorem can be used to express the momentum conservation equation. Considering the similar control volume used for continuity equation, the rate of change of pressure within the control volume can be written as [41]:

$$\begin{aligned} &PA - \left(P + \frac{\partial P}{\partial x}\delta x\right)A = \\ &\frac{\partial}{\partial t}\int_0^{\delta x}\left(\rho + \frac{\partial \rho}{\partial x}x\right)\left(u + \frac{\partial u}{\partial x}x\right)A\,dx - \rho u^2 A + \left(\rho + \frac{\partial \rho}{\partial x}\delta x\right)\left(u + \frac{\partial u}{\partial x}\delta x\right)^2 A \end{aligned} \tag{B.17}$$

Neglecting the small terms in the above equation, the momentum conservation equation can be written as follow:

$$\frac{\partial P}{\partial t} + \frac{\partial (u\rho)}{\partial t} + \frac{\partial (u^2\rho)}{\partial x} = 0 \tag{B.18}$$

B.5 Pressure Losses in Hydraulic Lines

Pressure losses in the hydraulic system can be categorized into two groups; losses in the straight pipes and losses due to sharp geometric changes within the system. The first group is mostly considered as the major losses and the second group is referred to as minor losses within the hydraulic system.

B.5.1 Pipe Pressure Losses

In hydraulic pipes, the pressure drop is a function of surface roughness, oil viscosity, Reynolds number, pipe length and radius [71]:

$$\Delta P = \frac{f \ell \rho v^2}{d} \tag{B.19}$$

where,

$$\begin{cases} f = \dfrac{64}{\mathrm{Re}} & \text{Laminar Flow} \\ f = \dfrac{0.3164}{\mathrm{Re}^{0.25}} & \text{Turbulent Flow} \\ f = 3.9e-6+0.0242 & \text{Transitional Flow} \end{cases}$$

B.5.2 Minor pressure Losses

As stated before, sudden expansion or contraction in flow passage can results in pressure drop within the flow. Therefore, valves, hydraulic fittings and flows into or from reservoir can lead to pressure losses. These losses can be formulated as below:

$$\Delta P = \frac{1}{2} K_L \rho V^2 \tag{B.20}$$

where K_L is a function of Reynolds number and the characteristic geometric features of the flow passage and can be found in hydraulic system handbooks.

B.6 Pressure Variation within a cylinder or Spring loaded Accumulator

The rate of hydraulic fluid mass change in the cylinder or accumulator can be determined as following equation:

$$\frac{dm}{dt} = \frac{d(\rho V)}{dt} = V\frac{d\rho}{dt} + \rho\frac{dV}{dt} \tag{B.21}$$

Assuming uniform pressure and density distribution within the system, the rate of change of the mass can be written as follows:

$$\frac{dm}{dt} = \rho Q \tag{B.22}$$

Using fluid bulk modulus, the rate of change in the hydraulic fluid density can be determined by:

$$\frac{\partial \rho}{\partial t} = \frac{\rho}{\beta}\frac{\partial P}{\partial t} \tag{B.23}$$

Substituting (B.22) and (B.23) in (B.21), the pressure variation in the accumulator or cylinder can be written as:

$$\frac{\partial P}{\partial t} = \frac{\beta}{V}\left(Q - \frac{dV}{dt}\right) \tag{B.24}$$

B.7 **Axial Leakage in Rotary Spool Valve**

In hydraulic components consisting of pistons and cylinders to reduce the friction force between moving parts, a clearance space filled with oil shall be considered. However, due to the existence of oil flow in the clearance space, some amount of oil is leaked from high pressure zone to low pressure zone. To increase the accuracy of the simulation, this leakage rate shall be modeled using the governing equation of motion for low-Reynolds-number flow. For a spool piston with radius R_i concentrically located in the valve cylinder with radius R_o with the clearance space (ε) filled with oil, the velocity profile can be determined as follow [41]:

$$u(r) = \frac{r^2}{4\mu}\frac{dP}{dx} + C_1 \ln(r) + C_2 \tag{B.25}$$

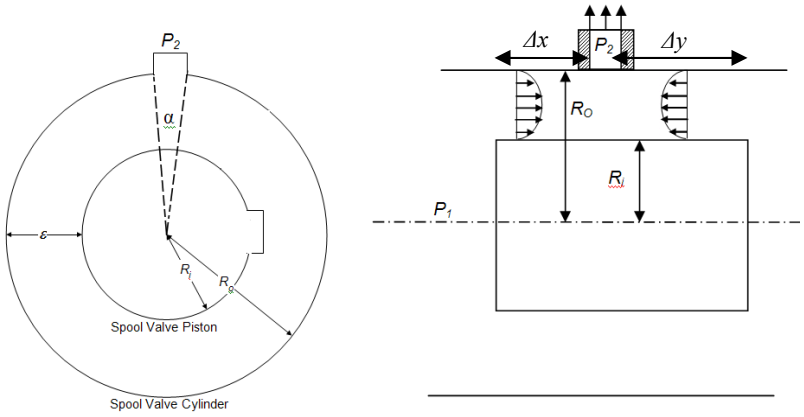

Figure B-2: End view of circular cylinder with a round insert

where,

$$C_1 = -\frac{R_o^{\,2} - R_i^{\,2}}{4\mu\left(\ln\left(R_o\right) - \ln\left(R_i\right)\right)}\frac{dp}{dx}$$

$$C_2 = -\frac{R_o^{\,2}}{4\mu}\frac{dp}{dx} - C_1\ln\left(R_o\right) \tag{B.26}$$

Therefore, the rate of leakage can be determined as follows:

$$Q_{leakage,axial} = 2\int_A u\left(r\right)dA = \left(\bar{R}\alpha\right)\int_{R_i}^{R_O}\left(\frac{r^2}{4\mu}\frac{dP}{dx} + C_1\ln(r) + C_2\right)dr \tag{B.27}$$

Simplifying the above equation, the axial leakage flow can be determined by:

$$Q_{leakage,axial} = 2\bar{R}\alpha\left(\frac{\left(R_o^3 - R_i^3\right)}{12\mu}\frac{\left(P_2 - P_1\right)}{\Delta x} + C_1\left(R_O.\left(\ln(R_o) - 1\right) - R_i.\left(\ln(R_i) - 1\right)\right) + C_2\left(R_o - R_i\right)\right) \tag{B.28}$$

where, $\bar{R}$ is the average radius

B.8 **Peripheral Leakage in Rotary Spool Valve**

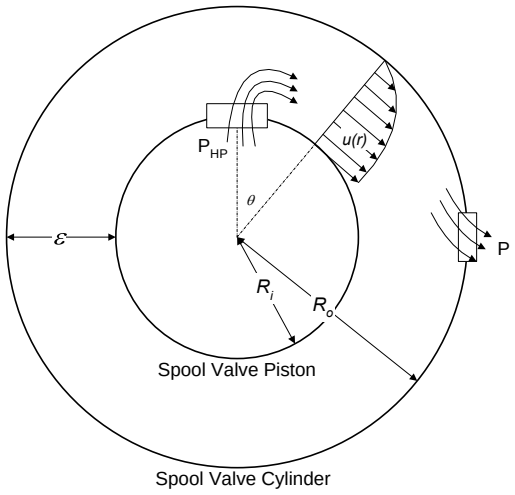

Figure B-3: The rotary spool valve cross section with magnified clearance between piston and cylinder

Assuming low Reynolds number flow, using the Navier-Stokes equations, the governing equation of motion for leaked fluid can be written as follow [41]:

$$\mu\nabla^2\vec{u} = \nabla P \tag{B.29}$$

Considering $\vec{u} = \begin{bmatrix} u_\theta & u_r & u_z \end{bmatrix}$, the above equation can be written as:

$$\mu\begin{bmatrix}\dfrac{\partial^2 u_\theta}{\partial r^2}+\dfrac{1}{r}\dfrac{\partial u_\theta}{\partial r}+\dfrac{1}{r^2}\dfrac{\partial^2 u_\theta}{\partial \theta^2}+\dfrac{\partial^2 u_\theta}{\partial z^2}\\ \dfrac{\partial^2 u_r}{\partial r^2}+\dfrac{1}{r}\dfrac{\partial u_r}{\partial r}+\dfrac{1}{r^2}\dfrac{\partial^2 u_r}{\partial \theta^2}+\dfrac{\partial^2 u_r}{\partial z^2}\\ \dfrac{\partial^2 u_z}{\partial r^2}+\dfrac{1}{r}\dfrac{\partial u_z}{\partial r}+\dfrac{1}{r^2}\dfrac{\partial^2 u_z}{\partial \theta^2}+\dfrac{\partial^2 u_z}{\partial z^2}\end{bmatrix}=\begin{bmatrix}\dfrac{\partial P}{r\partial\theta}\\ \dfrac{\partial P}{\partial r}\\ \dfrac{\partial P}{\partial z}\end{bmatrix} \tag{B.30}$$

Assuming one-dimensional flow field where velocity of the leaked fluid varies only in the r-direction and pressure varies in θ direction, the above equation is simplified to:

$$\mu\left(\frac{\partial^2 u_\theta}{\partial r^2}+\frac{1}{r}\frac{\partial u_\theta}{\partial r}\right)=\frac{\partial P}{r\partial\theta} \tag{B.31}$$

Because in the above equation the fluid pressure is independent of radial dimension and the velocity is independent of tangential dimension, by doing some manipulation, the above equation can be written as follow:

$$\mu\frac{1}{r}\frac{d}{dr}\left(r\frac{du}{dr}\right)=\frac{1}{r}\frac{dp}{d\theta} \tag{B.32}$$

Integrating the above equation twice with respect to r yields:

$$u(r)=\frac{r}{\mu}\frac{dp}{d\theta}+C_1\ln r+C_2 \quad , \begin{cases}u(R_o)=0\\ u(R_i)=R_i\omega\end{cases} \tag{B.33}$$

where, C_1 and C_2 are determined by imposing the boundary conditions:

$$\begin{aligned}C_1&=-\left(\frac{R_i\omega+\dfrac{(R_o-R_i)}{\mu}\dfrac{dp}{d\theta}}{\ln\dfrac{R_o}{r_i}}\right)\\ C_2&=\frac{-R_o}{\mu}\frac{dp}{d\theta}+\left(\frac{R_i\omega+\dfrac{(R_o-R_i)}{\mu}\dfrac{dp}{d\theta}}{\ln\left(\dfrac{R_o}{R_i}\right)}\right)(\ln R_o)\end{aligned} \tag{B.34}$$

Therefore, the total leakage flowrate can be determined by integrating the velocity with respect to flow area:

$$Q_{leakage,per}=\int_A u(r)\,dA=\int_{R_i}^{R_o}L_{Port}u(r)\,dr=L_{Port}\int_{R_i}^{R_o}\left(\frac{r}{\mu}\frac{dp}{d\theta}+C_1\ln r+C_2\right)dr \tag{B.35}$$

By approximating $dp/d\theta$ as $\left(P-P_{HP}\right)/\theta$, the peripheral leakage flowrate can be determined as follow:

$$Q_{leakage,per}=L_{Port}\left(\left(R_o^{\,2}-R_i^{\,2}\right)\left(P-P_{HP}\right)/2\mu\theta+ C_1\times\left(R_o\left(\ln\left(R_o-1\right)\right)-R_i\left(\ln\left(R_i-1\right)\right)\right)+C_2\left(R_o-R_i\right)\right) \tag{B.36}$$

B.9 **Hydraulic Energy**

For mechanical system, power is calculated by force times velocity or torque time angular velocity. For electrical systems, the power can be determined by multiplication of voltage and current. However, for the hydraulic systems the flow power can be defined as multiplication of volumetric flowrate and pressure.

$$\text{Power}=\frac{dW}{dt}=P\frac{dV}{dt}=PQ \tag{B.37}$$